Applications of Peptide Nucleic Acid (PNA) in Nanotechnology

by

Jing Kong

A dissertation submitted in partial fulfillment of the requirements for the degree of

Doctor of Philosophy in Chemistry

Carnegie Mellon University

Pittsburgh, Pennsylvania

February 2014

ABSTRACT

This dissertation is focused on the study of properties of PNA relevant for its use as a new material in nanotechnology applications. More specifically, it describes the synthesis and characterization of a molecular switch based on a ligand-modified PNA, the use of PNA for the sequence-specific functionalization of DNA origami, and the measurement of the rate constant for charge transfer through PNA in solution. Each of these three research projects covers an aspect of PNA relevant to nanotechnology.

The molecular switch described in Chapter II is based on a modified PNA that contains two different metal binding sites, one based on 8-hydroxyquinoline and one based on 2,2'-bipyridine. UV titration showed that it is possible to use this PNA as a scaffold to organize copper ions in different oxidation states at different coordination sites and to translocate these ions between the two sites in response to redox reagents. PNA can be used also as a linker for the sequence-specific functionalization of DNA origami, as shown in Chapter III. AFM images showed that PNA strands modified with functional groups can be attached to the DNA origami at predefined positions by either annealing or invasion and that the efficiency of this functionalization is higher than that of the current strategies based on DNA. The photo-induced electron transfer properties of PNA in solution have been studied in Chapter IV. This research showed that the number of base pairs and the sequence of a PNA duplex used to connect an electron donor to an acceptor affect the electron transfer rate between these two groups.

The research described in this thesis provides concepts and experimental results useful for the pursuit of PNA applications in nanotechnology.

ACKNOWLEDGEMENTS

First of all, I would like to sincerely thank my advisor, Dr. Catalina Achim, for guiding me with her professional instructions on research and personal advice throughout my PhD education. She is a great mentor with a lot of patience, kindness, integrity, and care. She is a role model for me to learn from in both teaching and research. I feel very lucky and appreciate her very much as my PhD advisor.

I would also like to thank my committee members, Dr. Danith Ly and Dr. Terrence Collins, for their constructive advice and inspiring comments for my progress report, proposal and thesis defense. I appreciate as well Dr. Rita Mihailescu from Duquesne University for accepting to be the external member of my Thesis Committee.

My work would not have been accomplished without the contributions of my collaborators from the University of Pittsburgh and the North Carolina State University. I would like to express my gratitude to Dr. David Waldeck and his group members, Xing Yin and Dr. Emil Wierzbinski, for the fluorescence experiments and valuable discussions and to Dr. Thomas LaBean and Ronnie Pedersen for the experiments on DNA origami and inspiring communications.

Special thanks to my lovely group members, Yookyung Bae, Heather Stout, Selma Ulku, Dilhara Jayarathna, Artur Sargun, Dr. Arnie de Leon, Dr. Silvia Bezer, Dr. Zhijie Ma and Dr. Richard Watson. They have been very supportive and helpful. My gratitude also extends to the colleagues in Mellon Institute and the teaching instructors, Dr. Susan Graul, Carolyn Neiderlander, and Robert Dalmasse. Without them, my life in Mellon and my teaching in Doherty would not have been so much fun.

I would like to dedicate this work to my family, my Mom Yufang Dong and my Dad Fanzhong Kong, my husband Dr. Hsiang-Kai Lin and my to-be-born baby Andrew. Their unlimited love and support motivated me to pursue my dream to be a PhD.

Last but not least, thank God for being with me all the time.

CONTENTS

LIST OF FIGURES

LIST OF TABLES

CHAPTER I. INTRODUCTION OF NON-MODIFIED AND MODIFIED NUCLEIC ACIDS AND THEIR APPLICATIONS IN NANOTECHNOLOGY

I-1. Introduction

Advances made in recent decades in understanding biological processes at the molecular level have stimulated progress in the quest for biomimetic approaches for the synthesis of artificial devices that perform various functions such as electron transfer, controlled changes in magnetic properties or mechanical motions in response to an electrochemical trigger, pH change, light signal, or presence of catalysis. The synthesis of these artificial devices is based on the rational and precise assembly by covalent and/or non-covalent interactions of a discrete number of molecular components. Particularly when assembled based on non-covalent interactions, the molecular devices can sense, communicate and respond to each other when a change in the environment takes place, because such a change can affect their components and/or the interactions that keep the components together. In this context, hybrid inorganic-nucleic acid molecules that contain one or more transition metal ions and whose assembly is based on coordination- and hydrogen-bonds have been pursued recently. The coexistence of metal complexes and nucleobase pairs in these hybrid molecules leads to a relatively large set of properties that can be adjusted to achieve the desired molecular architecture and function.

The typical synthesis of molecules that contain multiple metal ions is based either on the use of polytopic ligands (Figure I-1a), or on the self-assembly of small ligands and metal ions (Figure I-1b). The synthesis of polytopic ligands requires often several stepwise, different organic reactions and, consequently, has relatively low yield. The self-assembly of a large molecule from a set of different ligands and metal ions can generate many isomers. One recent strategy for creating homo- and hetero-metallic molecules is based on the use of ligand-containing, nucleic acid oligomers synthesized by only one, very high yield reaction between linkers to which various ligands are attached (Figure I-1c). Using this strategy, oligomers with different ligands arranged in any sequence can be obtained in relatively high yield. The difficulty that remains in the case of oligomers composed exclusively of ligand-containing monomers is the presence of multiple, different coordination sites that may have comparable affinity for metal ions; such oligomers could lead to several super molecules with different relative arrangement of the oligomers. This problem can be alleviated or avoided if the oligomers contain besides ligands another recognition component that drives the assembly of oligomers in a unique way independent of the metal ion(s) (Figure I-1d). Ligand-modified, nucleic acid duplexes such as the ones generically represented in Figure I-1d are an example of outcome of this strategy. The formation of the duplex is driven by the information stored in the sequence of nucleobases of the two strands, which interact through Watson-Crick base pairing. Subsequent to the duplex hybridization, metal coordination takes place at the ligand sites rather than at the nucleobases because, under a wide range of conditions, these sites have higher affinity for the metal ions than the nucleobases. Conversely, it is also possible to first self-assemble the ligand-modified nucleic acid oligomers through

metal coordination and then create the conditions for Watson-Crick hybridization, for example by a change in temperature or by the addition of a complementary oligomer.

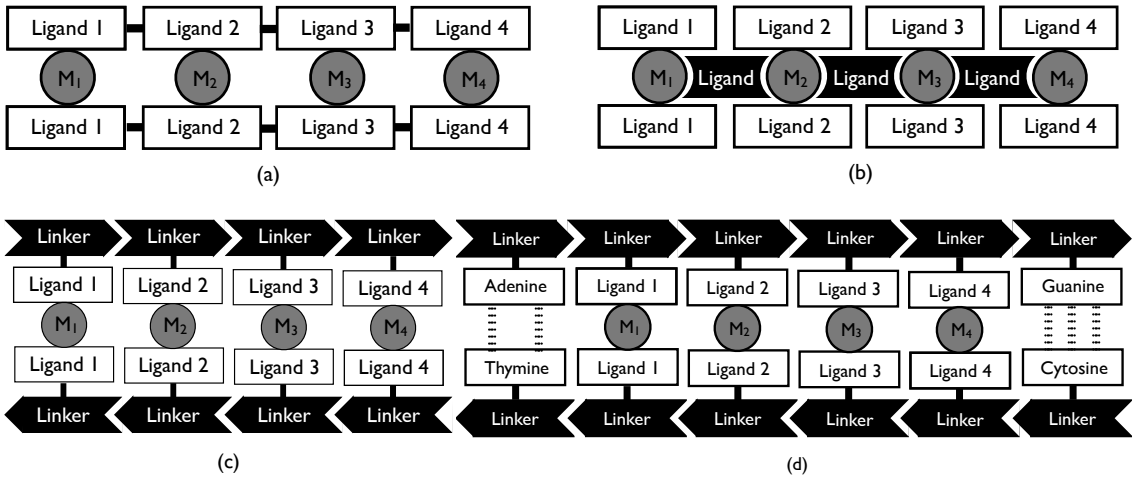

Figure I-1. Cartoon representation of strategies for the synthesis of heteroarrays of transition metal ions; Metal arrays based on (a) polytopic ligands; (b) self-assembly using small ligands; (c) polytopic ligands in which different ligands are attached to the same backbone made of monomers termed in the figure "linker"; (d) polytopic ligands in which different ligands and nucleobases are attached to the same nucleic acid backbone.

The use of ligand-modified nucleic acids to create hybrid inorganic-nucleic acid structures ensures that the metal binding is site specific rather than uniform, as is the case when the metal ions bind to either the backbone or the nucleobases of the non-modified nucleic acid. In DNA, the G-N7 and A-N7 positions are the most common coordination sites for transition metal ions with the G-N7 being preferred over the A-N7 site.[1-3] The factors that affect metal binding to DNA include *a)* the nucleophilicity of the phosphates and nucleobases and their hard and soft Lewis base character, respectively; *b)* the accessibility of these groups to metal ions; *c)* the molecular electrostatic potential of

DNA; *d)* the ability of the groups neighboring the metal coordination site to form hydrogen bonds with the water molecules coordinated to the metal; and, in the case of binding of multiple metal ions to the same DNA duplex, *e*) the changes in the secondary structure of the DNA and in the nucleophilicity of the phosphate and nucleobases induced by the first metal ions that bind to DNA.[4-18]

Although not site specific, metal binding to non-modified DNA was successfully exploited to create nano-size, hybrid inorganic-nucleic acid structures with interesting conducting or charge transfer properties. For example, a conductive silver wire was obtained by treatment of a DNA scaffold with Ag^+, followed by reduction of Ag^+ to metallic silver, and subsequent uniform deposition of Ag or Au on the initial Ag clusters formed on DNA.[19,20] Sequence specificity of the Ag deposition has been achieved by using RecA proteins for sequence-specific protection of the DNA.[21,22] While this strategy offered sequence specificity, the metal ion localization was with cluster/nanometer resolution rather than angstrom/atom resolution. A different strategy for the synthesis of hybrid inorganic-nucleic acid structures in which the metal ions are uniformly distributed on DNA was to coordinate 3d transition metal ions to non-modified DNA at high pH, which leads to the coordination of one metal ion per nucleobase pair to form M-DNA.[23-27] The structure, stability and electronic properties of M-DNA have been evaluated by theoretical methods too.[28-30]

In 1999 Shionoya and collaborators mentioned for the first time the possibility of substituting nucleobase pairs in DNA with pairs of ligands and binding of metal ions to these ligands to create metal-based alternative base pairs in duplexes that contain both

Watson-Crick and coordination bonds (Figure I-2).[31] They have synthesized several nucleosides and characterized metal complexes of these nucleosides with metal ions.[32-35] In 2000 Schultz published the first DNA duplex containing a metal-mediated alternative base pair based on a monodentate and a tridentate ligand coordinated to Cu^{2+},[36] shortly followed by Tor[37,38] and Shionoya,[39,40] who synthesized DNA duplexes modified with a pair of two bidentate ligands that bound 3d transition metal ions. Since then, several other groups including those of Switzer,[41-44] Müller,[45-49] and Carell[50-58] have applied this method to synthesize DNA duplexes containing one or several transition metal ions. The same strategy was applied to the successful modification of peptide nucleic acids (PNAs),[59-63] glycol nucleic acids (GNAs),[64,65] unlocked nucleic acid (UNA),[66-68] and locked nucleic acids (LNAs).[69,70]

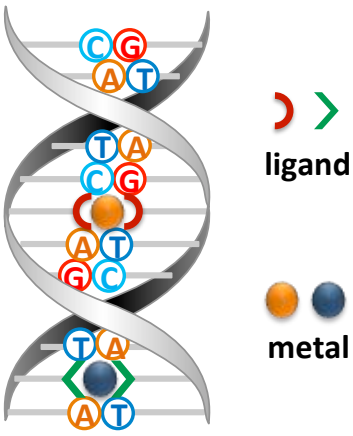

Figure I-2. Cartoon representation of nucleic acid duplex containing one metal-based alternative base pair and examples of complexes formed with the two ligands from the two single strands of the duplex.

To date, several strategies have been used to create systems based on synergetic formation of hydrogen and coordination bonds and p stacking interactions (Figure I-2).

Ligand incorporation in the center of nucleic acid oligomers (Figure I-3a) was used to create metal-containing, ligand-modified duplexes. In this approach, the coordination complex formed between the metal ion and the ligands plays the role of an artificial base pair and will be referred to as a metal-ligand alternative base pair or metal-mediated base pair. Ligands have also been used as connectors of ss nucleic acids (Figure I-3b). Terminal modification of nucleic acid oligomers with ligands was used to create a broad range of structures, including metal-containing, single strands, hairpins, duplexes and triplexes (Figure I-3c, d). Within these hybrid inorganic-nucleic acid structures, there are synergetic relationships between *a*) metal coordination and oligonucleotide hybridization, and *b*) the properties of the metal complexes and those of the nucleic acid structures that contain the metal complexes. For example, upon hybridization of ligand-modified oligonucleotides to form a duplex that contains ligands in complementary positions, the binding constant for a metal ion to the ligands brought in close proximity of each other by the duplex is generally larger than that to each independent ligand.[40,61] Conversely, ligand-modified oligonucleotides that may form two alternate structures such as a duplex or a hairpin (Figure I-3b), will adopt preferably one of these two structures in which the metal ion has its most common coordination number and geometry.[71]

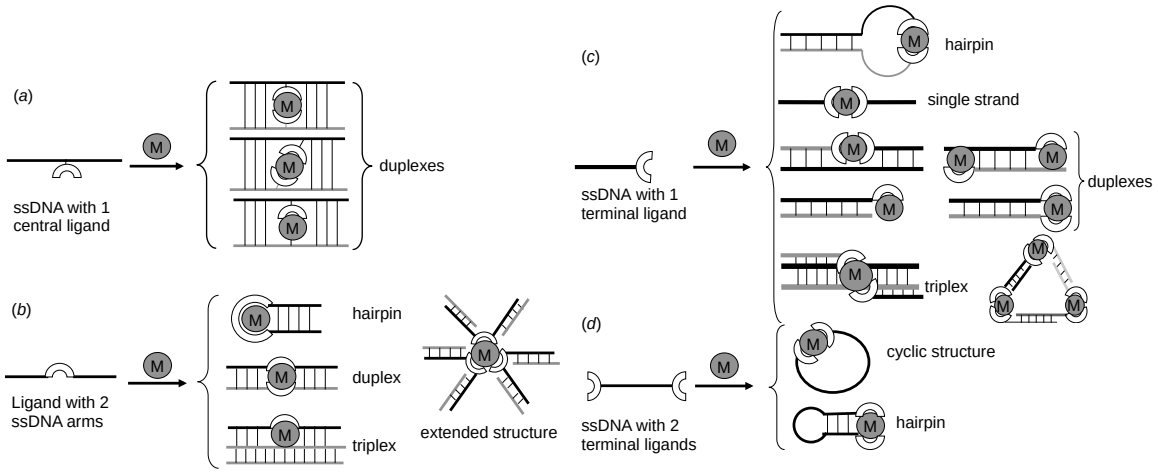

Figure I-3. Hybrid inorganic-nucleic acid structures based on four types of ligand-modified nucleic acid strands and transition metal ions.

I-2. Synthetic Analogues of DNA: PNA, LNA, UNA and GNA

Metal-based alternative base pairs have been incorporated to date in DNA, RNA and several of their synthetic analogues, including peptide nucleic acid (PNA), locked nucleic acid (LNA), unlocked nucleic acid (UNA), and glycol nucleic acid (GNA). These analogues can form duplexes by Watson-Crick base pairing with DNA and RNA, and thus have potential for antisense and antigene applications. Their backbone is different from that of DNA, which makes them chemically and biochemically more stable than DNA, and thus more appropriate in certain nanotechnology and biology applications.

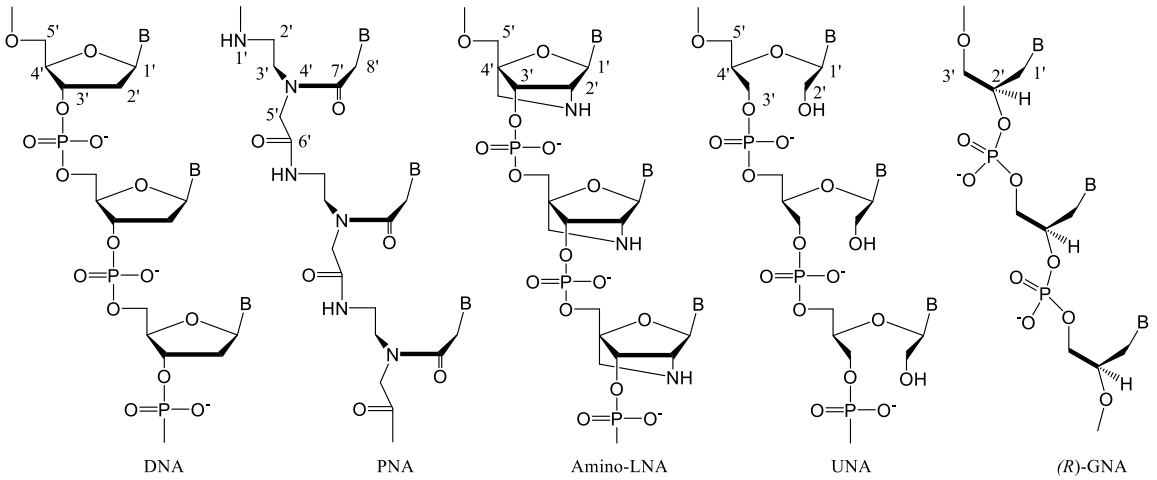

Figure I-4. Chemical structures of single strands of DNA, PNA, LNA, UNA, and GNA.

PNA, which was discovered in 1991, has a pseudo-peptide backbone originally based on N-(2-aminoethylglycine) (Aeg), which is neutral and achiral (Figure I-4).[72] The thermal stability of PNA•PNA duplexes is higher than that of PNA•DNA or DNA•DNA duplexes because the backbone is neutral. Hence, mismatches and in general chemical modifications that affect the base pairing have a larger effect on the thermal stability of PNA•PNA duplexes than on PNA•DNA or DNA•DNA duplexes. The synthesis of PNA monomers is relatively simple.[73] PNA monomers containing the A, G, C and T bases are commercially available from several suppliers. Numerous PNA monomers with different pseudo-peptide backbone or with alternative nucleobases have been prepared.[74-88] For example, alanyl PNA is a peptide-based nucleic acid structure with an alanyl-derived backbone having the nucleobases attached to the β-carbon.[89] PNA oligomers are prepared simply by modified solid phase synthesis using either Boc or Fmoc protection strategy.[90] The attachment of amino acids or carboxylic acid derivatives of ligands or metal

complexes to the amino end of the PNA oligomers is straightforward. Positively charged amino acids such as lysine and arginine and hydrophilic groups such as PEG have been introduced into PNA oligomers to improve their solubility, enabling the preparation of mM solutions of PNA.[90] Cysteine has also been introduced in PNA to form self-assembled monolayers (SAMs) on gold surfaces.[91,92]

In contrast to the chiral sugar-phosphate backbone of DNA, the amino-ethylglycine backbone of PNA does not contain stereocenters. A preferred helical handedness can be induced in the duplexes by the attachment of a D- or L-amino acid at the COOH terminus of the helix.[93] X-ray crystallography showed that the PNA•PNA duplexes, which adopt a distinct "p–form" helix in both crystals and solution, exist in crystals as right- and left-handed duplexes even if they contain an L-Lysine, which indicates that the chiral induction effect exerted by the lysine is comparable in strength to the packing forces.[94-96] A preferred handedness can also be induced in PNA duplexes by a stereogenic center at the α- or γ-position.[88,97-99] The incorporation of an (*S*)-Me stereogenic center at the γ-backbone position induced the formation of a right-handed structure in duplexes as well as in single stranded PNA.[88,100]

Several metal complexes have been attached to PNA because they can be used as IR (e.g., [Cr(benzene)$(CO)_3$]) or electrochemistry probes (e.g., ferrocene, cobaltocene, or $[Ru(bipy)_3]^{2+}$), or to quantify the cellular uptake of PNA. These complexes have been linked to PNA by using metal complex-containing PNA monomers or an alkyne-containing PNA monomer to which the metal complex could be linked by click chemistry (Figure I-5).[101]

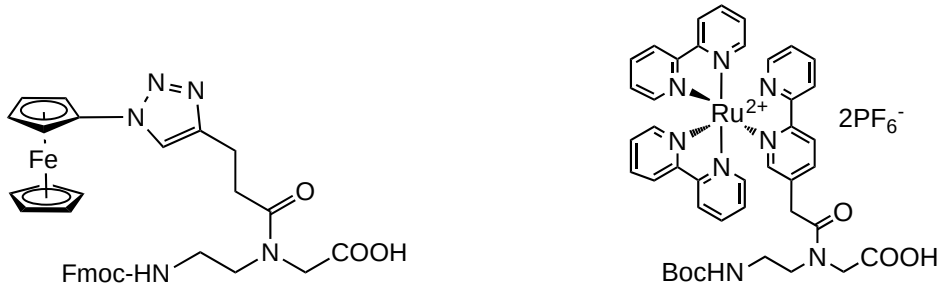

Figure I-5. PNA monomers used for the labeling of PNA-containing duplexes with transition metal complexes.[101-103] *These complexes do not function as alternative nucleobase pairs.*

Oxy-LNA is an RNA analogue developed in 1998,[104,105] in which the ribose group of the sugar phosphate backbone contains a methylene bridge between the 2'-oxygen atom of the ribose and the 4'-carbon atom (Figure I-4).[106,107] Unlocked nucleic acid (UNA) lacks the C2'-C4' bond normally found in ribonucleosides (Figure I-4). Several C-glycoside analogues of LNA have been prepared including an amino-LNA that has a 2'-NH group instead of the 2'-oxygen (Figure I-4). This chemical modification preorganizes the LNA monomer into a locked C3'-endo conformation similar to that observed in A-type DNA, and reduces the entropic penalty for the formation of duplexes containing LNA. As a consequence, LNA•LNA and hetero LNA•RNA and LNA•DNA duplexes are more stable than DNA•DNA or DNA•RNA ones. The NMR structures of partially- or completely modified LNA•RNA and LNA•DNA hybrids showed that the LNA nucleotides induce a preference for an A-type, right-handed duplex structure because of their C3'-endo conformation and because they steer the sugar conformations of neighboring nucleotides into similar C3'-endo conformations.[108] We note that it is

common to refer to a single strand of DNA that contains only several LNA (or GNA, see below) residues as single stranded LNA (or GNA).

The nucleobases of LNA are preorganized for good stacking interactions, which cause very high thermal stability of LNA-modified duplexes.[107] For example, the introduction of LNA into the DNA strand of a DNA•RNA duplex has been shown to increase the T_m by 1-8 °C per LNA monomer relative to the unmodified duplex. In contrast to LNA, UNA has a broken ribose bond between C2' and C3' instead of an extra bridge between C2' and C4' (Figure I-4), which was first reported earlier than LNA in 1995.[109] The high flexibility of UNA causes a destabilization of UNA-containing duplexes when compared to the ones lacking UNA.[107] For example, the T_m of a DNA•RNA duplex decreased by up to 10 °C per UNA monomer. However, strategic positioning of the UNA monomer can increase or decrease the discrimination of mismatches to manipulate the hybridization specificity.[110]

GNA has an acyclic three-carbon, propylene glycol-phosphodiester backbone that includes a stereocenter (Figure I-4).[65,111,112] GNA oligomers form antiparallel, helical duplexes based on Watson-Crick base pairing, which are more stable than the analogous DNA or RNA duplexes. Crystallographic studies of double stranded GNA that contained a brominated cytidine or uracil or a complex of copper with hydroxypyridone ligands showed that the existence of two forms of backbone conformations, a condensed N-type or an elongated M-type, respectively.[113] Molecular dynamics simulations of a non-modified GNA duplex showed an all-gauche conformation characteristic of M-type GNA but with the higher helical twist common to N-type GNA structures.[114] GNA and LNA

oligomers can be synthesized by standard solid state DNA synthetic methods because the backbone of both molecules is formed by phosphodiester bonds.

I-3. Metal-Containing, Ligand-Modified Nuclei Acid

The earliest attempt to incorporate metal ions in nucleic acids was by coordinating Hg^{2+} and Ag^{+} with natural bases.[115,116] The involvement of natural bases in both Watson-Crick hydrogen bond and metal-ligand coordination creates ambiguity in the rules of complementarity for base pair formation. This ambiguity is solved by the creation of ligand-containing nucleosides that are orthogonal to the natural bases, which is known as ligandosides.[37,117] Alternative base pairing formed between the ligandosides through metal complexation was first introduced by Tanaka and Shionoya, where a phenylenediamine-containing ligandoside was synthesized and characterized to form the 2:1 ligand:metal metal-mediated base pair with Pd^{2+}.[118] This study later led to the site-specific incorporation of metal ions by introducing multiple ligand-modified nucleosides into DNA duplexes.[36,38-40,119,120] Besides DNA, the same strategy was used to incorporate metal ions in other synthetic nucleic acids such as PNA, LNA, UNA and GNA.[121-124] The formed metal-mediated base pairs stack with the adjacent base pairs and contribute to the thermal stability of the duplex. This novel class of metal-DNA hybrid structures is of high interest for several reasons. First, it adds a novel dimension to the growing field of artificial base pairs, which were previously based either on alternative hydrogen bonding patterns or on hydrophobic interactions.[125,126] The higher stability of coordinative bonds when compared to that of hydrogen bonds bodes for the formation of alternative base pairs whose stability surpasses that of the natural, Watson-Crick base pairs and may be of

interest for applications in biotechnology. Second, metal-based alternative base could be used in the extension of the genetic code.[36] Recent work showed that indeed, metal-containing alternative basepairs can be recognized and extended by polymerases.[58,127,128] Third, for the inorganic chemist, the interest in such structures is related to the possibility of using the nucleic acid duplex as a scaffold in which metal ions are incorporated in a rational and controlled manner. The bridging of the gap between extended metal clusters, which have been produced by materials science, and metal clusters, which have been synthesized by supramolecular inorganic chemistry, makes the efforts aimed at using nucleic acids as scaffold for transition metal ions worthwhile.

To make possible the metal ion incorporation at specific locations in nucleic acid duplexes, ligands are included in the oligomers, typically in complementary positions. All ligands used to date to form metal-ligand alternative base pairs contain aromatic rings, and can participate in π–π stacking interactions with adjacent bases. Generally these ligands cannot form hydrogen bonds to bridge the two complementary oligonucleotides forming the duplex. In all studies published so far, the stability of the ligand-modified duplexes was similar or lower to that of the duplexes that have an A•T or G•C basepair instead of the pair of ligands.

The ligands chosen to create metal-containing nucleic acid duplexes form square-planar complexes, can participate in π stacking interactions (with the adjacent base pairs), and have been placed usually in complementary positions within nucleic acid duplexes. Most of the ligands fulfil this condition by having 1-3 metal binding sites that are part of aromatic rings. To ensure that the metal ions are incorporated only at the positions where

the duplex has been modified, the affinity of the ligands for the metal ions must be higher than that of the natural nucleobases, in particular that of the G bases, which bind in a monodentate fashion through GN7. Preferably the metal ions should have the ability to form either square-planar complexes or octahedral complexes with the ligands in equatorial positions and the axial positions occupied by donor atoms from the adjacent nucleobases or solvent molecules.

An important condition that artificial base pairs must fulfil to be useful for the extension of the genetic code is to be orthogonal to natural base pairs. Therefore, the metal ion should form complexes only with the extraneous ligands and not mixed-ligand complexes with the natural bases. This condition was verified when polymerases have been used to extend single stranded DNA containing either thymine or salicylaldehyde as ligands in the presence of Hg^{2+} or ethylene diamine and Cu^{2+}, respectively.[58,127,128] Bipyridine may be another candidate for genetic code expansion because metal coordination to bipyridine ligands introduced opposite a natural nucleobase in DNA (as well as PNA) duplexes had no effect on or caused a decrease in the thermal stability of the duplexes.[59,129] This result suggests that the metal ion does not form an alternative base pair with mixed bipyridine nucleobase coordination. The decrease in the melting temperature may have been caused by metal coordination to bipyridine only, which in turn may cause a distortion of the duplex and/or a loss of stacking interactions.

Incorporation of multiple metal ions in adjacent positions within the duplexes is likely to depend on the overall charge of the metal complex and of the nucleic acid. In DNA duplexes, the phosphodiester backbone can act as intrinsic counter anion for positively-

charged metal complexes incorporated in the duplex and thus can mitigate electrostatic repulsion between adjacent metal-ligand complexes. In DNA analogues that are neutral, these interactions are weak if neutral metal complexes are incorporated in the duplex.

I-4. Research in Our Group

The research in our group has several aims: 1) The synthesis of new ligand-modified PNA monomers that have interesting chiral, electrochemical, and optical properties in the presence of transition metal ions; 2) The investigation of electronic properties of PNA to understand the charge transfer and electron capture properties of PNA; 3) The pursuit of nucleic-acid based devices whose properties can be changed in a controlled manner by relatively small environmental perturbations; 4) The arrangement of functional groups on DNA origami using PNA as anchor. Previous work in our group has demonstrated the incorporation into PNA duplexes of different ligands , such as 8-hydroxyquinoline, 1,2-hydroxypyridone, hydroxamate, pyridine, 2,2'-bipyridine, 5'-methyl-2,2'-bipyridine, terpyridine, and tetrazole, or metal complexes, such as ferrocene or tris(bipyridine) ruthenium.[63,121,130-132] Using the above-mentioned ligands, a variety of metal ions such as Al^{3+}, $Cu^{2+/+}$, $Fe^{2+/3+}$, Co^{2+}, Zn^{2+}, Ni^{2+}, and Eu^{3+} have been introduced into the PNA duplexes.

Chapter II reports a molecular switch created based on PNA. The switch is based on two different ligands, 8-hydroxyquinoline and 2,2'-bipyridine, whose binding constants with copper in different oxidation states are very distinct from each other. Both ligands are inserted at the complementary positions in a PNA duplex such that they can form alternative base pairs in the presence of copper. Due to the difference in the binding

constants, Cu^{2+} prefers binding with 8-hydroxyquinoline while Cu^{+} prefers binding with 2,2'-bipyridine. Upon oxidation or reduction reaction, a copper ion can migrate from one binding site to the other. Rather than the traditional molecular switch with difficulty to manipulate, the PNA-based molecular switch can be altered easily by a new sequence design followed by the same solid phase peptide synthesis protocol. The new "LEGO" like molecular switch makes possible assembly of different ligand combination and different metal incorporation with a uniform strategy. This molecular switch has potential applications as control units or sensor in creating nanodevices. In Chapter II, I present the experiments that prove the binding preferences of copper ion in different oxidation states for the two ligands situated in PNA duplexes and the successful migration of copper ion triggered by redox reactions.

Chapter III presents data on photo-induced charge transfer through PNA duplex in solution. Previous studies of charge transfer through PNA have been conducted on self-assembled monolayers of PNA on Au electrodes and were done mainly by electrochemistry. In this thesis I describe experiments done by fluorescence spectroscopy to determine the rate of electron transfer in PNA duplexes in solution. A $[Ru(bpy)_3]^{2+}$ donor and a $[CuQ_2]$ acceptor have been chosen to facilitate the electron transfer through PNA (Figure I-6). Fluorescence quenching is realized by the electron transfer from $[Ru(bpy)_3]^{2+}$ to $[CuQ_2]$ through the PNA bridge that connects the two metal complexes. The rate of electron transfer is derived from the decay curve of fluorescence quenching. A distribution of experimentally-determined fluorescence lifetimes bears similarity to a distribution in the donor-acceptor distance calculated based on molecular dynamics

simulations. This study also addresses the dependence of charge transfer through PNA on factors such as the length, the sequence, and the conformation of the PNA.

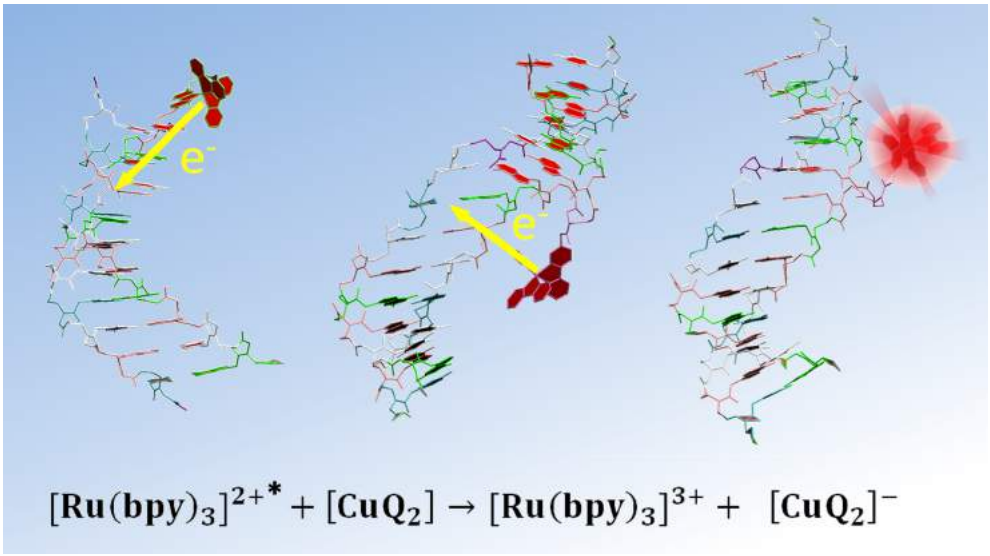

Figure I-6. Cartoon representative of the photo-induced electron transfer in PNA.

Chapter IV demonstrates the application of PNA as linker for the functionalization of DNA origami.[133-137] PNA, as an analogue of DNA with neutral or positively-charged character is introduced after the pre-annealing of DNA origami. AFM images show the successful modification of PNA at the predefined positions on DNA origami (Figure I-7). Statistic results indicate the binding efficiency of PNA depends on the relative location on the DNA origami. Specifically, the binding of PNA on the center of DNA origami has a significant advantage over DNA due to the reduced electrostatic repulsion.

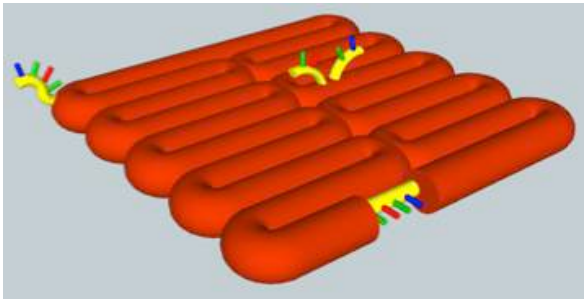

Figure I-7. Illustration of different PNA binding sites on DNA origami. Orange cylinders represent the DNA duplex forming the structure. Yellow cylinders represent single stranded regions complementary to PNA.

I-5. References

(1) Derose, V. J.; Burns, S.; Kim, N. K.; Vogt, M. *Comprehensive Coordination Chemistry II* **2004**, *8*, 787.

(2) Martin, R. B. *Metal Ions in Biological Systems* **1996**, *32*, 61.

(3) Martin, R. B. *Accounts of Chemical Research* **1985**, *18*, 32.

(4) Schoenknecht, T.; Diebler, H. *Journal of Inorganic Biochemistry* **1993**, *50*, 283.

(5) Gueron, M.; Demaret, J. P.; Filoche, M. *Biophysical Journal* **2000**, *78*, 1070.

(6) Van Steenwinkel, R.; Campagnari, F.; Merlini, M. *Biopolymers* **1981**, *20*, 915.

(7) Zimmer, C.; Luck, G.; Triebel, H. *Biopolymers* **1974**, *13*, 425.

(8) Moldrheim, E.; Andersen, B.; Froystein, N. A.; Sletten, E. *Inorganica Chimica Acta* **1998**, *273*, 41.

(9) Froeystein, N. A.; Davis, J. T.; Reid, B. R.; Sletten, E. *Acta Chemica Scandinavica* **1993**, *47*, 649.

(10) Vinje, J.; Parkinson, J. A.; Sadler, P. J.; Brown, T.; Sletten, E. *Chemistry-A European Journal* **2003**, *9*, 1620.

(11) Vinje, J.; Sletten, E. *Chemistry-A European Journal* **2006**, *12*, 676.

(12) Jia, X.; Zon, G.; Marzilli, L. G. *Inorganic Chemistry* **1991**, *30*, 228.

(13) Pullman, A.; Pullman, B.; Lavery, R. *Theochem* **1983**, *10*, 85.

(14) Abrescia, N. G. A.; Malinina, L.; Fernandez, L. G.; Huynh-Dinh, T.; Neidle, S.; Subirana, J. A. *Nucleic Acids Research* **1999**, *27*, 1593.

(15) Abrescia, N. G. A.; Tam, H.-D.; Subirana, J. A. *Journal of Biological Inorganic Chemistry* **2002**, *7*, 195.

(16) Labiuk, S. L.; Delbaere Louis, T. J.; Lee, J. S. *Journal of biological inorganic chemistry* **2003**, *8*, 715.

(17) Soler-Lopez, M.; Malinina, L.; Tereshko, V.; Zarytova, V.; Subirana, J. A. *JBIC, Journal of Biological Inorganic Chemistry* **2002**, *7*, 533.

(18) Kagawa, T. F.; Geierstanger, B. H.; Wang, A. H. J.; Ho, P. S. *Journal of Biological Chemistry* **1991**, *266*, 20175.

(19) Braun, E.; Eichen, Y.; Sivan, U.; Ben-Yoseph, G. *Nature* **1998**, *391*, 775.

(20) Jayaraman, S.; Tang, W.; Yongsunthon, R. *J. Electrochem. Soc.* **2011**, *158*, K123.

(21) Keren, K.; Krueger, M.; Gilad, R.; Ben-Yoseph, G.; Sivan, U.; Braun, E. *Science* **2002**, *297*, 72.

(22) Keren, K.; Berman, R. S.; Braun, E. *Nano Letters* **2004**, *4*, 323.

(23) Aich, P.; Labiuk, S. L.; Tari, L. W.; Delbaere, L. J. T.; Roesler, W. J.; Falk, K. J.; Steer, R. P.; Lee, J. S. *Journal of Molecular Biology* **1999**, *294*, 477.

(24) Wettig, S. D.; Li, C.-Z.; Long, Y.-T.; Kraatz, H.-B.; Lee, J. S. *Analytical Sciences* **2003**, *19*, 23.

(25) Wettig, S. D.; Wood, D. O.; Aich, P.; Lee, J. S. *Journal of Inorganic Biochemistry* **2005**, *99*, 2093.

(26) Wood, D. O.; Dinsmore, M. J.; Bare, G. A.; Lee, J. S. *Nucleic Acids Research* **2002**, *30*, 2244.

(27) Wood, D. O.; Lee, J. S. *Journal of Inorganic Biochemistry* **2005**, *99*, 566.

(28) Alexandre, S. S.; Murta, B. J.; Soler, J. M.; Zamora, F. *Phys. Rev. B: Condens. Matter Mater. Phys.* **2011**, *84*, 045413/1.

(29) Brancolini, G.; Di, F. R. *Journal of Chemical Physics* **2011**, *134*, 205102/1.

(30) Rubin, Y. V.; Belous, L. F.; Yakuba, A. A. *J. Mol. Model.* **2011**, *17*, 997.

(31) Tanaka, K.; Shionoya, M. *Journal of Organic Chemistry* **1999**, *64*, 5002.

(32) Cao, H.; Tanaka, K.; Shionoya, M. *Chemical & Pharmaceutical Bulletin* **2000**, *48*, 1745.

(33) Shionoya, M.; Tanaka, K. *Bulletin of the Chemical Society of Japan* **2000**, *73*, 1945.

(34) Tanaka, K.; Tasaka, M.; Cao, H.; Shionoya, M. *European Journal of Pharmaceutical Sciences* **2001**, *13*, 77.

(35) Tasaka, M.; Tanaka, K.; Shiro, M.; Shionoya, M. *Supramolecular Chemistry* **2001**, *13*, 671.

(36) Meggers, E.; Holland, P. L.; Tolman, W. B.; Romesberg, F. E.; Schultz, P. G. *Journal of the American Chemical Society* **2000**, *122*, 10714.

(37) Weizman, H.; Tor, Y. *Chemical Communications* **2001**, 453.

(38) Weizman, H.; Tor, Y. *Journal of the American Chemical Society* **2001**, *123*, 3375.

(39) Tanaka, K.; Tengeiji, A.; Kato, T.; Toyama, N.; Shiro, M.; Shionoya, M. *Journal of the American Chemical Society* **2002**, *124*, 12494.

(40) Tanaka, K.; Yamada, Y.; Shionoya, M. *Journal of the American Chemical Society* **2002**, *124*, 8802.

(41) Switzer, C.; Shin, D. *Chemical Communications* **2005**, 1342.

(42) Switzer, C.; Sinha, S.; Kim, P. H.; Heuberger, B. D. *Angewandte Chemie, International Edition* **2005**, *44*, 1529.

(43) Shin, D.; Switzer, C. *Chemical Communications* **2007**, 4401.

(44) Heuberger, B. D.; Shin, D.; Switzer, C. *Organic Letters* **2008**, *10*, 1091.

(45) Boehme, D.; Duepre, N.; Megger, D. A.; Müller, J. *Inorganic Chemistry* **2007**, *46*, 10114.

(46) Polonius, F.-A.; Müller, J. *Angewandte Chemie, International Edition* **2007**, *46*, 5602.

(47) Megger, D. A.; Müller, J. *Nucleosides, Nucleotides & Nucleic Acids* **2010**, *29*, 27.

(48) Megger, D. A.; Fonseca Guerra, C.; Bickelhaupt, F. M.; Müller, J. *Journal of Inorganic Biochemistry* **2011**, *105*, 1398.

(49) Megger, D. A.; Guerra, C. F.; Hoffmann, J.; Brutschy, B.; Bickelhaupt, F. M.; Müller, J. *Chemistry--A European Journal* **2011**, *17*, 6533.

(50) Clever, G. H.; Polborn, K.; Carell, T. *Angewandte Chemie, International Edition* **2005**, *44*, 7204.

(51) Clever, G. H.; Soeltl, Y.; Burks, H.; Spahl, W.; Carell, T. *Chemistry-A European Journal* **2006**, *12*, 8708.

(52) Tanaka, K.; Clever, G. H.; Takezawa, Y.; Yamada, Y.; Kaul, C.; Shionoya, M.; Carell, T. *Nature Nanotechnology* **2006**, *1*, 190.

(53) Clever, G. H.; Carell, T. *Angewandte Chemie, International Edition* **2007**, *46*, 250.

(54) Clever, G. H.; Kaul, C.; Carell, T. *Angewandte Chemie, International Edition* **2007**, *46*, 6226.

(55) Tanaka, K.; Clever, G. H.; Takezawa, Y.; Yamada, Y.; Kaul, C.; Shionoya, M.; Carell, T. *Nature Nanotechnology* **2007**, *2*, 63.

(56) Gaub, B. M.; Kaul, C.; Zimmermann, J. L.; Carell, T.; Gaub, H. E. *Nanotechnology* **2009**, *20*, 434002/1.

(57) Clever, G. H.; Reitmeier, S. J.; Carell, T.; Schiemann, O. *Angewandte Chemie, International Edition* **2010**, *49*, 4927.

(58) Kaul, C.; Mueller, M.; Wagner, M.; Schneider, S.; Carell, T. *Nature Chemistry* **2011**, *3*, 794.

(59) Popescu, D.-L.; Parolin, T. J.; Achim, C. *Journal of the American Chemical Society* **2003**, *125*, 6354.

(60) Watson, R. M.; Skorik, Y.; Patra, G. K.; Achim, C. *Journal of the American Chemical Society* **2005**, *127*, 14628.

(61) Franzini, R.; Watson, R. M.; Patra, G. K.; Achim, C. *Inorganic Chemistry* **2006**, *45*, 9798.

(62) Bezer, S.; Rapireddy, S.; Skorik, Y. A.; Ly, D. H.; Achim, C. *Inorganic Chemistry* **2011**, *50*, 11929.

(63) Ma, Z.; Olechnowicz, F.; Skorik, Y. A.; Achim, C. *Inorganic Chemistry* **2011**, *50*, 6083.

(64) Seubert, K.; Guerra, C. F.; Bickelhaupt, F. M.; Mueller, J. *Chem. Commun.* **2011**, *47*, 11041.

(65) Zhang, L.; Peritz, A.; Meggers, E. *Journal of the American Chemical Society* **2005**, *127*, 4174.

(66) Hansen, A. G.; Salvatore, P.; Karlsen, K. K.; Nichols, R. J.; Wengel, J.; Ulstrup, J. *Phys. Chem. Chem. Phys.* **2013**, *15*, 776.

(67) Karlsen, K. K.; Jensen, T. B.; Wengel, J. *Journal of Organic Chemistry* **2009**, *74*, 8838.

(68) Karlsen, K. K.; Wengel, J.; Jensen, T. B. *Abstracts of Papers, 239th ACS National Meeting, San Francisco, CA, United States, March 21-25, 2010* **2010**, ORGN.

(69) Babu, B. R.; Hrdlicka, P. J.; McKenzie, C. J.; Wengel, J. *Chemical Communications* **2005**, 1705.

(70) Kalek, M.; Madsen, A. S.; Wengel, J. *Journal of the American Chemical Society* **2007**, *129*, 9392.

(71) Kuklenyik, Z.; Marzilli, L. G. *Inorganic Chemistry* **1996**, *35*, 5654.

(72) Nielsen, P. E.; Egholm, M.; Berg, R. H.; Buchardt, O. *Science* **1991**, *254*, 1497.

(73) Beck, F. *Methods in Molecular Biology* **2002**, *208*, 29.

(74) Bahal, R.; Sahu, B.; Rapireddy, S.; Lee, C.-M.; Ly, D. H. *ChemBioChem* **2012**, *13*, 56.

(75) Corradini, R.; Sforza, S.; Tedeschi, T.; Totsingan, F.; Marchelli, R. *Current topics in medicinal chemistry* **2007**, *7*, 681.

(76) D'Costa, M.; Kumar, V.; Ganesh, K. *Organic Letters* **1999**, *1*, 1513.

(77) Dragulescu-Andrasi, A.; Rapireddy, S.; Frezza, B.; Gayathri, C.; Gil, R.; Ly, D. *Journal of the American Chemical Society* **2006**, *128*, 10258.

(78) Ganesh, K. N.; Nielsen, P. E. *Current Organic Chemistry* **2000**, *4*, 931.

(79) Govindaraju, T.; Kumar, V.; Ganesh, K. *The Journal of organic chemistry* **2004**, *69*, 1858.

(80) Govindaraju, T.; Kumar, V.; Ganesh, K. *The Journal of organic chemistry* **2004**, *69*, 5725.

(81) Govindaraju, T.; Kumar, V.; Ganesh, K. *Chemical communications* **2004**, 860.

(82) Govindaraju, T.; Kumar, V.; Ganesh, K. *Journal of the American Chemical Society* **2005**, *127*, 4144.

(83) Govindaraju, T.; Madhuri, V.; Kumar, V.; Ganesh, K. *The Journal of organic chemistry* **2006**, *71*, 14.

(84) Haaima, G.; Hansen, H.; Christensen, L.; Dahl, O.; Nielsen, P. *Nucleic Acids Research* **1997**, *25*, 4639.

(85) Kumar, R.; Singh, S. K.; Koshkin, A. A.; Rajwanshi, V. K.; Meldgaard, M.; Wengel, J. *Bioorganic & Medicinal Chemistry Letters* **1998**, *8*, 2219.

(86) Lagriffoule, P.; Eriksson, M.; Jensen, K. K.; Nielsen, P. E.; Wittung, P.; Nordén, B.; Buchardt, O. *Chemistry-A European Journal* **1997**, *3*, 912.

(87) Pokorski, J.; Witschi, M.; Purnell, B.; Appella, D. *Journal of the American Chemical Society* **2004**, *126*, 15067.

(88) Rapireddy, S.; He, G.; Roy, S.; Armitage, B. A.; Ly, D. H. *Journal of the American Chemical Society* **2007**, *129*, 15596.

(89) Diederichsen, U. *Angewandte Chemie, International Edition in English* **1996**, *35*, 445.

(90) Nielsen, P. E.; Editor *Peptide Nucleic Acids: Protocols and Applications, Second Edition*, 2004.

(91) Wolak, M. A.; Balaeff, A.; Gutmann, S.; Helmrich, H. J.; Vosloo, R.; Beerbom, M. M.; Wierzbinski, E.; Waldeck, D. H.; Bezer, S.; Achim, C.; Beratan, D. N.; Schlaf, R. *Journal of Physical Chemistry C* **2011**, *115*, 17123.

(92) Paul, A.; Watson, R. M.; Lund, P.; Xing, Y.; Burke, K.; He, Y.; Borguet, E.; Achim, C.; Waldeck, D. H. *Journal of Physical Chemistry C* **2008**, *112*, 7233.

(93) Wittung, P.; Eriksson, M.; Lyng, R.; Nielsen, P. E.; Norden, B. *Journal of the American Chemical Society* **1995**, *117*, 10167.

(94) Rasmussen, H.; Kastrup, J. S.; Nielsen, J. N.; Nielsen, J. M.; Nielsen, P. E. *Nature structural biology* **1997**, *4*, 98.

(95) Yeh, J. I.; Pohl, E.; Truan, D.; He, W.; Sheldrick, G. M.; Du, S.; Achim, C. *Chemistry-A European Journal* **2010**, *16*, 11867.

(96) Yeh Joanne, I.; Pohl, E.; Truan, D.; He, W.; Sheldrick George, M.; Du, S.; Achim, C. *Chemistry-A European Journal* **2011**, *17*, 12227.

(97) Sforza, S.; Tedeschi, T.; Corradini, R.; Marchelli, R. *European Journal of Organic Chemistry* **2007**, 5879.

(98) Sforza, S.; Haaima, G.; Marchelli, R.; Nielsen, P. E. *European Journal of Organic Chemistry* **1999**, 197.

(99) Pensato, S.; Saviano, M.; Bianchi, N.; Borgatti, M.; Fabbri, E.; Gambari, R.; Romanelli, A. *Bioorganic Chemistry* **2010**, *38*, 196.

(100) He, W.; Hatcher, E.; Balaeff, A.; Beratan, D. N.; Gil, R. R.; Madrid, M.; Achim, C. *Journal of the American Chemical Society* **2008**, *130*, 13264.

(101) Sosniak, A. M.; Gasser, G.; Metzler-Nolte, N. *Organic & Biomolecular Chemistry* **2009**, *7*, 4992.

(102) Kise, K. J., Jr.; Bowler, B. E. *Inorganic Chemistry* **2002**, *41*, 379.

(103) Nickita, N.; Gasser, G.; Bond, A. M.; Spiccia, L. *Eur. J. Inorg. Chem.* **2009**, 2179.

(104) Singh, S. K.; Nielsen, P.; Koshkin, A. A.; Wengel, J. *Chemical Communications* **1998**, 455.

(105) Obika, S.; Nanbu, D.; Hari, Y.; Andoh, J.-I.; Morio, K.-I.; Doi, T.; Imanishi, T. *Tetrahedron Letters* **1998**, *39*, 5401.

(106) Wengel, J.; Petersen, M.; Frieden, M.; Koch, T. *Letters in Peptide Science* **2004**, *10*, 237.

(107) Doessing, H.; Vester, B. *Molecules* **2011**, *16*, 4511.

(108) Nielsen, K. E.; Rasmussen, J.; Kumar, R.; Wengel, J.; Jacobsen, J. P.; Petersen, M. *Bioconjugate Chemistry* **2004**, *15*, 449.

(109) Nielsen, P.; Dreioe, L. H.; Wengel, J. *Bioorg Med Chem* **1995**, *3*, 19.

(110) Langkjaer, N.; Pasternak, A.; Wengel, J. *Bioorganic & Medicinal Chemistry* **2009**, *17*, 5420.

(111) Meggers, E.; Zhang, L. *Accounts of Chemical Research* **2010**, *43*, 1092.

(112) Zhang, L.; Meggers, E. *Journal of the American Chemical Society* **2005**, *127*, 74.

(113) Schlegel, M. K.; Essen, L.-O.; Meggers, E. *Chem. Commun.* **2010**, *46*, 1094.

(114) Johnson, A. T.; Schlegel, M. K.; Meggers, E.; Essen, L.-O.; Wiest, O. *Journal of Organic Chemistry* **2011**, *76*, 7964.

(115) Katz, S. *Biochim. Biophys. Acta, Spec. Sect. Nucleic Acids Relat. Subj.* **1963**, *68*, 240.

(116) Miyake, Y.; Togashi, H.; Tashiro, M.; Yamaguchi, H.; Oda, S.; Kudo, M.; Tanaka, Y.; Kondo, Y.; Sawa, R.; Fujimoto, T.; Machinami, T.; Ono, A. *J. Am. Chem. Soc.* **2006**, *128*, 2172.

(117) Weizman, H.; Tor, Y. *J. Am. Chem. Soc.* **2001**, *123*, 3375.

(118) Tanaka, K.; Shionoya, M. *J. Org. Chem.* **1999**, *64*, 5002.

(119) Zimmermann, N.; Meggers, E.; Schultz, P. G. *J. Am. Chem. Soc.* **2002**, *124*, 13684.

(120) Atwell, S.; Meggers, E.; Spraggon, G.; Schultz, P. G. *Journal of the American Chemical Society* **2001**, *123*, 12364.

(121) Popescu, D.-L.; Parolin, T. J.; Achim, C. *J. Am. Chem. Soc.* **2003**, *125*, 6354.

(122) Hirva, P.; Nielsen, A.; Bond, A. D.; McKenzie, C. J. *Journal of Physical Chemistry B* **2010**, *114*, 11942.

(123) Schlegel, M. K.; Essen, L.-O.; Meggers, E. *Journal of the American Chemical Society* **2008**, *130*, 8158.

(124) DeLeon, A.; Kong, J.; Achim, C. In *Metallofoldamers: Supramolecular Architectures from Helicates to Biomimetics*; Maayan, G., Albrecht, M., Eds.; Wiley-VCH: Weinheim, 2012.

(125) Henry, A. A.; Romesberg, F. E. *Current Opinion in Chemical Biology* **2003**, *7*, 727.

(126) Kool, E. T. *Accounts of Chemical Research* **2002**, *35*, 936.

(127) Park, K. S.; Jung, C.; Park, H. G. *Angewandte Chemie, International Edition* **2010**, *49*, 9757.

(128) Urata, H.; Yamaguchi, E.; Funai, T.; Matsumura, Y.; Wada, S.-i. *Angewandte Chemie, International Edition* **2010**, *49*, 6516.

(129) Brotschi, C.; Leumann, C. J. *Nucleosides, Nucleotides & Nucleic Acids* **2003**, *22*, 1195.

(130) Watson, R. M.; Skorik, Y. A.; Patra, G. K.; Achim, C. *J. Am. Chem. Soc.* **2005**, *127*, 14628.

(131) Franzini, R. M.; Watson, R. M.; Patra, G. K.; Breece, R. M.; Tierney, D. L.; Hendrich, M. P.; Achim, C. *Inorg. Chem.* **2006**, *45*, 9798.

(132) Bezer, S.; Rapireddy, S.; Skorik, Y. A.; Ly, D. H.; Achim, C. *Inorg. Chem.*, *50*, 11929.

(133) Yan, H. *Science* **2004**, *306*, 2048.

(134) Krishnan, Y.; Simmel, F. C. *Angew. Chem., Int. Ed.* **2011**, *50*, 3124.

(135) Bhatia, D.; Sharma, S.; Krishnan, Y. *Curr. Opin. Biotechnol.* **2011**, *22*, 475.

(136) Dietz, H.; Douglas, S. M.; Shih, W. M. *Science* **2009**, *325*, 725.

(137) Rothemund, P. W. K. *Nature* **2006**, *440*, 297.

CHAPTER II. Molecular Switch Based on PNA

II.1 Introduction

The growing interest in nanotechnology is stimulating research on molecular assemblies that can act as wires, sensors, diodes, logic gates, memory, switches, and motors.[1-6] Among these molecular assemblies, molecular switch as the control unit of the molecular assemblies receives extensive studies. Nucleic acids have emerged as a new material for molecular assemblies in recent decades because of their predictable and programmable hybridization encoded in the Watson-Crick base pairing and precise control of positioning decorations on up to three dimensional architectures at the nanoscale.[7-11] Furthermore, the well-developed synthetic protocols for nucleic acids and their derivatives provide ready access to nucleic acids of desired sequences and modifications in adequate quantity. Therefore, beyond a carrier for genetic information, nucleic acid is considered a novel substance for the development of nanotechnology.[12] Among several artificial nucleic acids, PNA caught great attention due to the enhanced stabilization effect on the formed duplex and triplex induced by the pseudopeptide backbone composed of N-(2-aminoethyl)-glycine units.[13] Instead of the negatively charged phosphate-deoxyribose backbone of deoxyribonucleic acid (DNA), the neutral backbone of PNA makes the complementary binding between PNA and DNA stronger than between DNA and DNA.[14] Furthermore, PNAs are not recognized by nucleases and proteases, and thus are resistant to digestion and degradation in a biological environment.[15,16] In addition, using ligand-modified monomers as building blocks, the

solid phase peptide synthesis significantly simplifies the organic synthesis for diverse designs of molecular assemblies.[17,18] These properties of PNA make it a good candidate for both biological and nanotechnological applications.

DNA is one of the most delicate molecules from nature with complex structures, functions and operations to perform its biological role. On the other hand, the artificial nucleic acids mimicking the operation of DNA typically undergo structural or conformational changes caused by duplex formation or dissociation, which are triggered by the addition of fuse strands with the complementary sequence to the targeting sequence.[19,20] The introduction of metal ions in nucleic acids adds another dimension of operation to the molecular assemblies with additional electronic, magnetic, photoelectric or catalytic properties synergetically determined by the components.[21-26]

The earliest attempt to incorporate metal ions in nucleic acids was realized by coordinating metal ions such as Hg^{2+} and Ag^{+} with natural bases.[27,28] However, the involvement of natural bases in both Watson-Crick hydrogen bond and metal-ligand coordination creates ambiguity in the rules of complementarity for duplex formation. The synthesis of novel nucleosides orthogonal to natural bases for alternative base pairing through metal complexation was first introduced by Tanaka and Shionoya, where a phenylenediamine-containing nucleoside was synthesized and characterized to form a 2:1 ligand:metal complex with Pd^{2+}.[29] This study led to the site-specific incorporation of transition metal by introducing different types of ligand-modified nucleosides into DNA duplexes.[30-35] The same strategy was then applied to incorporate metal ions in other synthetic nucleic acids, including PNA, LNA and GNA.[36-39] The formed metal-ligand

complexes act as alternative base pairs, stacking with the adjacent natural base pairs by the aromatic ring in the ligands. The fitting of the artificial metal-ligand base pairs into the surrounding natural ones is determined by the size, shape, charge and geometry of the metal-ligand complexes. Linear (Hg^{2+} and Ag^{+}) or square planar (Cu^{2+}, Ni^{2+} and Co^{2+}) coordination geometries offer the corresponding complexes better π-stacking and less distortion to the adjacent natural base pairs, imparting the modified nucleic acid duplex with improved stability.[25] The charge of the metal-ligand complex matters when the complex is placed in the hydrophobic interior of the nucleic acids and when several metal-ligand complexes are adjacent or close to each other creating electrostatic repulsion in between.[40,41]

Previous work in our group has demonstrated the ability to incorporate six different ligands into PNA duplexes, 8-hydroxyquinoline, pyridine, 2,2'-bipyridine, 5'-methyl-2,2'-bipyridine, terpyridine and tetrazole, which introduce metal ions such as Cu^{2+}, Ni^{2+} and Co^{2+} into PNA duplexes.[36,42-45] The coexistence of different types of ligands in the same PNA duplex creates the opportunity to incorporate different metal ions at predefined locations within the PNA duplex, which leads to the formation of metal array with specific sequence determined by the sequence of the ligand-modified PNA duplex. The concept to manipulating metal ions by arranging the ligands in nucleic acid facilitates the design of molecular assemblies such as nanowires, sensors, and circuits with DNA origami as template and metal-containing ligand-modified PNA as surface decorations.

As one of the most important components of molecular assemblies, molecular switches play the role of the control unit, which is in charge of turning on and off a certain function of the molecular assembly. Created from metal and nucleic acid, the bioinorganic hybrid structure takes advantages of both metal ions with alterable oxidation states, electronic and magnetic properties, and nucleic acids as a scaffold with programmable architecture.[46,47] The preferential coordination of metal ions to different ligands can be adjusted by factors such as pH, solvent, oxidation state, and coordination geometry of the ligands.

The selection of ligands is a crucial factor for a successful design of the molecular switch. Zelikovich et al. first reported a redox triggered molecular switch based on triple-stranded helical complexes, wherein an iron ion translocated between two different ligand cavities.[48] One ligand cavity was a hydroxamate moiety, which was a hard base with a preference of the hard acid, ferric ion. The other ligand cavity was a bipyridyl moiety, which was a soft base with the preference of the soft acid, ferrous ion. Chemical reduction of the ferric ion triggered the metal migration from hydroxamate to bipyridyl cavity, and vice versa. Kalny et al. further developed the molecular switch and synthesized a double-stranded ditopic ligand, which was composed of 8-hydroxyquinoline and bipyridyl moieties.[49] In response to auxiliary redox reactions, a copper ion translocated between these two ligand sites. The driving force of the molecular switch was the preference of hard acid to hard base and of soft acid to soft base. Later Petitjean et al. also used these two ligands to assemble a [2×2] grid structure and a molecular switch with the assistance of metal ions Zn^{2+} and Cu^{+}.[50,51] These results have shown that 8-hydroxyquinoline and 2,2-bipyridine are good ligands for the design

of a molecular switch. Both ligands are versatile ligands in coordination chemistry that they have diverse varieties of derivatives for supramolecular assemblies.[52,53] They were frequently used and have shown robust redox stability and easy functionalization, which are crucial properties for building molecular switches triggered by redox reactions.

The "hard" ligand 8-hydroxyquinoline (**Q**) coordinates metal ion as a bidentate monoanion N,O-donor chelate.[54,55] Zhang et al. and Watson et al. first investigated the introduction of ligand **Q** and Cu^{2+} as an alternative metal-ligand base pair in DNA and PNA, respectively.[42,56] UV titrations indicated that a 1:2 metal:ligand complex was formed within the duplex as [**Q**-Cu-**Q**]. The melting temperature of the ligand modified nucleic acid duplex increased significantly by 29 °C and 33 °C for DNA and PNA, respectively, when one eq. Cu^{2+} was added to the duplex. Ma et al. have studied the effect of complex [**Q**-Cu-**Q**] on the thermal stability of PNA duplexes quantitively by calorimetric studies.[43] They found out that the linkers between the ligand and the backbone have an effect on the stability constants of the formed complexes. Consequently, the complex with a larger stability constant rendered the PNA duplex a higher stability.

The "soft" ligand 2,2'-bipyridine (**B**) is a neutral bidentate N-donor ligand with flexible chelating size due to the rotational single bond between the two aromatic rings.[57] Weizman and Tor first used the ligand to replace natural bases to mimic DNA nucleoside.[31,58] UV titrations with Cu^{+} or Cu^{2+} indicated the formation of a 1:2 metal:ligand complex [**B**-Cu-**B**]$^{+}$ or [**B**-Cu-**B**]$^{2+}$ within the DNA duplex, respectively. Frazini el al. also investigated the interaction between Cu^{2+} and ligand **B** in PNA duplex

by UV titration, EPR spectroscopy and thermal denature experiment.[44] They found that the formed complex [**B**-Cu-**B**]$^{2+}$ bestowed a higher thermal stability than the PNA duplex by 10 °C. They have also incorporated multiple ligands **B** in PNA duplex since the neutral feature of B does not produce electrostatic repulsion when situated adjacently.

These preliminary results proved that both ligand **Q** and **B** modified PNAs coordinate well with Cu^{2+} to form PNA duplex with alternative base pair and enhanced thermal stability. In addition, ligand **B** modified PNA coordinates well with Cu^{+}. With the reduction potential E^*_f being -375 mV and +120 mV for [**Q**-Cu-**Q**] and [**B**-Cu-**B**]$^{2+}$, respectively, the redox-active copper complexes are suitable for the design of a redox triggered molecular switch.[59] Moreover, copper is involved in critical cellular processes such as oxygen transfer, catalytic cofactor for enzymes, iron intake, blood clotting and many others, which is the driving force for the extensive study of copper metabolism.[60,61]

Here we report the synthesis of a molecular switch based on 2,2'-bipyridine- and 8-hydroxyquinoline-modified PNA duplexes, in which a copper ion preferentially binds to one of two distinct ligand-sites depending on the oxidation state of the copper ion (Scheme II-1). Taking advantage of the significant difference in the stability constants of the complexes of Cu^{+} and Cu^{2+} with the "soft" ligand **B** and the "hard" ligand **Q**, we constructed this PNA-based system in which a copper ion behaves like a shuttle between two ligand stations in response to a change in the oxidation state. The significant difference in the stability constants of the complexes formed between the copper ion and the different ligands insures the mechanism of the molecular switch (Table II-1).[43,59,62] The significant increase of the stability constants of the complex formed by the PNA

based ligand over the free ligand is a chelating effect endorsed by the PNA duplex. Chemical redox reaction of the copper ion triggers the translocation of the copper ion from one ligand cavity to the other. The translocation process was monitored quantitatively by UV spectroscopy thanks to the distinct spectral features of the copper complexes with the two ligands **Q** and **B**. CD spectroscopy and melting curve analysis also showed supporting evidences of the switch behavior of the copper ion. The results of this chapter show that it is possible to construct molecular switches with PNA building blocks made of ligand-modified PNA monomers.

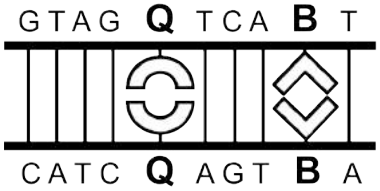

*Scheme II-1. Cartoon Representation of a Molecular Switch Based on Ligand-Modified PNA Duplex (ligands **Q** and **B** are represented by half circle and open triangles shapes)*

Table II-1. Stability Constants of Different Complexes[43,59,62]

Ligand	$\log\beta_1$	$\log\beta_2$
Q	14.7	25.4
Q-PNA		29.0
B	8.15	13.65
B-PNA		19.7

II.2 Results

II.2.i PNA sequences

The first well investigated PNA duplex N_α:N_β (Chart II-1a) since the discovery of PNA was modified with two different ligands **Q** and **B** at the middle and the end of the 10-mer PNA sequence N_α and N_β.[63,64] In other words, the complementary base pairs A:T in the middle of the duplex and the C:G at the end of the duplex were replaced by a pair of ligands **Q**:**Q** and **B**:**B**, respectively (Chart II-1b). To study the metal binding to each ligand site exclusively without the interference of the other ligand site, corresponding ligand modified PNAs were also synthesized. In this case, either the base pair A:T in the middle of the duplex was replaced by a pair of ligands **Q**:**Q** (Chart II-1c), or the base pair C:G at the end of the duplex was replaced by a pair of ligands **B**:**B** (Chart II-1d).

Chart II-1. PNA Sequences and Duplexes

	1 2 3 4 5 6 7 8 9 10	
dsN	H-GTAG**A**TCA**C**T-Lys-NH_2 H_2N-Lys-CATC**T**AGT**G**A-H	(a)
dsQ^5B^9	H-GTAG**Q**TCA**B**T-Lys-NH_2 H_2N-Lys-CATC**Q**AGT**B**A-H	(b)
dsQ^5	H-GTAG**Q**TCA**C**T-Lys-NH_2 H_2N-Lys-CATC**Q**AGT**G**A-H	(c)
dsB^9	H-GTAG**A**TCA**B**T-Lys-NH_2 H_2N-Lys-CATC**T**AGT**B**A-H	(d)

II.2.ii Melting Curves by UV-Vis Spectroscopy

In the absence of metal ions, substitution of natural base pairs with ligands that cannot form hydrogen bonds leads to destabilization of the nucleic acid duplexes.[25] Addition of metal ions causes formation of metal-ligand coordination bonds and partly or completely restores the thermal stability of nucleic acid duplexes, depending on the interactions of the metal complex with the adjacent base pairs. Variable-temperature UV-Vis spectroscopy was used to evaluate the stability of the metal-containing, ligand-modified PNA duplexes by measuring the melting temperature T_m of the duplexes, which is derived from the melting curve.

Melting curves of dsPNA had typical sigmoidal shape, indicating a cooperative transition between ss and dsPNA. Melting curves of ds$\mathbf{Q}^5\mathbf{B}^9$ also showed sigmoidal shape, but not as steep as of ds$\mathbf{Q}^5$ and ds$\mathbf{B}^9$,[42,44] suggesting lower cooperativity in the denaturation (Figure II-1a). In the absence of copper ion, the melting temperature for ds$\mathbf{Q}^5\mathbf{B}^9$ was 28 ˚C, which was 38 ˚C lower than the non-modified dsN (Table II-2). Compared with single-ligand pair modified dsPNA, the T_m of ds$\mathbf{Q}^5\mathbf{B}^9$ was 17 ˚C lower than that of ds$\mathbf{Q}^5$ and 36 ˚C lower than that of dsB^9. The larger decrease in T_m of ds$\mathbf{Q}^5\mathbf{B}^9$ from ds$\mathbf{B}^9$ than from ds$\mathbf{Q}^5$ was due to the different position of ligand substitution in PNA duplex. The first eq. of Cu^{2+} recovered the T_m of ds$\mathbf{Q}^5\mathbf{B}^9$ back to 42 ˚C, and the second eq. of Cu^{2+} further restored the T_m to 48 ˚C. From the titration result of ds$\mathbf{Q}^5\mathbf{B}^9$ by Cu^{2+}, it was indicated that the first eq. of Cu^{2+} bond to the ligand **Q** site and the second eq. of Cu^{2+} bond to the ligand **B** site. Therefore, the recovery of first eq. of Cu^{2+} in T_m by 14 ˚C was gained by the formation of complex [**Q**-Cu-**Q**]. Consequently, the increase of T_m by

6 ˚C was due to the formation of complex [**B**-Cu-**B**]$^{2+}$. This inference is in agreement with preliminary results on the thermal stability study.[42,44]

The coordination impact of Cu^{+} on the thermal stability of ds$\mathbf{Q}^{5}\mathbf{B}^{9}$ was not as significant as of Cu^{2+}. The T_m of ds$\mathbf{Q}^{5}\mathbf{B}^{9}$ in presence of one eq. of Cu^{+} is 31 ˚C, which was only 3 ˚C higher than the T_m of ds$\mathbf{Q}^{5}\mathbf{B}^{9}$ (Figure II-1b). The slight increase was induced by the complex formation of [**B**-Cu-**B**]$^{+}$ since the first eq. of Cu^{+} bond to the ligand **B** site according to the UV titration. In contrast with the large increase in T_m of ds$\mathbf{Q}^{5}\mathbf{B}^{9}$ in presence of one eq. of Cu^{2+}, the small increase induced by one eq. of Cu^{+} demonstrated the different nature of the metal ion. The second eq. of Cu^{+} did not change the T_m of ds$\mathbf{Q}^{5}\mathbf{B}^{9}$, indicating that the second eq. of Cu^{+} may not bind with ds$\mathbf{Q}^{5}\mathbf{B}^{9}$ and thus, it does not enhance the stability of the duplex.

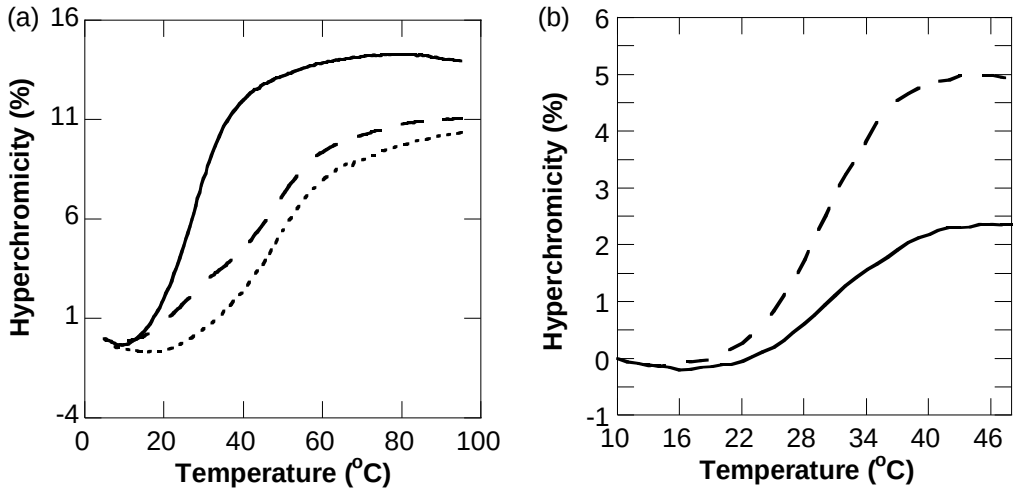

Figure II-1. Denaturation profiles measured at 260 nm for 5 µM solutions of ds$\mathbf{Q}^{5}\mathbf{B}^{9}$ in the absence (solid line) and presence of 5 µM (long dashed line) or 10 µM (dotted line) CuCl2 (a) or CuCl (b) in pH 7.7 10 mM Tris buffer in acetonitrile/water (1/3, v/v) solvent.

Table II-2.Melting Temperatures T_m (˚C) in the Absence of and Presence of $Cu^{2+/+}$

dsPNA	non	Cu^{2+}		Cu^{+}		Ref.
		1 eq.	2 eq.	1 eq.	2 eq.	
dsN	67	67	-	-	-	[36]
dsQ^5	46	>79	-	-	-	[42]
dsB^9	65	75	-	58	58	[44]
dsQ^5B^9	28	42	48	31	31	-

II.2.iii CD Spectroscopy

CD spectroscopy was exploited to study the secondary structure of the ligand-modified PNA duplexes and to identify their conformational change upon metal binding to different ligand sites within the PNA duplexes. Unlike DNA, the handedness of PNA is determined by the handedness of the chiral centers introduced in PNA such as an amino acid attached to the C-terminus, which is l-lysine in this case.[65] Therefore, a left handed helical structure is expected for the CD spectra in this study. Since the handedness is propagated through the π-π stacking between adjacent base pairs, ligand substitutions of natural base pairs may disrupt the transmission of the chiral induction effect of l-lysine. The addition of metal ion can further impact the handedness and helicity of the PNA duplexes depending on the geometry of the complex formed between the metal and the ligands.

The positive peak in a CD spectrum represents the right-handedness, while the negative peak represents the left-handedness. In the absence of metal ion, the CD spectra of all ligand-modified PNA duplexes used in this study have shown the left-handedness with a predominant negative peak at 256 nm (Figure II-2a), which is similar to that of the

non-modified PNA duplex.[65] The single-ligand modified PNA ds**B**^{9} and ds**Q**^{5} exhibited more intense CD spectra than the double-ligand modified PNA ds**Q**^{5}**B**^{9} since the π-π stacking in single-ligand modified PNA is less interrupted than the double-ligand modified PNA. Yet the CD spectrum of ds**B**^{9} was stronger than that of ds**Q**^{5}, suggesting the position or the nature of the ligand modification has influence on the helicity and handedness of the PNA duplex.

In the presence of one eq. of Cu^{2+}, ligand **Q** modified PNA duplex had a significant increase in the intensity of the peak at 256 nm, indicating that [**Q**-Cu-**Q**] is sufficient medium for π-π stacking and chirality transmission (Figure II-2a). On the other hand, the ligand **B** modified PNA duplex ds**B**^{9} did not show much change in handedness upon the addition of either Cu^{2+} or Cu^{+} (Figure II-2b and c), indicating that either the formed complexes [**B**-Cu-**B**]$^{2+/+}$ are poor media for π-stacking or the base pairs at the end of the duplex do not play an important role in the chirality. Considering the square planar structure of complex [**Q**-Cu-**Q**] and the tetrahedral structure of complex [**B**-Cu-**B**]$^{2+/+}$,[42,44,50] the observation in CD spectra is in agreement with the geometry of the complex formed.

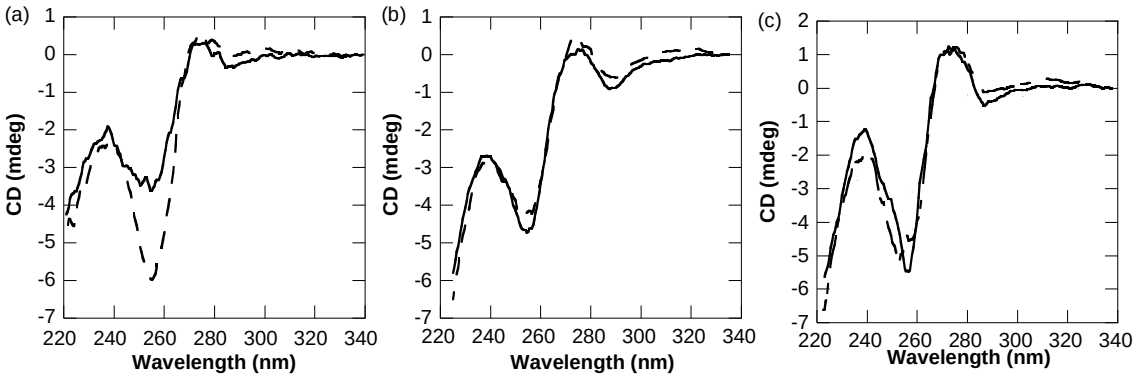

*Figure II-2. CD spectra of 10 μM ds**Q**^{5} (a) or ds**B**^{9} (b and c) in the absence (solid line) and in the presence (dashed line) of 10 μM Cu^{2+} (a and b) or Cu^{+} (c) at 20 °C in pH 7.7 10 mM Tris buffer in acetonitrile/water (1/3, v/v).*

The CD spectra of ds**Q**^{5}**B**^{9} showed a similar result upon the addition of Cu^{2+} to that of ds**Q**^{5} and ds**B**^{9} (Figure II-3b). The first eq. of Cu^{2+} greatly increased the CD intensity at 256 nm by coordinating with the ligand Q site to form the square planar complex [**Q**-Cu-**Q**], while the second eq. of Cu^{2+} slightly increased the CD intensity at 256 nm since the formed complex [**B**-Cu-**B**]$^{2+}$ is tetrahedral with poor π-stacking effect with the adjacent base pairs. In the case of Cu^{+}, the CD spectra of ds**Q**^{5}**B**^{9} barely changed upon addition of one or two eq. of Cu^{+} (Figure II-3c). Again, this observation demonstrated that the first eq. of Cu^{+} binds with ligand B site and no further binding event happens for the second eq. of Cu^{+}, which is in agreement with the UV titration result of ds**Q**^{5}**B**^{9} by Cu^{+}.

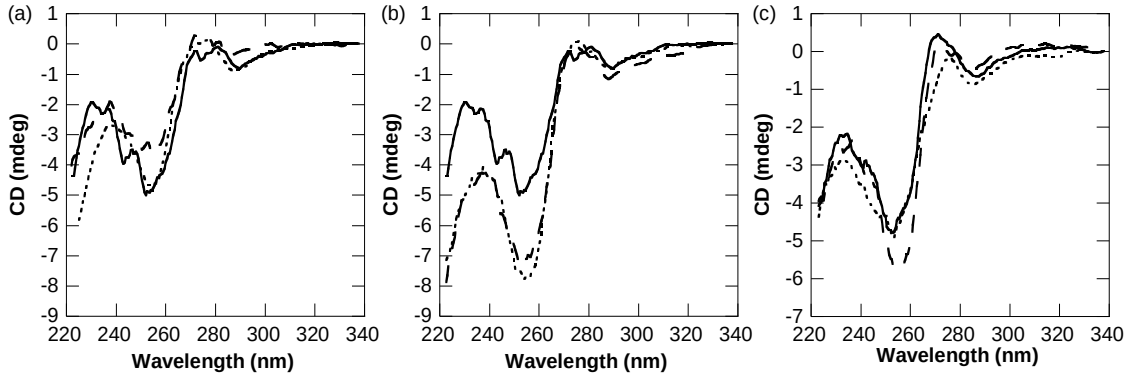

*Figure II-3. CD spectra of 10 μM ds**Q**^{5}**B**^{9} (solid line), ds**Q**^{5} (dashed line) and ds**B**^{9} (dotted line) in the absence (a) and in the presence of 10 μM (dashed line) and 20 μM (dotted line) of (b) $CuCl_2$ and (c) CuCl at 20 °C in pH 7.7 10 mM Tris buffer in acetonitrile/water (1/3, v/v).*

II.2.iv UV-Vis Spectroscopy Titrations

In order to monitor the copper translocation between the two distinct ligand sites by UV-Vis spectra, single-ligand modified PNA duplexes ds**Q**^{5} and ds**B**^{9} and their complexes with copper ion were first investigated by UV-Vis titrations in 10 mM pH 7.7 Tris buffer at room temperature. Different ligand modified PNA duplexes showed a distinguishable bathochromic shift upon addition of copper.

II.1.i.a Cu^{2+} Titrations

Ligand **Q** modified PNA ds**Q**^{5} has two major absorption bands at 247 and 260 nm, characteristic to the π-π* transition of ligand **Q** and the nucleobases, respectively (Figure II-4a).[42] Upon addition of 1 eq. of Cu^{2+}, the band at 247 nm was shifted to 260 nm due to the binding of Cu^{2+} to ligand **Q**. One isosbestic point was observed at 252 nm. Titration curve of ds**Q**^{5} showed an inflection point of Cu^{2+}/ds**Q**^{5} at around 1 (Figure II-4b),

indicating the formation of a 1:2 metal:ligand complex [**Q**-Cu-**Q**] (Scheme II-2a). Ligand **B** modified PNA ds**B**[9] showed one major band at 260 nm (Figure II-4c).[31,44] The intensity of the band at 260 nm slightly increased upon the addition of Cu^{2+}, indicating the slightly enhanced π-stacking induced by the binding of Cu^{2+} with ligand **B**. Additionally, the shoulder at 280 nm representing the π-π* transition of ligand **B** was shifted to 300-320 nm, which was the predominant change of ds**B**[9] upon copper addition. Two isosbestic points were observed at 264 and 297 nm. Titration curves of ds**B**[9] by Cu^{2+} showed an inflection point of Cu/dsPNA at 1 (Figure II-4d), demonstrating the formation of 1:2 metal:ligand complex [**B**-Cu-**B**] within the PNA duplex (Scheme II-2b).

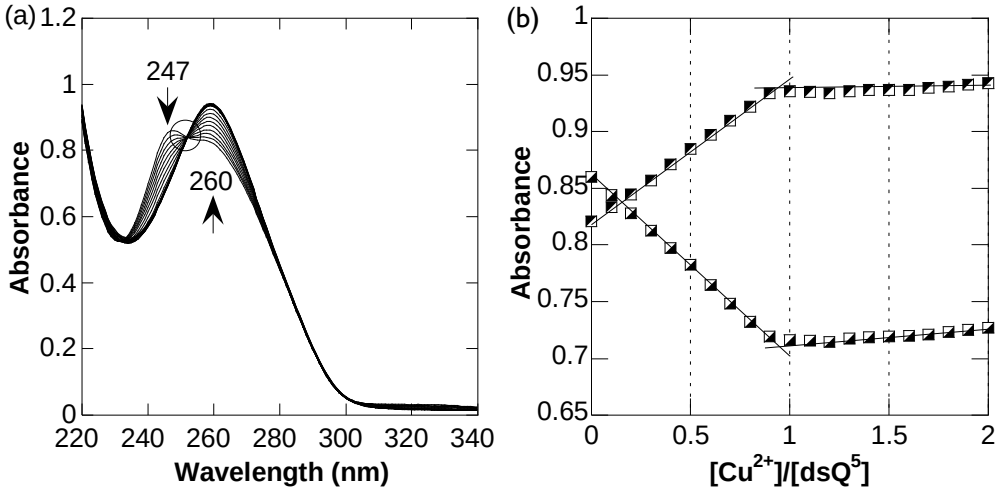

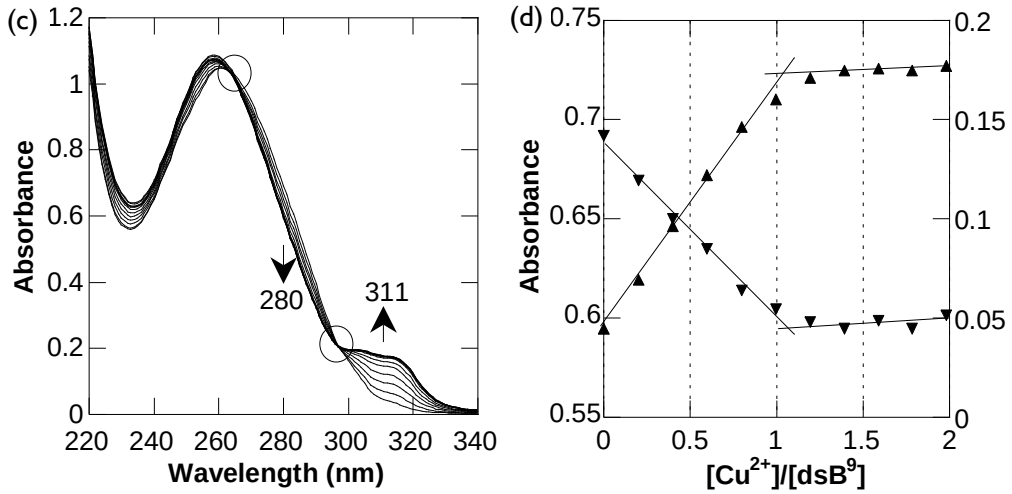

*Figure II-4. UV spectra of titration of 5 μM solution of ds**Q**[5] (a) and ds**B**[9] (c) with a 0.5 mM $CuCl_2$ solution, and titration curves of dsQ[5] (b) and dsB[9] (d) at 247 nm (◪), 260 nm (◩), 280 nm (▼) or 311 nm (▲) in pH = 7.7 10 mM Tris buffer in acetonitrile/water solvent (1/3, v/v).*

*Scheme II-2. Complexes from between Cu and (a) **Q**- or (b) **B**-Modified PNA.*

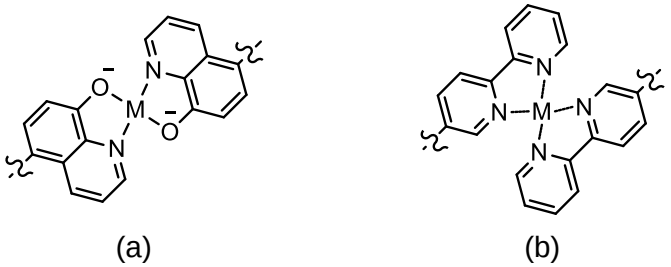

Based on the UV-Vis titrations of Cu^{2+}, we determined the specific, "diagnostic" wavelengths that can be used to monitor Cu^{2+} coordination with different ligand sites: 1) changes at 247 or 260 nm represent the binding of Cu^{2+} to ligand **Q** site; 2) changes at 280 or 311 nm indicate the binding of copper to ligand **B** site. Thereafter, the titrations of

ds**Q**^{5}**B**^{9} by Cu^{2+} were conducted to evaluate the relative affinity of ligand **Q** and ligand **B** sites for Cu^{2+}. Titration spectra closely resembled the spectroscopic features of both ds**Q**^{5} and ds**B**^{9}, meaning the decrease at 247 and 280 nm, and the increase at 260 and 311 nm (Figure II-5a). The curves have shown that Cu^{2+} binds to ligand **Q** with a higher affinity than ligand **B** (Figure II-5b), which can be also predicted with the binding constants from preliminary results (Table II-1). Upon addition of Cu^{2+}, the first changes in absorbance were observed at 247 and 260 nm, which are the diagnostic bands for the formation of [**Q**-Cu-**Q**] (Figure II-4a). Meanwhile, the absorbance at 280 and 311 nm remained constant, which means that Cu^{2+} did not bind at the ligand **B** site. The first isosbestic point was observed at 252 nm, which is also found in the titration of ds**Q**^{5}. The addition of more than one eq. of Cu^{2+} caused bathochromic shift from 280 nm to 311 nm, but did not produce further changes at 247 and 260 nm. These observations imply that the second eq. of Cu^{2+} binds to ligand **B** exclusively, in which the changes of the spectra strictly resembled the titration of ds**B**^{9}. The second set of isosbestic points were observed at 264 and 297 nm, similar as the ones seen in the titration of ds**B**^{9} (Figure II-4c). After the second eq. of Cu^{2+} bound at ligand **B**, the absorbance at 247, 260, 280 and 311 nm remained unchanged up to the third eq. of Cu^{2+} (Figure II-5b).

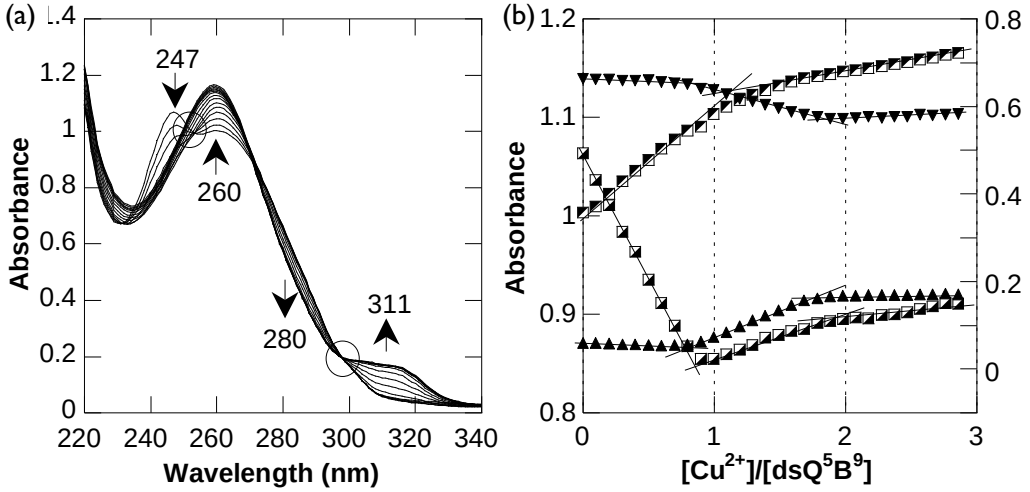

*Figure II-5. (a) UV spectra of titration of 5 μM solution of ds**Q**^{5}**B**^{9} with a 0.5 mM $CuCl_2$ solution, and (b) titration curves at 247 nm (◪), 260 nm (◩), 280 nm (▼) or 311 nm (▲) in pH = 7.7 10 mM Tris buffer in acetonitrile/water solvent (1/3, v/v).*

II.1.i.b Cu^+ Titrations

The titration spectra of ds**Q**^{5} by Cu^+ showed no change before and after the addition of metal ion, which demonstrated that Cu^+ does not bind to ds**Q**^{5} in pH 7.7 Tris buffer (Figure II-6a and b). In the case of dsB^9, although the bands of the bathochromic shifts of dsB^9 titrations for Cu^+ were identical to Cu^{2+}, the magnitude of changes in absorbance was obviously different (Figure II-6c). The absorbance change of Cu^{2+} was larger than that of Cu^+, indicating the difference in the local structure of the complexes formed. Similar with the titration of ds**B**^{9}, the intensity of the 260 nm band slightly increased as Cu^+ was added to the solution. The bathochromic shift from 280 to 300-320 nm indicated the coordination between Cu^+ and ligand **B**, which was also observed in the titration of ds**B**^{9} by Cu^{2+}. Two isosbestic points at 264 and 297 nm were observed. An inflection point of Cu:dsPNA at 1:1 was shown in the titration curves of ds**B**^{9} by Cu^+ (Figure II-6d),

demonstrating the formation of 1:2 metal:ligand complex [**B**-Cu-**B**] within the PNA duplex (Scheme II-2b).

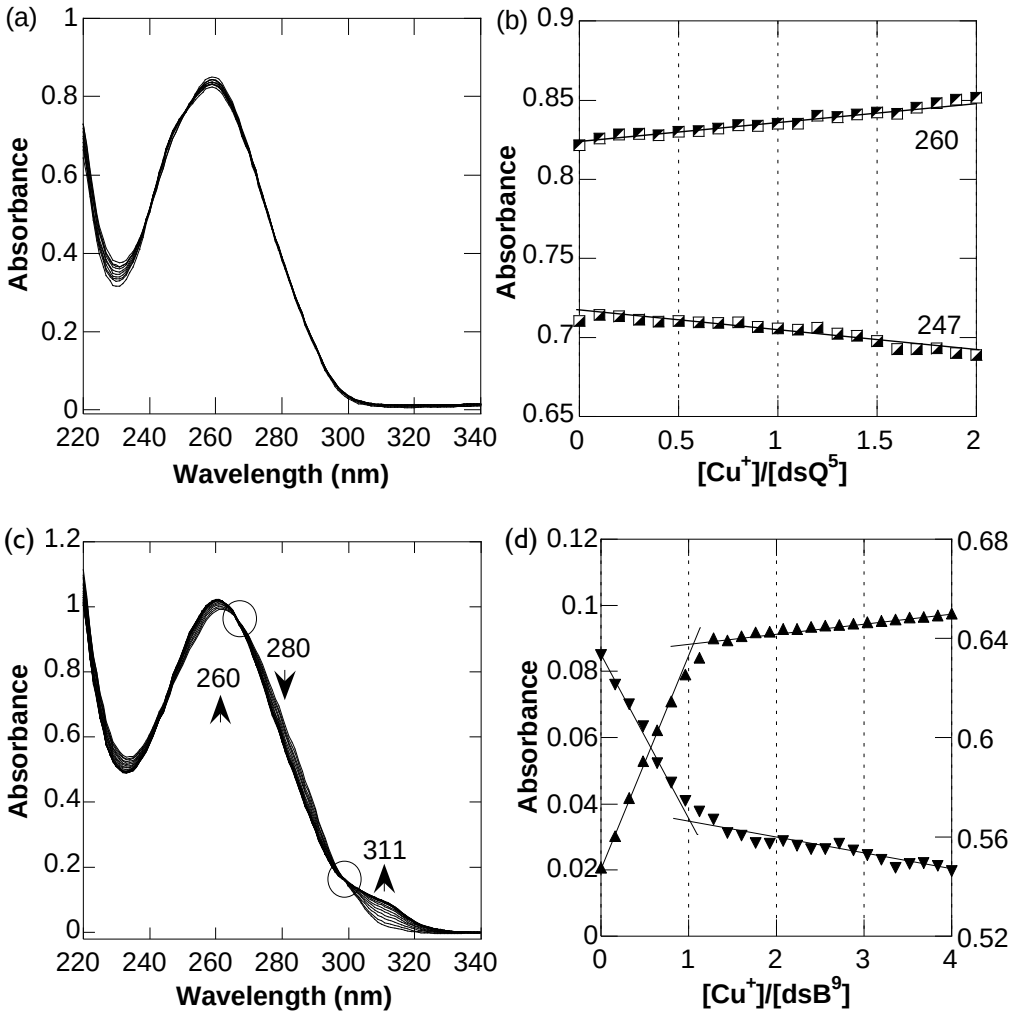

*Figure II-6. UV spectra of titration of 5 μM solution of ds**Q**^{5} (a) and ds**B**^{9} (c) with a 0.5 mM CuCl solution, and titration curves ds**Q**^{5} (b) and ds**B**^{9} (d) at 247 nm (◪), 260 nm (◩), 280 nm (▼) or 311 nm (▲) in pH = 7.7 10 mM Tris buffer in acetonitrile/water solvent (1/3, v/v).*

The titration of ds$\mathbf{Q}^5\mathbf{B}^9$ by Cu^+ was very different from that by Cu^{2+}, with only one binding event observed at ligand **B** site (Figure II-7a). The addition of one eq. of Cu^+ caused absorbance changes at 280 and 311 nm, indicating that Cu^+ coordinates at the ligand **B** site and forms a [**B**-Cu-**B**]$^+$ complex. No further spectral change occurred at the addition of up to three eq. of Cu^+ (Figure II-7b). This result is in agreement with the titration of ds$\mathbf{Q}^5$ and ds$\mathbf{B}^9$ by Cu^+ (Figure II-6). These titration results proved the feasibility of the hypothesized molecular switch based on the ligand modified PNA ds$\mathbf{Q}^5\mathbf{B}^9$ and copper ion.

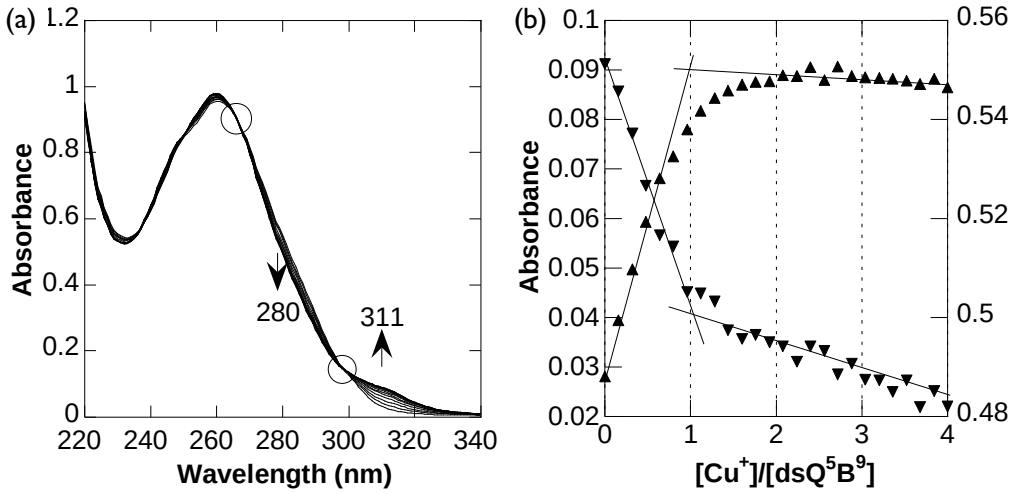

Figure II-7. Spectrophotometric titration spectra of 5 μM solution of ds$\boldsymbol{B}^9$ (a) or ds$\boldsymbol{Q}^5\boldsymbol{B}^9$ (b) with a 0.5 mM CuCl solution in pH = 7.7 10 mM Tris buffer in acetonitrile/water solvent (1/3, v/v); Titration curves of ds$\boldsymbol{B}^9$ (c) or ds$\boldsymbol{Q}^5\boldsymbol{B}^9$ (d) with CuCl at 280 nm (▼) or 311 nm (▲). The slope after 1eq Cu^+ is due to the binding of Cu^+ to the solvent.

The clear selectivity of different ligand sites for copper ions in different oxidation states promises a successful design of molecular switch. One can translocate the copper ion between the two ligand-sites, namely **Q** and **B** of ds$\mathbf{Q}^5\mathbf{B}^9$, by changing the oxidation state of copper. To verify the possibility of this translocation experimentally, we added one eq. of Cu^+ or Cu^{2+} to ds$\mathbf{Q}^5\mathbf{B}^9$ and then treated the solution with an oxidant, *tert*-butyl hydroperoxide (*ox*), or a reductant, sodium dithionite (*red*). As described above, the complex formed in the solution of ds$\mathbf{Q}^5\mathbf{B}^9$ and Cu^+ was [**B**-Cu-**B**]$^+$. Therefore, the two absorption bands representing free ligand **Q** site at 247 and 260 nm are intact. Addition of *ox* caused transformation of Cu^+ into Cu^{2+}, which also changed the coordination site of copper from ligand **B** to ligand **Q**. The absorption band shift for ligand **Q** from 247 to 260 nm was therefore observed in the UV-Vis spectra, indicating that the newly formed Cu^{2+} form the complex [**Q**-Cu-**Q**] with ligand **Q** (Figure II-8a). In addition, the small band at 311 nm representing the complex [**B**-Cu-**B**]$^+$ disappeared, which is another evidence that the copper translocated from ligand **B** to **Q**. The reverse process occurred when a mixture of ds$\mathbf{Q}^5\mathbf{B}^9$ and one eq. of Cu^{2+} was treated with *red*. Before addition of *red*, Cu^{2+} coordinated to the ligand **Q** site; the spectrum of the mixture displayed only one absorption band at 260 nm as expected for the complex [**Q**-Cu-**Q**]. Addition of *red* caused Cu^{2+} to become Cu^+ and also changed the preference of copper from ligand **Q** to **B**. The hypochromatic shift from 260 to 247 nm indicated the release of unbound ligand **Q** from complex [**Q**-Cu-**Q**]. Meanwhile, the increase of absorbance at 300-320 nm indicated the formation of [**B**-Cu-**B**]$^+$, demonstrating the translocation of copper from ligand **Q** to **B**. The new band at 300 nm is caused by the reductant, sodium dithionite (Figure II-8b).[66]

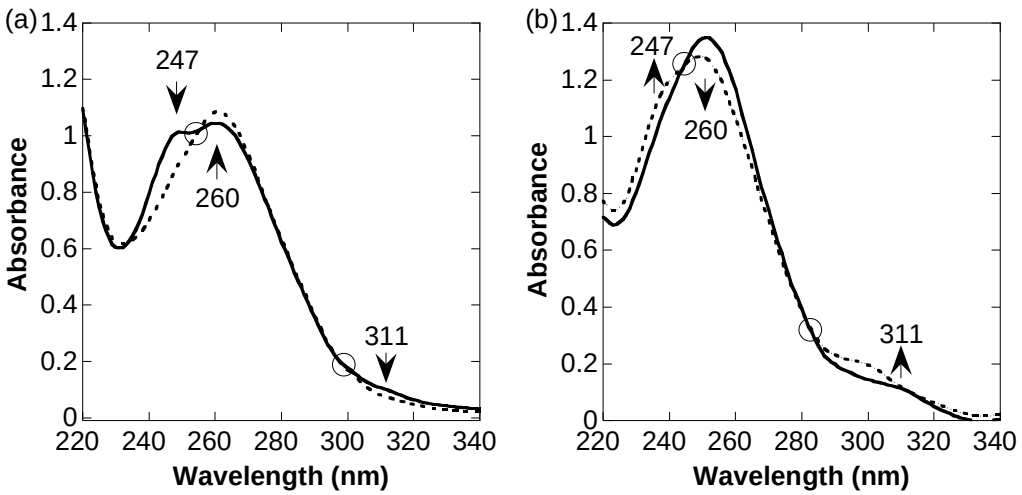

*Figure II-8. Spectrophotometric titration spectra of (a) a mixture of 5 μM solution of ds**Q**^{5}**B**^{9} and 5 μM solution of CuCl (solid line) treated by tert-butyl hydroperoxide (dotted line) and (b) a mixture of 5 μM solution of ds**Q**^{5}**B**^{9} and 5 μM solution of $CuCl_2$ (solid line) treated by sodium dithionite (dotted line) in pH 7.7 10 mM Tris buffer in acetonitrile/water solvent (1/3, v/v).*

II.3 Discussion

This chapter presented the result of a molecular switch built from metal ion and ligand-modified PNA that can be triggered by chemical reduction or oxidation. The strong coordination bonds that are formed between ligand at complementary position and metal ion make possible the alternative base pairs in replacement of the natural base pairs. Site-specific binding of metal ion to ligand-modified PNA is realized by the incorporation of different ligands in PNA, allowing the selective binding of different metal ion at different ligand site according to their stability constants. With an auxiliary redox trigger, the metal ion switches its position between different ligand-sites as a consequence of the change in its oxidation state.

The feasibility of the redox driven molecular switch has to do with the fact that the stoichiometry of the metal ion to the PNA duplex remains the same regardless of the oxidation state of the metal ion. The supramolecular chelate effect is responsible for maintaining the same stoichiometry of the metal ion to each ligand. The PNA duplex brings the two ligands at complementary positions to close proximity that once the metal ion binds with one of the ligands, the other ligand bind immediately as well. This critical feature of the complex formed within the PNA duplex promotes a mononuclear complex rather than a binuclear complex, thus ensuring the feasibility of redox trigger metal translocation within PNA duplex. Besides this, binuclear complex can induce metal ions into nucleic acids, but cannot improve thermal stability of the duplex in lack of the coordination bonds crosslinking the two ss PNAs within a duplex. Moreover, mononuclear complex is also the key to metal-mediated holiday junction, which has potential in building complex DNA origami with hierarchic thermal stability.

The change in the oxidation states of copper ion changes the preference of metal ion to different ligands according to the dramatic difference in the stability constants of the corresponding complexes. While the hard acid Cu^{2+} prefers the hard base **Q**, the soft acid Cu^{+} prefers the soft base **B**. The change in oxidation states triggered by the redox reagent drives the copper ion from one ligand site to the other because of this preference. This preference is in agreement with literature data and preliminary results.[43,48-50,62] Similar observations of metal translocation triggered by redox reagents are witnessed in non-nucleic acid systems with ligand **Q** and **B**.[48,49] In these non-nucleic acid systems, ligand **Q** and **B** are synthesized into either duplex or triplex of organic molecules to accommodate the octahedral or tetrahedral geometry of the metal ions. Upon the addition

of redox reagents, the metal ion translocate from one ligand site to the other. The importance of the research presented in this chapter is multifold. First, the design of the molecule is not limited by the organic synthesis. Customized molecular switches with different ligands at different positions coordinating with different metal ions could follow the same protocol of solid phase peptide synthesis once the ligand-modified PNA monomer is made. Secondly, the produced molecular switch has a motional precision at the nanoscale. The positioning of the metal ion is controlled by the location of each ligand pair in PNA. The distance of the adjacent bases in PNA is 3.2-3.4 Å,[22] which allows the positioning of ligand or metal ion at angstrom resolution. Thirdly, the PNA scaffold offers stronger chelating effect of the incorporated ligand, which makes possible molecular switch from the ligand or metal with weaker binding affinity. Last but not the least, the created molecular device can be easily arranged and targeted on the substrate of DNA origami as desired with an anchoring strand.

In addition to the stationary stoichiometry, the mononuclear formula from supramolecular chelate effect is also a premise of the thermal stability of the duplex. Besides the formed coordination bonds between the metal ion and the ligands that crosslink the two ss PNAs within the duplex, the metal ion also organizes the pair of ligands into the coordination geometry of the metal complex. Therefore, the mononuclear complex is as well in charge of the π-stacking and thus the stability of the duplex. Due to the square planar structure of complex [**Q**-Cu-**Q**], the π-stacking of [**Q**-Cu-**Q**] with the adjacent base pairs is better than the tetrahedron complex [**B**-Cu-**B**]$^{2+}$, rendering ds**Q**[5] a ΔT_m > 33 °C and dsB[9] a ΔT_m of 10 °C upon the addition of Cu^{2+}. This geometry difference also explains the reason for the ΔT_m of 14 °C with the addition of the first eq.

Cu^{2+} into ds$\mathbf{Q}^5\mathbf{B}^9$ and the ΔT_m of 6 °C with the addition of the second eq. Cu^{2+} into ds$\mathbf{Q}^5\mathbf{B}^9$. The tremendous recovery of thermal stability induced by ligand **Q** and Cu^{2+} has also been observed in other nucleic acids such as DNA and GNA.[56] In the case of DNA, the substitution of natural base pair in the middle of a 15-mer dsDNA lowers the T_m by 9 ˚C and addition of Cu^{2+} restores the T_m by 29 ˚C. The effect of ligand **B** in nucleic acids has also been studied extensively in DNA and PNA.[31,36,67-69] In the case of DNA, the addition of ligand **B** in the middle of a 10-mer DNA duplex did not change the T_m of the duplex, but damaged the cooperativity of the melting. The addition of Cu^{2+} increased the T_m by 7.5 ˚C.[31] In the context of PNA, the substitution of ligand **B** in the center of a 11-mer DNA decreased the T_m by 21˚C and addition of Ni^{2+} restores the T_m by 11 ˚C.[36]

The melting point of ligand modified PNA without metal ion depends mainly on the position of the ligand modification. Since the terminal position is vulnerable to fraying, substitution at terminal position does not decrease the stability of the duplex as much as the substitution at middle position. Ligand modification at the middle of the strand opens a gap in the duplex, creating two new pseudo-terminals that are vulnerable to fraying. This explains the large ΔT_m of -21 ˚C for dsQ^5 and the small ΔT_m of -2 ˚C for dsB^9 compared with non-modified dsN.

As observed in the thermal stability of the ligand modified PNA, the position of the ligand modification has influence on the conformation of the PNA duplex. Even though ligand **Q** possesses a more rigid aromatic conjugation structure for better π-stacking than ligand **B**, the CD intensity of ds$\mathbf{Q}^5$ is still weaker than that of ds$\mathbf{B}^9$. With this comparison in the absence of metal ion, the exceeding intensity gained upon metal addition of ds$\mathbf{Q}^5$

over ds**B**^{9} is very impressive, which again proves that the geometry of [**Q**-Cu-**Q**] is indeed square planar and that [**B**-Cu-**B**]$^{2+}$ is tetrahedral. The CD spectrum of ds**Q**^{5}**B**^{9} is actually another piece of evidence for the stepwise binding event since the first eq. of copper significantly increased the chirality, indicating the formation of the square planar [**Q**-Cu-**Q**]. If the first eq. of copper binds to ligand **B** instead, then the helicity would not restore as much referring to the poor helicity recovery shown for ds**B**^{9}. However, the second eq. of copper coordinates at the ligand **B** site, which leads to a tetrahedral geometry of the complex formed, corresponding to the slight increase of the CD intensity. The excellent performance of [**Q**-Cu-**Q**] in helicity transmission demonstrates that the dipole-dipole interaction between the π-stacked base pairs is the main source for propagation of helicity.[65]

This chapter reports a molecular switch based on metal-containing ligand-modified PNA duplex. 8-hydroxyquinoline and 2,2'-bipyridine are incorporated in PNA duplex to create the scaffold to accommodate copper ion of different oxidation states with different ligand sites. The copper ion is driven by a redox reaction to switch the preference of different ligand site. PNA is an ideal material to build elemental components for nanotechnology. As the first molecular switch built with ligand-modified PNA, the system can be easily customized as desired due to the convenience of the building blocks made of ligand modified PNA in both nanotechnological and biological applications.

II.4 Conclusions

Substitution of natural nucleobases with different types of ligands in peptide nucleic acid (PNA) oligomers makes possible the incorporation of diverse metal ions at predefined positions within PNA duplexes. In this chapter, 8-hydroxyquinoline and 2,2'-bipyridine ligands were introduced in a 10-base PNA duplex, thus creating a molecular switch in which a copper ion could be driven back and forth like a shuttle between two distinct ligand stations by alternating the oxidation state of the copper ion. Due to the different stability constants of the metal complexes formed between the ligands and the copper ion in different oxidation states, the translocation of the copper ion between the ligand stations was triggered by auxiliary redox reactions. This PNA-based molecular switch facilitates flexible design with building blocks made of PNA monomers, which can be used as signal receiver, operation component, information storage, or control unit of protein with specific function.

II.5 Experimental

Materials. Boc-protected ligand-modified PNA monomers 2-(N-(tert-butyloxycarbonyl-2-amino ethyl)-2-(8-hydroxyquinolin-5-yl)acetamido)acetic acid (**Q**, Scheme II-3a) and 2-(2,2'-bipyridin-5-yl)-2-(N-(tert-butyloxycarbonyl-2-aminoethyl) acetamido)acetic acid (**B**, Scheme II-3b) were prepared according to published procedures.[42,44] All other reagents were commercially available, analytical grade quality, and used without further purification. Reagents that were involved with Cu^{+} experiments

were treated with five cycles of freeze-pump-thaw degassing to remove dissolved oxygen. Titrations with Cu^{+} were performed under an inert atmosphere.

Scheme II-3. (a) ***Q****- or (b)* ***B****-Modified PNA Monomer.*

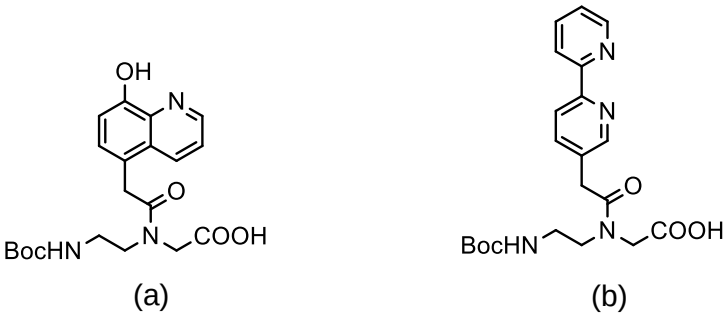

Synthesis of Ligand-Modified PNA. PNA oligomers were synthesized with the Boc-protection strategy. PNA monomers were purchased from Applied Biosystems and ASM Research Chemicals and were used without further purification. PNA was precipitated using diethyl ether after cleavage and was purified by reversed-phase HPLC using a C18 silica column on a Waters 600 model. Absorbance was measured at 260 nm with a Waters 2996 Photodiode Array Detector. Characterization of the oligomers was performed by MALDI-ToF mass spectrometry on an Applied Biosystems Voyager Biospectrometry Workstation with Delayed Extraction and an R-cyano-4-hydroxycinnamic acid matrix (10 mg/mL in 1:1 water/acetonitrile, 0.1% TFA). m/z for $(M+H)^{+}$ were calculated and found to be $\mathbf{Q}^{5}$-α 2864.9/2867.0, $\mathbf{Q}^{5}$-β 2873.9/2876.1, $\mathbf{B}^{9}$-α 2899.9/2901.0, $\mathbf{B}^{9}$-β 2859.9/2861.0, $\mathbf{Q}^{5}\mathbf{B}^{9}$-α 2909.9/2911.1, $\mathbf{Q}^{5}\mathbf{B}^{9}$-β 2878.9/2879.2.

CD Spectroscopy. CD measurements were conducted on a JASCO J-715 spectropolarimeter equipped with a thermoelectrically controlled, single-cell holder. CD spectra were measured for 10 μM PNA duplexes in 10 mM pH 7.7 Tris buffer (1:3 acetonitrile/water solvent). CD spectra were collected using a bandwidth of 1 nm, response time of 1s, speed of 50 nm/min, sensitivity of 20 mdeg, and scan accumulation of 10.

UV-Vis Spectroscopy Titrations. UV-Vis titrations were performed on a Varian Cary 50 Bio spectrophotometer with a 10 mm quartz cell. PNA stock solutions were prepared with nanopure water (> 18.3 MΩ.cm^{-1}) and have been stored at -18 °C to avoid depurination. The concentration of PNA oligomers was determined by UV absorption at 95 °C using the sum of the extinction coefficients of the constituent nucleosides ε_{260} taken from the literature.[17] The extinction coefficients for 8-hydroxyquinoline ε_{260} = 2570 M^{-1} cm^{-1} and 2,2'-bipyridine ε_{260} = 9770 M^{-1} cm^{-1} (at pH 7.0) were determined from the slope of the calibration curve A_{260} versus concentration. PNA solutions were prepared in 10 mM pH 7.7 Tris buffer (1:3 acetonitrile/water solvent). To prepare each PNA duplex for titrations, the PNA solutions were held at 95 °C for 10 min first and then annealed from 95 °C to 10 °C at a rate of 1 °C/min. Concentration of the annealed PNA duplex were 5 μM. UV-Vis titrations were carried out by addition of 0.5 mM $CuCl_2$ solutions to PNA solutions at room temperature. The absorbance after each addition was corrected for dilution.

UV-Vis Spectroscopy Melting Curves. UV melting curves were recorded at 260 nm in the temperature range of 10-95 °C for both cooling and heating modes, at the rate of 1

°C/min. For the melting of Cu^{+} coordinated duplex, the rate of heating mode is 4 °C/min to avoid possible oxidation during the heating process. Prior to the measurement of the melting profiles, solutions of 5 μM of each ss PNA in 10 mM pH 7.7 Tris buffer (1:3 acetonitrile/water solvent) were kept at 95 °C for 10 min before cooling down. T_m is the inflection point of a sigmoidal function used to fit the melting curve. All measurements were performed in at least triplicate.

II.6 References

(1) Bojinov, V.; Georgiev, N. *J. Univ. Chem. Technol. Metall.* **2011**, *46*, 3.

(2) Fages, F.; Wytko, J. A.; Weiss, J. *C. R. Chim.* **2008**, *11*, 1241.

(3) Kumar, M. J. *Recent Pat. Nanotechnol.* **2007**, *1*, 51.

(4) Magri, D. C.; Vance, T. P.; Prasanna de Silva, A. *Inorg. Chim. Acta* **2007**, *360*, 751.

(5) Otsuki, J.; Akasaka, T.; Araki, K. *Coord. Chem. Rev.* **2008**, *252*, 32.

(6) Hess, H. *Annu. Rev. Biomed. Eng.* **2011**, *13*, 429.

(7) Yan, H. *Science* **2004**, *306*, 2048.

(8) Krishnan, Y.; Simmel, F. C. *Angew. Chem., Int. Ed.* **2011**, *50*, 3124.

(9) Bhatia, D.; Sharma, S.; Krishnan, Y. *Curr. Opin. Biotechnol.* **2011**, *22*, 475.

(10) Dietz, H.; Douglas, S. M.; Shih, W. M. *Science* **2009**, *325*, 725.

(11) Rothemund, P. W. K. *Nature* **2006**, *440*, 297.

(12) Seeman, N. C. *Annu. Rev. Biochem.* **2010**, *79*, 65.

(13) Beck, F.; Nielsen, P. E. *Artificial DNA* **2003**, 91.

(14) Nielsen, P. E.; Egholm, M. *Curr. Issues Mol. Biol.* **1999**, *1*, 89.

(15) Mischiati, C.; Borgatti, M.; Bianchi, N.; Rutigliano, C.; Tomassetti, M.; Feriotto, G.; Gambari, R. *J. Biol. Chem.* **1999**, *274*, 33114.

(16) Saviano, M.; Romanelli, A.; Bucci, E.; Pedone, C.; Mischiati, C.; Bianchi, N.; Feriotto, G.; Borgatti, M.; Gambari, R. *J. Biomol. Struct. Dyn.* **2000**, *18*, 353.

(17) Nielsen, P. E.; Editor *Peptide Nucleic Acids: Protocols and Applications, Second Edition*, 2004.

(18) Toy, P. H.; Lam, Y. *Solid-Phase Organic Synthesis: Concepts, Strategies, and Applications*; John Wiley & Sons, 2011.

(19) Seeman, N. C. *Trends Biochem. Sci.* **2005**, *30*, 119.

(20) Seeman, N. C. *Mol. Biotechnol.* **2007**, *37*, 246.

(21) Mallajosyula, S.; Pati, S. *Angew. Chem. Int. Ed. Engl.* **2009**, *48*, 4977.

(22) He, W.; Franzini, R. M.; Achim, C. *Prog. Inorg. Chem.* **2007**, *55*, 545.

(23) Mueller, J. *Eur. J. Inorg. Chem.* **2008**, 3749.

(24) Lynam, J. M. *Dalton Trans.* **2008**, 4067.

(25) Takezawa, Y.; Shionoya, M. *Acc. Chem. Res.*, ASAP.

(26) Nakanishi, Y.; Kitagawa, Y.; Shigeta, Y.; Saito, T.; Matsui, T.; Miyachi, H.; Kawakami, T.; Okumura, M.; Yamaguchi, K. *Polyhedron* **2009**, *28*, 1714.

(27) Katz, S. *Biochim. Biophys. Acta, Spec. Sect. Nucleic Acids Relat. Subj.* **1963**, *68*, 240.

(28) Miyake, Y.; Togashi, H.; Tashiro, M.; Yamaguchi, H.; Oda, S.; Kudo, M.; Tanaka, Y.; Kondo, Y.; Sawa, R.; Fujimoto, T.; Machinami, T.; Ono, A. *J. Am. Chem. Soc.* **2006**, *128*, 2172.

(29) Tanaka, K.; Shionoya, M. *J. Org. Chem.* **1999**, *64*, 5002.

(30) Zimmermann, N.; Meggers, E.; Schultz, P. G. *J. Am. Chem. Soc.* **2002**, *124*, 13684.

(31) Weizman, H.; Tor, Y. *J. Am. Chem. Soc.* **2001**, *123*, 3375.

(32) Tanaka, K.; Yamada, Y.; Shionoya, M. *J. Am. Chem. Soc.* **2002**, *124*, 8802.

(33) Tanaka, K.; Tengeiji, A.; Kato, T.; Toyama, N.; Shiro, M.; Shionoya, M. *J. Am. Chem. Soc.* **2002**, *124*, 12494.

(34) Meggers, E.; Holland, P. L.; Tolman, W. B.; Romesberg, F. E.; Schultz, P. G. *J. Am. Chem. Soc.* **2000**, *122*, 10714.

(35) Atwell, S.; Meggers, E.; Spraggon, G.; Schultz, P. G. *J. Am. Chem. Soc.* **2001**, *123*, 12364.

(36) Popescu, D.-L.; Parolin, T. J.; Achim, C. *J. Am. Chem. Soc.* **2003**, *125*, 6354.

(37) Hirva, P.; Nielsen, A.; Bond, A. D.; McKenzie, C. J. *J. Phys. Chem. B* **2010**, *114*, 11942.

(38) Schlegel, M. K.; Essen, L.-O.; Meggers, E. *J. Am. Chem. Soc.* **2008**, *130*, 8158.

(39) DeLeon, A.; Kong, J.; Achim, C. In *Metallofoldamers: Supramolecular Architectures from Helicates to Biomimetics*; Maayan, G., Albrecht, M., Eds.; Wiley-VCH: Weinheim, 2012.

(40) Tanaka, K.; Clever, G. H.; Takezawa, Y.; Yamada, Y.; Kaul, C.; Shionoya, M.; Carell, T. *Nat. Nanotechnol.* **2006**, *1*, 190.

(41) Li, G.; Liu, H.; Chen, X.; Zhang, L.; Bu, Y. *J. Phys. Chem. C* **2011**, *115*, 2855.

(42) Watson, R. M.; Skorik, Y. A.; Patra, G. K.; Achim, C. *J. Am. Chem. Soc.* **2005**, *127*, 14628.

(43) Ma, Z.; Olechnowicz, F.; Skorik, Y. A.; Achim, C. *Inorg. Chem.* **2011**, *50*, 6083.

(44) Franzini, R. M.; Watson, R. M.; Patra, G. K.; Breece, R. M.; Tierney, D. L.; Hendrich, M. P.; Achim, C. *Inorg. Chem.* **2006**, *45*, 9798.

(45) Bezer, S.; Rapireddy, S.; Skorik, Y. A.; Ly, D. H.; Achim, C. *Inorg. Chem.*, *50*, 11929.

(46) Lehn, J. M. *Science* **1985**, *227*, 849.

(47) Waldron, K. J.; Rutherford, J. C.; Ford, D.; Robinson, N. J. *Nature* **2009**, *460*, 823.

(48) Zelikovich, L.; Libman, J.; Shanzer, A. *Nature* **1995**, *374*, 790.

(49) Kalny, D.; Elhabiri, M.; Moav, T.; Vaskevich, A.; Rubinstein, I.; Shanzer, A.; Albrecht-Gary, A.-M. *Chem. Commun.* **2002**, 1426.

(50) Petitjean, A.; Kyritsakas, N.; Lehn, J.-M. *Chem. Commun.* **2004**.

(51) Petitjean, A.; Kyritsakas, N.; Lehn, J.-M. *Chem.--Eur. J.* **2005**, *11*, 6818.

(52) Kaes, C.; Katz, A.; Hosseini, M. *Chem. Rev.* **2000**, *100*, 3553.

(53) Albrecht, M.; Fiege, M.; Osetska, O. *Coord. Chem. Rev.* **2008**, *252*, 812.

(54) Boraei, A. A. A.; Ahmed, I. T. *Synth. React. Inorg. Met.-Org. Chem.* **2002**, *32*, 981.

(55) Ahn, G. O.; Ware, D. C.; Denny, W. A.; Wilson, W. R. *Radiat. Res.* **2004**, *162*, 315.

(56) Zhang, L.; Meggers, E. *J. Am. Chem. Soc.* **2005**, *127*, 74.

(57) Kruszynski, R. *Struct. Chem.* **2010**.

(58) Weizman, H.; Tor, Y. *Chem. Commun.* **2001**, 453.

(59) James, B. R.; Williams, R. J. P. *J. Chem. Soc.* **1961**, 2007.

(60) Tapiero, H.; Townsend, D. M.; Tew, K. D. *Biomedicine & Pharmacotherapy* **2003**, *57*, 386.

(61) Kim, B.-E.; Nevitt, T.; Thiele, D. J. *Nature Chemical Biology* **2008**, *4*, 176.

(62) Ma, Z. *Dissertations* **2011**, *Paper 35*, 80.

(63) Wittung, P.; Nielsen, P. E.; Buchardt, O.; Egholm, M.; Norden, B. *Nature* **1994**, *368*, 561.

(64) Egholm, M.; Buchardt, O.; Christensen, L.; Behrens, C.; Freier, S. M.; Driver, D. A.; Berg, R. H.; Kim, S. K.; Norden, B.; Nielsen, P. E. *Nature* **1993**, *365*, 566.

(65) Wittung, P.; Eriksson, M.; Lyng, R.; Nielsen, P. E.; Norden, B. *J. Am. Chem. Soc.* **1995**, *117*, 10167.

(66) Dixon, M. *Biochim. Biophys. Acta, Bioenerg.* **1971**, *226*, 241.

(67) Weizman, H.; Tor, Y. *J. Am. Chem. Soc.* **2001**, *123*, 3375.

(68) Franzini, R.; Watson, R. M.; Popescu, D.-L.; Patra, G. K.; Achim, C. *Polym. Prepr. (Am. Chem. Soc., Div. Polym. Chem.)* **2004**, *45*, 337.

(69) Yeh, J.; Pohl, E.; Truan, D.; He, W.; Sheldrick, G.; Du, S.; Achim, C. *Chemistry* **2010**, *16*, 11867.

CHAPTER III. PNA Functionalization on DNA Origami

III.1 Introduction

The rapid development of nanotechnology creates great opportunities for assembling molecular-scale devices with desired functions. During the last decade, nucleic acids have emerged as a promising material for nanotechnology due to the highly predictable and programmable nature of Watson-Crick hybridization of complementary nucleic acid sequences. The high fidelity and hybridization of complementary sequences allows the formation of diverse structures through sequence design. Of particular success has been an approach based on folding a single, long strand of DNA using short DNA staple strands into a scaffold, which is known as DNA origami.[1-5] Current synthetic methods for natural and artificial nucleic acids allow the access to milligram of material, which is adequate for fundamental studies and some practical applications.[6] The high-resolution control of the geometry and shape of the nucleic acid structures has enabled extensive investigations of nucleic acid as a substrate for the assembly of devices with smart behavior and desired functions such as tissue culture, drug delivery, and immunotechnology.[7-9]

A crucial property of the practical use of these nucleic acid-based structures is the ability to functionalize them with different chemical groups that vary from a few atoms to nanocrystals, proteins and nucleic acids. Several research groups have explored various means of functionalization. A common approach relies on incorporating DNA oligos that

have been chemically modified with solid phase phosphoramidite chemistry during synthesis. For example incorporation of oligos with terminal thiol groups allows binding to gold nanoparticles (AuNP). Due to their electronic, optical and magnetic properties, AuNPs have been extensively incorporated into different nanostructures formed from thiol-modified DNAs.[10-19] DNA oligos modified with terminal amines or click-chemistry partners allows for chemical modification of resulting nanostructures with NHS-esters and through click chemistry.[20] Enzymatic modifications of DNA oligonucleotides with terminal transferase allows for addition of deoxynucleotides to the 3' end of one oligonucleotide or to several different ones in parallel. In addition, the appended deoxynucleotide can carry a wide variety of chemical groups that are thus displayed on the final assembled nanostructure.[21] As opposed to termini modification of DNA oligos, internal purines can be sequence specifically alkylated using pyrrole-imidazole polyamide enabling modification with functional groups such as biotin.[22]

Proteins naturally have a great range of functionalities and catalytic activities and also share buffer compatibility with DNA. As such they are extremely desirable components to incorporate in DNA nanostructures. Previously it has been shown that incorporation of an antigen allows for programmed patterning of antibodies on DNA nanostructures.[23] A simpler approach utilized the ligand recognition of aptamers to attach thrombin and platelet derived growth factor to DNA nanostructures.[24] The same thiol modification of DNA oligonucleotides used to link AuNPs to DNA was used to make maleimide-based modifications of the DNA structures. For example, a maleimide-linked nitrilotriacetic acid (NTA) was coupled to a thiol group; Ni^{2+} binding to NTA in turn allowed the binding of his-tagged proteins to the Ni^{2+}-NTA complex.[25] Thiols can also be used for

covalent coupling to amine groups using maleimide-N-hydroxysuccinimide heterobifunctional linkers.[26] The N-hydroxysuccinimide reactive group have been used to incorporate snap- and halo-tags allowing for covalent incorporation of fusion proteins into DNA nanostructures.27,28 Illustrating the diverse functionality of peptides; DMTMM (4-(4,6-Dimethoxy-1,3,5-triazin-2-yl)-4-methyl morpholinium chloride) was used to incorporate AuNP binding peptides enabling nanoscale patterning of AuNP without thiol chemistry.[29] Besides chemistry targeting the termini of DNA oligos, sequence specific binding of zinc-finger motifs have been used to link fluorescent proteins to DNA-based nanostructures.[30]

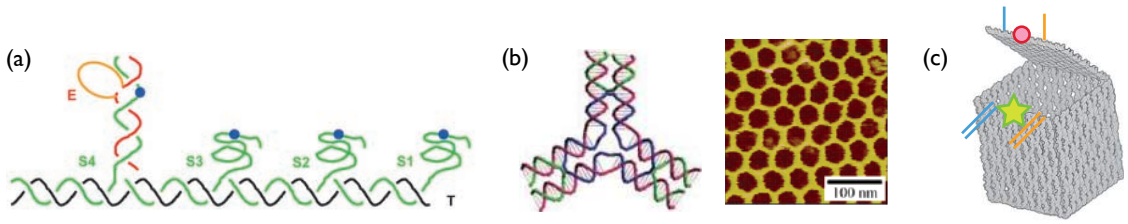

Figure III-1. A variety of self-assembled DNA shapes. The images are adapted from references.[31-33] We envision that when modified with appropriate electroactive groups, these structures can constitute the scaffold of 1-D, 2-D and 3-D electron transfer chains in which the charge transfer occurs unidirectionally, in manner similar to that in the membrane of mitochondria.

Nucleic acids, such as DNA and peptide nucleic acid (PNA), are known to self-assemble not only into the iconic double helical structures, but also into a variety of two- and three-dimensional structures that can be tailored with astounding variety and precision (Figure III-1). Recently developed technologies have led to rectangular grids,

crosses, nuts, blocks, bridges, wheels, baskets, and nano-sized boxes with flexible lids.[34] DNA has been used as framework for nanoassembly of nanoparticles,[35,36] and DNA lattices are being exploited for organizing photonic devices that perform elementary logic operations.[37] DNA-based functional devices[38,39] including nanorobots,[40] have been also extensively studied.

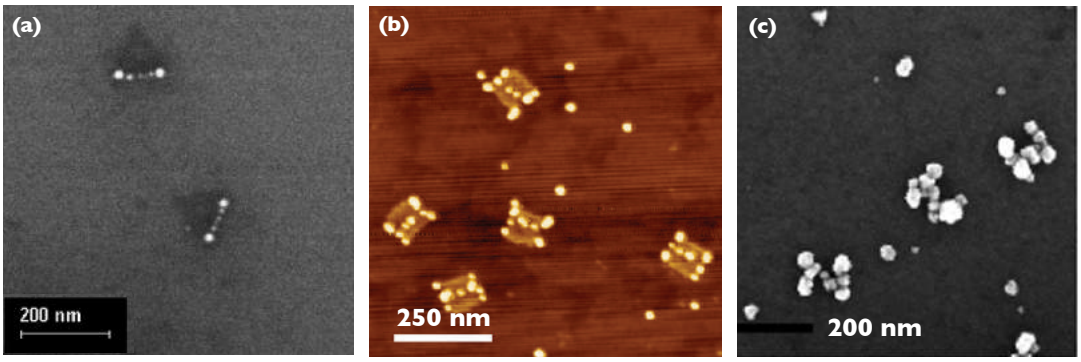

Figure III-2. (a) SEM image of linear AuNPs organized by triangular DNA origami. AFM image of a pair of parallel bars of AuNPs on a rectangular DNA origami before (b) and after (c) metallization.

DNA assemblies with 1-D, 2-D and 3-D arbitrary shapes provide a programmable template for bottom-up method to build complex nanostructures. Different modifications have been done to improve the functionality of DNA origami. Metallic nanoparticles such as gold and silver are first placed on DNA origami to challenge the limitation on the current top-down lithography techniques. One interesting aspect is that silver deposit on DNA template can create conducting nanowires in the scale of tens of nanometers.[41,42] The size and the granular morphology of the nanowire depends largely on the grain size

of the silver particles. Linear chain of separated gold nanoparticles (AuNPs) with progressively decreasing sizes and precise control of spacing was also placed on DNA origami by gluing the sticky ends thiolated on AuNPs with the potential of large field enhancement (Figure III-2a).[43,44] The same strategy was applied to arrange the distance between a fluorescence dye and AuNPs to study the distance dependence of fluorescence quenching. It is proved that the enhanced quantum efficiency observed when the distance is below 30 nm.[45] To fabricate nano-scale structure for potential electronic and plasmonic applications, procedure of metallization was performed after the placement of AuNPs on predefined positions to enlarge and fuse the AuNPs together. Different shapes such as "H" and other complex shapes were successfully assembled on DNA origami (Figure III-2b and c).

Modification with functional group such as protein is particularly desirable to realize the application of DNA origami as template for assembling device for sensing, catalysis, or enzymatic activity. A face-shaped DNA origami was used to demonstrate the selective immobilization of different proteins.[46] AFM images revealed that the staple strands with biotin, benzylguanine, or chlorohexane were able to fuse with the tagged proteins of interest to pattern mouth, eyes and nose on a face-like DNA origami (Figure III-3). With appropriate modification of ssDNA, virus capsid was also attached to DNA origami to form a capsid array organized by connected rectangular DNA origami (Figure III-4a and b).[47] Alternative procedures and conditions of placing the capsid and connecting the DNA origami were investigated to optimize the binding efficiency. DNA wrapped carbon nanotubes with fixed length can also be attached to the DNA origami with ssDNA on both carbon nanotubes and DNA origami (Figure III-4c).[48] Another interesting

application of DNA origami is drug delivery. DNA nano cage with large cavity were designed to load drugs and/or programmably release the drug by opening the cavity upon the triggering.[49-53] ssDNA are used to fuse the lid and the container and the addition of key strand that is complementary to the fuse strand release the content in the container (Figure III-5).

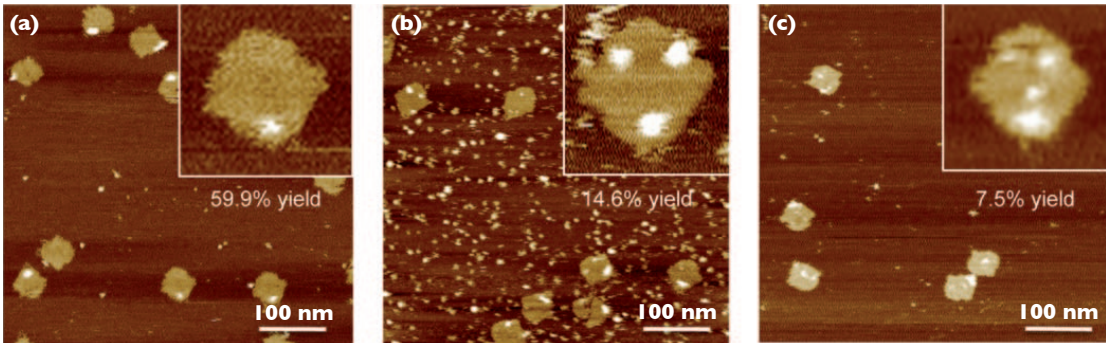

Figure III-3. AFM images of face-like DNA origami with 1, 2, and 3 proteins representing mouth (a), eyes (b), and nose (c).

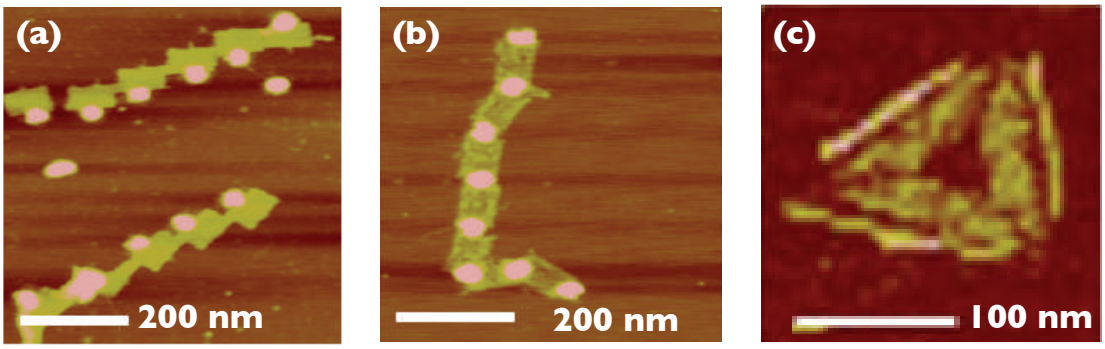

Figure III-4. AFM images of capsid array on the edge (a) and center (b) of DNA origami. Triangle DNA origami modified SWNT.

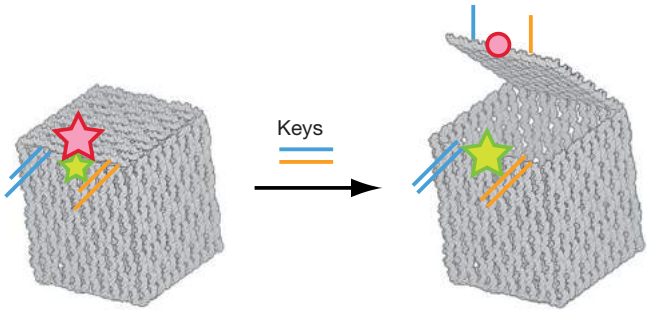

Figure III-5. Cartoon of DNA nano box that can close and open upon the addition of single stranded key DNA. Star and circle represent the fluorescent dyes.

As discussed in the functionalization on DNA origami above, ssDNA key or fuse strand, sticky ends, and anchoring staple strands that are identical in their physical properties with the DNA template are the conventional method to label or modify DNA origami. However, to hybridize the sticky ends or the key strands, same or similar condition of annealing for the DNA origami has to be applied, which poses challenge to dissembling the DNA origami and leads to low yield. The melting temperature for the well-known rectangular DNA origami made from M13mp18 scaffold is 57 °C, which is very close to a 20-bp dsPNA (Figure III-6a).[54] Another challenge of using ssDNA as the method for functionalization of DNA origami is that *in vivo* applications such as drug delivery require the enzymatic stability of the device itself. The cellular stability of ssDNA, dsPNA and DNA origami were examined by treating with cell lysate.[55] Based on the gel electrophoresis result, ssDNA and dsDNA are digested by the enzymes in the cell lysate while the DNA origami remained stable.

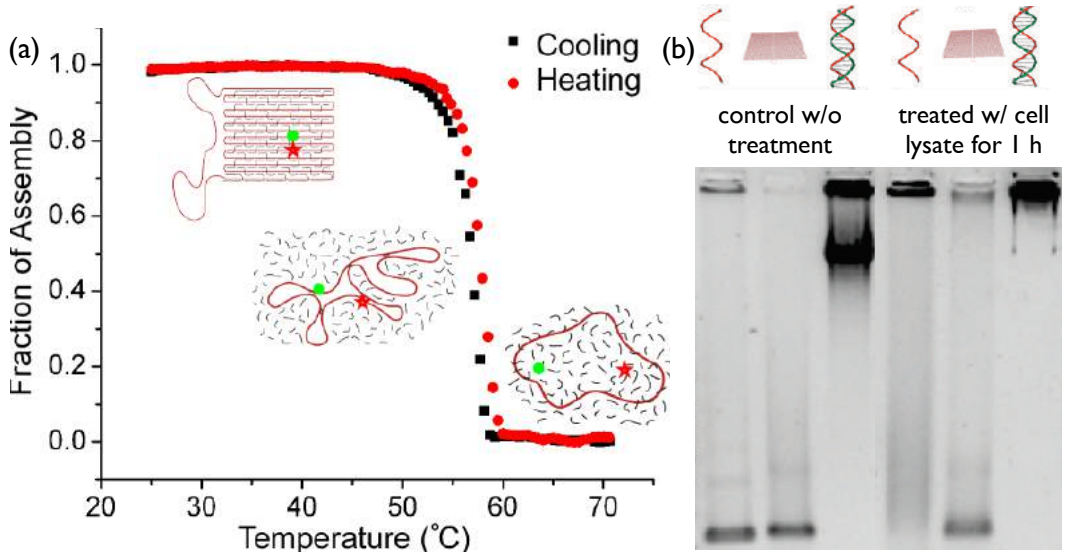

Figure III-6. (a) Thermal stability of rectangular DNA origami modified with FRET dye pair. (b) Gel electrophoresis of ssDNA, dsDNA and DNA origami before and after cell lysate treatment.

To concur the two obstacles mentioned above, recently attention has been directed toward using peptide nucleic acids (PNA). PNA is a synthetic DNA analog consisting of a backbone of repeating N-(2-aminoethyl)-glycine units to which purine and pyrimidine bases are linked by amide bonds.[56] The neutral backbone affords PNA characteristics different from those of DNA, such as increased affinity towards complementary strands at low salt concentrations.[57,58] Since PNA is synthesized by the same solid phase chemistry as peptides, it is easy to make PNA-peptide chimeras and consequently to incorporate peptides at well-defined locations in DNA nanostructures.[59] The structure of PNAs are not recognized by nucleases and proteases, and thus are resistant to enzymatic hydrolysis.[60,61] The unique properties of PNA can also be used to construct nanostructures with different handedness than that of DNA•DNA duplexes[62] and with low tolerance of base mismatches useful in detection systems.[63,64] One of the most

interesting features of PNA molecules is that their high affinity for complementary DNA allows for sequence specific invasion of DNA duplexes.[56,65,66] This property can be used to create nanoscale assemblies using double stranded DNA as a scaffold[67,68] or as a way to manipulate dynamic nanostructures by addition of PNA without the use of predesigned toeholds.[69,70] PNA holds promise for greatly expanding of the toolbox of DNA nanotechnology both by introducing chemical reactivity in the form of peptides and by aiding in the fine tuning of nanostructure designs.

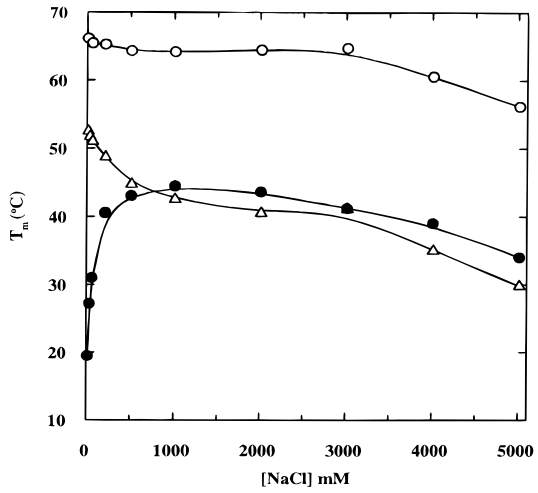

Figure III-7. Effects of ionic strength on the T_m of PNA complexes compared to the corresponding DNA•DNA duplex: (a) PNA•PNA (O), N/3′ PNA•DNA (Δ), and DNA•DNA (•) 10-mer duplexes in 10 mM sodium phosphate, pH 7.0.

Dynamic targeting of DNA nano structures is desirable when creating devices for drug delivery or nano-scale assembly.[71,72] The increased affinity between PNA and DNA compared to DNA and DNA affords a possibility of targeting DNA nano structures with

smaller and stronger-binding constructs. The ionic effect on thermal stability of DNA•DNA, DNA•PNA and PNA•PNA shows different trends with increasing salt concentration (Figure III-7).[73] The thermal stability of DNA•DNA (•) and PNA•DNA (Δ) is crucial for successful PNA invasion in DNA origami. As shown in Figure III-7, the thermal stability of DNA•DNA and PNA•DNA approximately equals each other beyond 700 mM NaCl, which is far larger than the salt concentration that we used for the modification, which is 150 mM NaCl and below, down to 0.125 mM $MgCl_2$.

Here in this chapter, we have investigated the incorporation of PNA in DNA nanostructures. To test the incorporation of this PNA molecule into DNA structures, we employed a two dimensional DNA origami structure of Rothemunds original design herein labelled RRO (regular rectangular origami) following previous convention.[74] We modified RRO to include three PNA binding sites at different locations, labelled as sites center, side and corner. The attachment of the PNA to these sites was assayed using streptavidin (STV), which can bind with high affinity to biotin.

The increased stability of a hetero DNA•PNA duplex when compared to a homo DNA•DNA duplex allows PNA to invade a DNA homo duplex. This invasion represents a method for DNA modification that is orthogonal to the widely used toehold-mediated strand displacement for the introduction of controlled dynamic behavior in nano devices.[75] However the relative stability of the hetero and homo duplexes is highly dependent on ionic strength. Hence, we decided to first evaluate the kinetics of invasion of a DNA duplex by the PNA molecule and its dependence on salt concentration. We employed the method of initial rates and a DNA duplex labelled with a fluorophore and a

quencher to monitor by fluorescence the dissociation of the DNA duplex in the presence of PNA. Building on knowledge learned from this kinetic experiment, we designed a linear array[76,77] to display invasion sites in order to visualize invasion of the biotinylated PNA strand.

III.2 Results

III.2.i PNA Synthesis and DNA Origami

Two PNA strands were synthesized for this study, a short 8-base PNA with one cysteine (Cys) at the C end (PNA1) and a long 16-base PNA with three lysines (Lys) at the C end (PNA2). The side group of lysine has a pK_a of 10.5; hence at pH 8.00 each PNA strand has three positive charges. We also included a biotin group at the N end of the longer PNA. The sequences of the two strands are H_2N-Cys-T_3GT_4-H (PNA1) and H_2N-Lys_3-$ATGA_2TATAGT_2G_3A$-$C_4C_4C_2$-SH (PNA2). PNA1 is designed to target a complementary ssDNA stretching out of the DNA origami. Two such stretches were situated at the corners of the DNA origami and one was placed on the side of the origami. The cysteine at the C-end of PNA1 is incorporated to bind AuNPs to the DNA origami (refer to Figure III-8). PNA2 has a linker that contains a thiol group to couple the biotin group at the N-end. The three target sites for PNA2 on DNA origami are at corner, on side and at center (refer to Figure III-9). The side site consists of a stretch of exposed, uncomplemented M13 scaffold strand along the edge of the rectangular structure complementary to the PNA sequence. The center site is placed in the center of the two dimensional origami and consists of overhangs from two staple strands forming a V-

shaped binding site; each overhang is complementary to half of the PNA molecule. The corner site is located at the corner and consists of an overhang from a staple strand and has a sequence fully complementary to that of the PNA molecule. The DNA array designed for the invasion kinetics is shown in Figure III-10.

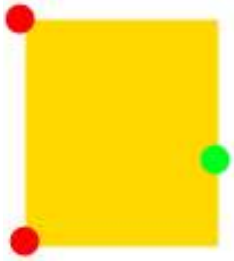

Figure III-8. DNA origami for PNA1 binding with position of target strands identified in red and green. The red dots designate location of two single strands with 3 consecutive complementary sequences. The green dot designates location of a single intrinsic complementary sequence in the m13 scaffold, looping out on the side;

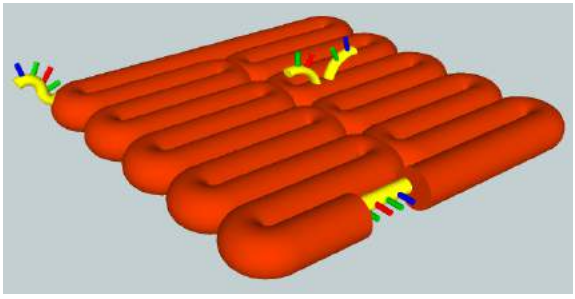

Figure III-9. Illustration of 3 different PNA2 binding sites on the DNA origami structure. Red cylinders represent the DNA duplex forming the origami structure. Yellow cylinders represent single stranded regions complementary to PNA2. The binding site in the front of the picture and "inline" with the orange duplex cylinders are located on the m13 scaffold.

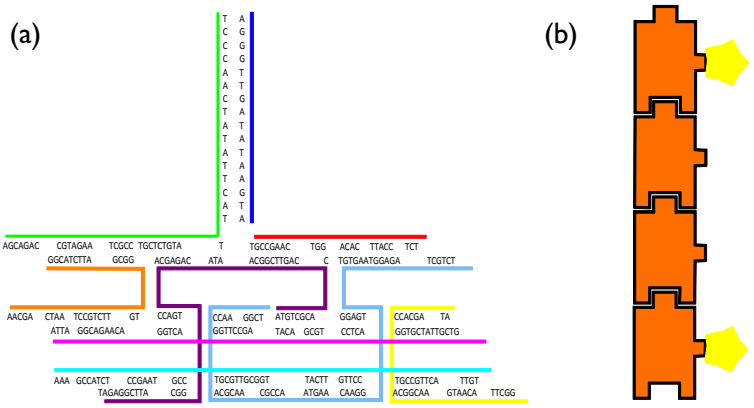

Figure III-10. (a) An array consists of several linking tiles fully illustrated with sequences. The top protruding duplex allows for invasion of complementary PNA strand. (b) Multiple tiles form linear arrays. This enables estimation of the efficiency of PNA invasion when using biotinylated PNA as the bound streptavidin can be counted in AFM. The streptavidin molecule attached to some of the tiles is represented as yellow pentagram.

III.2.ii UV-Vis Spectroscopy Melting Curves

The melting curves were measured to evaluate the feasibility of the functionalization of DNA origami by PNA invasion. The enhanced thermal stability of the hetero PNA•DNA duplexes over the homo DNA•DNA duplexes was observed in solutions of different salt concentrations. The melting temperatures (T_m) of PNA•DNA duplex under different salt concentrations is above 70 °C in all cases, which is more than 30 °C higher than that of the DNA•DNA duplex at 41 °C (Table III-1). The melting temperatures of the 16-bp duplexes are in agreement with the literature values of 15-bp duplexes.[78]

Table III-1. The melting temperature (T_m/˚C) of homo- DNA and hetero- PNA•DNA duplexes in pH 7.0 sodium phosphate or pH 8.5 1X TAE buffer at different concentrations of NaCl or $MgCl_2$.

	Buffer	Salt	Salt Conc. (mM)	T_m (°C)	Ref.
PNA•DNA[a]	10 mM NaPi	NaCl	20	72	[73]
			150	70	
DNA•DNA[a]	10 mM NaPi	NaCl	0	40	[73]
			20	48	
PNA2•DNA	H_2O	NaCl	15	72	
	10 mM NaPi		150	74	
	1 mM NaPi		0.125	66	
	10 mM NaPi		12.5	75	
		$MgCl_2$	1	78	
	1X TAE		6	77	
			12.5	76	
DNA•DNA	H_2O	$MgCl_2$	0.125	43	
	1 mM NaPi		0.125	41	
			1	40	
	1X TAE		6	56	
			12.5	57	

[a] The 15-bp hetero- and homo-PNA•DNA duplex has the same sequence N(5)'-TAGACGTCA CAACTA-C(3)'. The complementary DNA strand is 3'-ATCTGCAGTGTTGAT-5'.[73]

Representative melting curves are shown in Figure III-11. The melting curve of DNA•DNA duplex has a slightly sharper transition around the melting temperature of duplex than the PNA•DNA duplex, which demonstrated a higher cooperativity of the base pairs formation in the DNA•DNA duplex than that of the PNA•DNA duplexes. However, the melting curves of PNA•DNA duplex shifted significantly to higher temperature compared to DNA•DNA duplex, indicating the great thermodynamic driving force of the strand invasion of PNA in DNA origami. The same result is found for both pH 7.0 sodium phosphate buffer (Figure III-11a) and pH 8.5 1X TAE buffer (Figure III-11b).

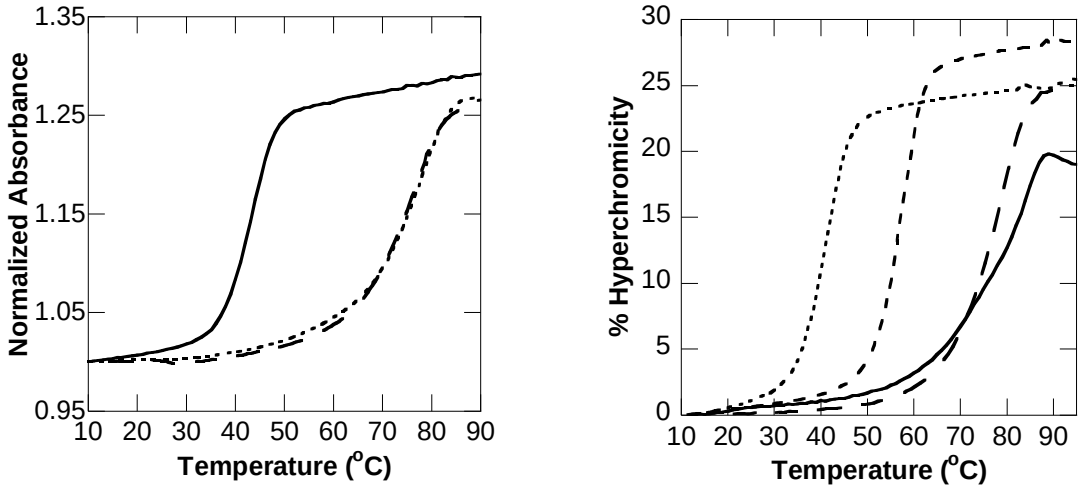

(a) (b)

Figure III-11. (a) Melting curves of DNA•DNA duplex in 0.125 mM $MgCl_2$ (solid line), PNA•DNA duplex in 150 mM NaCl (dotted line) or 12.5 mM $MgCl_2$ (dashed line) solutions. (b) Comparison of the ionic effect on melting temperatures of 1 mM $MgCl_2$ for DNA•DNA duplex (dotted line) and PNA•DNA duplex (solid line) or 12.5 mM $MgCl_2$ for DNA•DNA duplex (short dashed line) and PNA•DNA duplex (long dashed line) on the melting temperatures of homo- and hetero-duplexes in 1X TAE buffer.

III.2.iii Binding of PNA to DNA origami

To test the feasibility of PNA modification on DNA origami, a short sequence PNA1 was used first to modified three sites on the DNA origami. Two of the sites are located at the corners of the origami with the same protruding single strand. The third site is located at one edge of the origami with the intrinsic sequence inside the DNA origami. AFM image showed that both types of sites at the corner and on the edge could be modified with PNA strands labeled with AuNPs (Figure III-12b and c). However, some DNA origami remains unmodified (Figure III-12a). Additionally, aggregations of AuNPs were also observed due to the lack of charge on PNA. Therefore, a different strategy of visualization of PNA binding with streptavidin is applied for the following study.

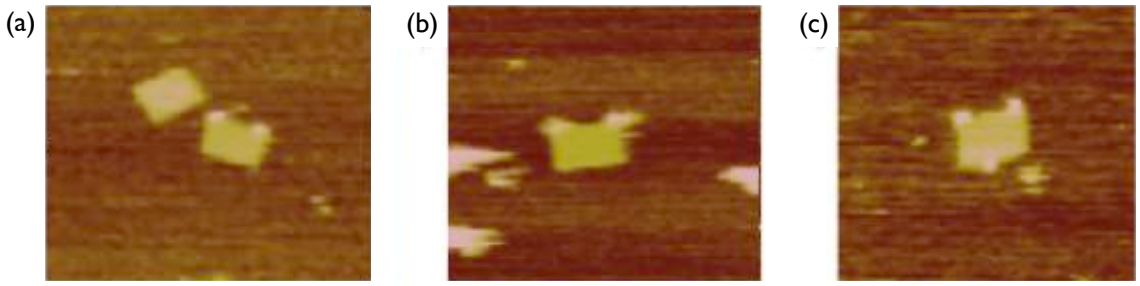

Figure III-12. From left to right, (a) origami with both corner sites bound and one without any bound AuNPs; (b) origami with both corner sites bound; (c) origami with all 3 sites bound to AuNPs. This occurs far less frequently due to the low affinity of the single intrinsic site.

To further evaluate the binding efficiency of PNA modification at different geometry sites on the DNA origami, we modified a DNA origami with three different binding sites for PNA2. The sites were chosen with different geometries and locations on the origami. These geometries include a single strand protruding at a corner. An imbedded site on the m13 scaffold along the edge of the origami structure and two protruding single strands complementary each to half of the PNA sequence so that they form a V shaped binding site at the center of the origami. To identify energy minima, we annealed DNA origami structures with both PNA2 and a DNA strand of identical sequence (DNAi). To bind streptavidin on the DNA origami, PNA2 was biotinylated through the thiol group, which gives PNA2b. Streptavidin was then added to a concentration of 2 uM and then the sample was imaged with AFM.

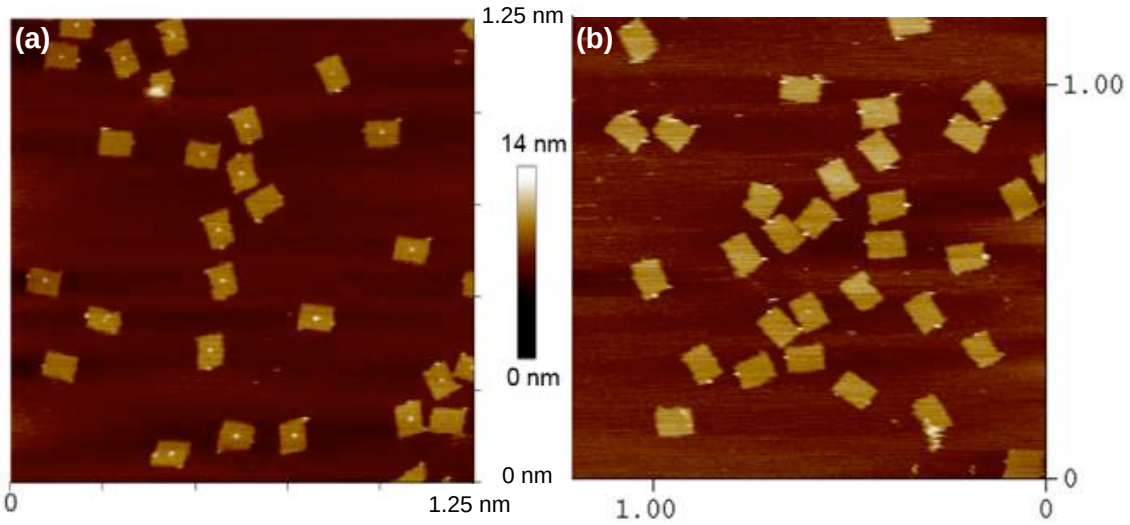

Figure III-13. AFM image of streptavidin attached DNA origami with PNA2b (a) or DNAi (b) bound to three different sites.

AFM analysis of the resulting structures illustrates the degree of binding at the three different locations (Figure III-13a and b). In order to archive statistical significant results, a total of 10 different micrographs were collected and analysed. The number of structures and binding events counted are listed in Table III-2. For each individual micrograph the binding rate was calculated. The mean value is displayed in Figure III-14.

An oligomer of 16 nucleotides generally does not have a high enough (higher than the melting temperature than the DNA origami itself) melting temperature to effectively target DNA nanostructures. Despite this, Figure III-13a shows that PNA2 targets the center site with a degree of binding and significantly higher than the two other sites. The 16 nucleotides DNA sequence on the other hand achieves almost zero binding at the

center site (Figure III-13b). Interestingly, it does show higher binding to the side site compared to the corner site.

Table III-2. Total number of counted origami structures and binding events.

	PNA2b	% of PNA2b	DNAi	% of DNAi
Origami	596	n/a	883	n/a
Center site	510	85.6 %	5	0.5 %
Edge site	322	54.0 %	458	51.9 %
Corner site	344	57.7 %	276	31.2 %

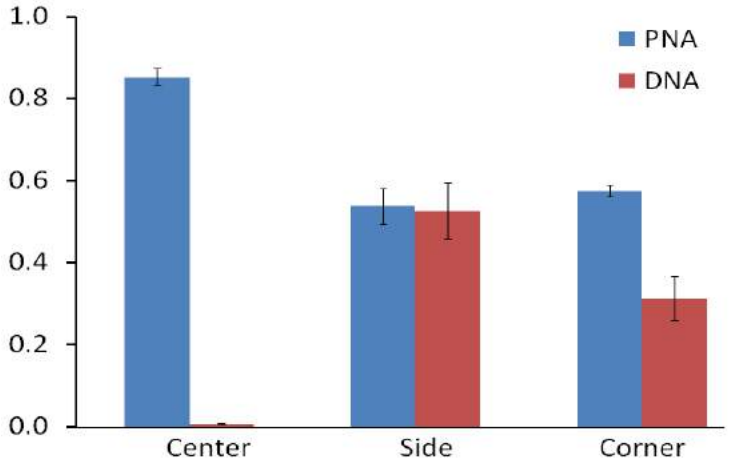

Figure III-14. Degree of binding of PNA2b and DNAi to the three different binding sites. Each micrograph was treated individually and the mean displayed with error bars representing standard deviation.

III.2.iv Duplex Invasion

We employed the method of initial rates to monitor the kinetics of the invasion by PNA of a DNA duplex attached to the DNA tiles (Figure III-10) that form a DNA array. The DNA duplex was labelled with a fluorophore and a quencher, such that the fluorescence of the fluorophore is quenched in the DNA duplex but turned on when PNA invades the duplex. The initial rates of the invasion were measured for different concentrations of both DNA duplex and PNA, which allowed us to determine the exponents in the rate equation $r = k[DNA]^X[PNA]^Y$. In this equation, [DNA] is the concentration of pre-annealed DNA duplex and [PNA] is the concentration of single stranded PNA. Figure III-15a shows representative graphs of the concentration of dissociated duplex following the addition of PNA; analysis of the data leads to values of 0.3 and 0.7 for X and Y, respectively. These values indicate the formation in the rate limiting step of a PNA•DNA hetero-structure that contains ss PNA and ds DNA in a 2:1. This result is in agreement with previous reports on the invasion by poly-T PNA of DNA duplexes.[79] Figure III-15c shows representative graphs of the initial rates of duplex dissociation at different ionic strengths. The initial rate constants are listed in Table III-3. The rate constant increases by almost an order of magnitude in going from 1 mM $MgCl_2$ to the 12.5 mM $MgCl_2$ solutions; the latter concentration is typically used for annealing DNA nanostructures.

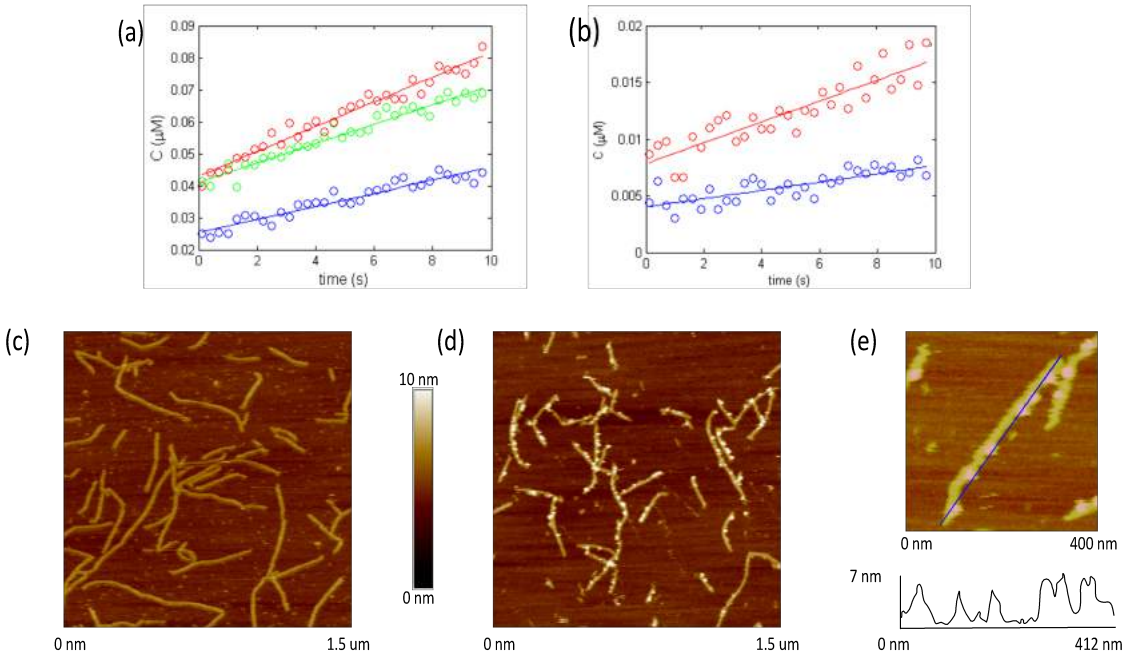

Figure III-15. (a) Representative graphs of initial rates at the following concentrations: O Red; 0.5 μM duplex and 1 μM PNA. O Green; 0.5 μM duplex and 2 μM PNA. O Blue; 1 μM duplex and 2 μM PNA. (b) Initial rates at O red; 6 mM $MgCl_2$ and O blue 12.5 mM $MgCl_2$. (c) Control sample with biotinylated DNA. (d) DNA arrays incubated at 1 mM MgCl2 with PNA2b and then imaged with STV. (e) Zoom of array with section contour.

Table III-3. Rate constants at different $MgCl_2$ concentrations.

	1 mM $MgCl_2$	6mM $MgCl_2$	12.5 mM $MgCl_2$
k ($s^{-1}M^{-1}$)	0.0025	0.00072	0.00034

Based on this information, we have annealed the DNA arrays that contained duplex invasion sites in 12.5 mM $MgCl_2$ buffer and then exchanged the buffer to one that contained 1 mM $MgCl_2$. We then added to the solution biotinylated PNA and incubated for >2 hours before depositing the DNA on mica. The samples deposited on mica were incubated with 1-2 μM solutions of STV in pH 7.0 12.5 mM $MgCl_2$ buffer and then

imaged with AFM. The control sample with biotinylated DNA added showed no STV localization on the arrays (Figure III-15c). The DNA samples treated with biotinylated PNA showed the STV protein localized as beads on a string (Figure III-15d). Figure III-15e shows an expanded view of 412 nm section of a DNA array that has 6 attached STVs. As each tile is 52 nucleotides long and the DNA base pair rise is ~0.3 nm, the 412 nm long array contains 24 tiles of which 6 display an STV. Hence, the yield of invasion for the array is 25%.

III.3 Discussion

To date, there is no publication on PNA modification on DNA origami. We are the first investigating the potential of PNA as a novel material for functionalization of DNA origami with significant advantage than DNA itself. The higher thermal stability of PNA•DNA than that of DNA•DNA is the key to successful hybridization of PNA to the complementary sites on DNA origami after the DNA origami is pre-annealed. The melting temperature of the 16-bp DNA is barely over 40 °C, which is far below the melting temperature of the DNA origami around 57 °C.[54] On the other hand, the melting temperature for the hetero-duplex PNA•DNA is as high as 78 °C (almost 40 °C higher than that of DNA•DNA), making the modification by PNA much more favorable. DNA, especially if designed to be at the center of the origami, linked with a functional group has to be annealed together with the DNA origami as one of the staple DNA to obtain a higher yield, while PNA can be added to modify the DNA origami after it is formed. This advantage of PNA over DNA offers the post treatment of DNA origami with different

PNA sequences each labeled separately with different functional groups such as proteins, AuNPs or capsids.

All of the three geometry-different sites on DNA origami showed a better binding efficiency (Table III-2 and Figure III-14) of PNA than that of DNA. Except the side location, which is only 2.1 % higher in binding efficiency, both locations at the corner and in the center of the DNA origami showed significant improvement on binding efficiency of PNA than that of DNA. At the corner, DNA only has 31.2 % of the sites successfully modified while PNA almost doubled the efficiency with 57.7 % of binding efficiency. DNA modification on the center of the DNA origami almost failed completely with only 0.5 % chance to bind with DNA origami. However for PNA, an excellent binding efficiency of 85.6 % was observed on the center of the DNA origami. Therefore, if a center modification is required post annealing, PNA is clearly a better choice than DNA to ensure successful modification. Notice that the facing preference of the DNA origami on mica for AFM imaging would have an effect on the binding efficiencies, especially at center of the DNA origami. However, the slight curvature of the DNA origami introduces a preference of DNA origami to land with one face upwards on the mica surfaced conditioned with Mg^{2+}. Even though this preference is 100 %, it does not pose any problem to change the result or the conclusion. Actually, with STV bond to biotin either beyond or beneath the structure, the STV is still visible under AFM. In the case of the DNA origami facing downward, the biotin is flexible enough to poke out of the DNA origami and binds with STV. In our experiments, to minimize the effect of the "hindered" biotin, the DNA origami is incubated with STV prior to putting the DNA origami on mica.

The other strategy to functionalize the DNA origami by invasion also showed an undeniable advantage over DNA. While no invasion was found by invasion of ssDNA, the invasion efficiency of 25 % by PNA is evidence that PNA invasion is a feasible method to modify DNA origami after the DNA origami is formed with all staple strands added instead of either leaving the exposed ssDNA without adding the complementary staple strands or using anchoring ssDNA as the extension on staple strand with extra targeting sequence added on the staple strand.

Another advantage of PNA over DNA, which is not examined in this study, is the cellular stability. The stability of PNA and of the PNA•DNA chimera in the presence of cellular enzymes were studied extensively and both are stable unlike DNA or peptide.[80-83] For cellular applications such as nano robot or nano device for drug delivery, which requires the introduction of key and fuse strands that are mostly single stranded, the stability of the single stranded nucleic acid is crucial for the device to function properly. In these applications, peptide nucleic acid is again a good candidate with excellent stability as DNA origami.[55]

Last but not the least, PNA functionalization of DNA origami opens a door to the dynamic nano structures with spontaneous changes such as structure transformation induced by the key and fuse strands made of PNA, real time signal of fluorescence or electrochemistry produced by the functional group on PNA target strand, or even instant collaboration between the functional groups on DNA origami. The dynamic changes can only be achieved by PNA given the current strategies in modification on DNA origami. The reason is that 1) modifications made by covalent bond cannot be formed or broken

easily at ambient conditions, 2) modifications made by ssDNA can only be achieved by lifting the temperature above the melting temperature of the DNA origami and slowly cooling down. For either cases listed above, there is no spontaneous dynamic changes happening on the DNA origami but only the final outcome.

III.4 Conclusions

We have shown that PNA behave differently than DNA in the context of DNA nanostructures as evidenced by the different binding distribution of DNA and PNA to a two dimensional DNA origami. Positive PNA probes can exploit the large density of negative charge at the center of DNA based nanostructures to more effectively bind targets with shorter complementary sequences, a feature that can be exploited in the design of DNA-based structures and devices. The strand invasion ability of PNA increases the toolbox for creating diverse, functional DNA devices. However more research is needed to understand the invasion mechanism before accurate and predictable nanoscale machinery can be built.

III.5 Experimental

Solid Phase PNA Synthesis. The PNA oligomer was synthesized by solid phase peptide synthesis using the Boc-protection strategy.[84] MBHA resin was downloaded with Boc-L-Lys-(4-MeOBzl)-OH (NovaBiochem) to an estimated loading of 0.05 mequiv/g. Boc group on resin is deprotected with 5 % *m*-cresol in trifluoroacetic acid (TFA). According to the sequence of the PNA oligomer, a Boc-protected PNA monomer (A, G,

T, or C) (ASM Research Chemicals) was coupled to the resin using O-Benzotriazole-N,N,N',N'-tetramethyluronium hexafluoro-phosphate (HBTU) (Peptides International) as a coupling agent. Unreacted $-NH_2$ sites on resin were capped by acetic anhydride. Finally, 5-aminovaleric acid (C_4) as a linker and 3-mercaptopropionic acid (C_2) as a source of –SH group were coupled at the end of the PNA oligomer to allow the functionalization of biotin. PNA oligomers were cleaved from the resin with TFA and trifluoromethanesulfonic acid (TFMSA), precipitated in diethyl ether, and dried with nitrogen. PNA oligomers were purified by reversed-phase HPLC using a C18 silica column on a Waters 600 model. Absorbance was measured at 260 nm with a Waters 2996 Photodiode Array Detector. Characterization of the oligomers was performed by MALDI-ToF mass spectrometry on an Applied Biosystems Voyager Biospectrometry Workstation with Delayed Extraction and an R-cyano-4-hydroxycinnamic acid matrix (10 mg/mL in 1:1 water/acetonitrile, 0.1% TFA). The PNA sequence synthesized for this study is Lys_3-ATGAATATAGTTGGGA-$C_4C_4C_2$. m/z for the PNA molecule $(M+H)^+$ were calculated and found to be 5127.2/5130.0. PNA solutions were prepared in nanopure water (>18.3 MΩ cm^{-1}) and stored at -18 °C to avoid depurination reactions. The concentration of PNA solutions was determined by UV-Vis spectrophotometry using ε at 260nm of 6,600, 8,600, 11,700, and 13,700 cm^{-1} M^{-1} for the C, T, G, and A monomers, respectively. For biotinylation, the PNA was first reduced using immobilized TCEP (Thermo Scientific) and then biotinylated with EZ-Link Maleimide-PEG2-Biotin2 (Thermo Scientific). The final product was purified by reverse phase HPLC.

UV-Vis Spectroscopy Melting Curves. UV melting curves were recorded at 260 nm in the temperature range of 10-95 °C for both cooling and heating modes, at the rate of 1

°C/min. Prior to cooling, the 3 μM solutions of the complementary ss PNAs in 1X TAE and different concentration of $MgCl_2$ were kept at 95 °C for 10 min. T_m is the inflection point of a sigmoidal function used to fit the melting curve. The DNA strands used in melting curves were purchased from Integrated DNA Technologies.

DNA Origami. Origami structures were annealed with 10x concentration of staple strands (Integrated DNA Technologies) in 1xTAE/Mg2+ (Tris, 40 mM; acetic acid, 20 mM; EDTA, 2 mM; and magnesium acetate, 12.5 mM; pH 8.0) and annealed from 90 to 4 °C over the course of 2 hours. Origami structures were purified using Microcon 100,000 MWCO filter spin units.

PNA Biotinylation. PNA2 was biotinylated to create PNA2b. Biotinylatin was done by reducing the terminal thiol with immobilized TCEP (Thermo scientific) and then incubating ON with biotin-maleimide (sigma-aldrich).

Binding of PNA, AuNPs and Streptavidin to DNA Origami. PNA was included in the annealing procedure at 10x excess in order to probe the thermodynamic rather than the kinetic binding landscape. Streptavidin was added to samples in solution and incubated for at least two hours at room temperature before imaging with AFM. 3 mg of bis(p-sulfonatophenyl)phenylphosphine (BSPP, Sigma-Aldrich) were added to 10 ml of purchased AuNP solution (British Biocell International). After overnight incubation, the AuNPs were concentrated by adding 260 mg of NaCl and centrifuging for 30 min at 800 g. The supernatant was removed without disturbing the visible Au pellet. 200 ml of methanol and 200 ul of BSPP (3 mg in 10 ml DI water) were added, after which the

solution was centrifuged a second time for 30 min. The supernatant was again removed and the AuNPs were resuspended in the same BSPP solution to a total volume of 200 ul. Typical AuNP concentrations were 2-3 mM. PNA was added at a ratio of 2 strands per gold particle (more strands induce aggregation). Functionalized particles where added to origami adsorbed on mica surface and incubated for 30 min before AFM imaging.

AFM. Origami samples were mixed incubated in 1-2 μM STV solutions at room temperature for 1-2 hours. Then 5 μl samples were placed on freshly cleaved mica. DNA array samples were placed directly on freshly cleaved mica to which 1-2 μM STV solutions were added. AFM images were obtained on a Digital Instruments Nanoscope III (Vecco, USA) using NP–S oxide-sharpened silicon nitride tips (Vecco, USA) with a multimode head and fluid cell in tapping mode under buffer.

Fluorescence Spectroscopy. Fluorescence data were collected using a Cary Eclipse Fluorescence Spectrophotometer from Varian, with temperature controller set to 23°C. Excitation and emission wavelengths were 648 and 668 nm with a 5 nm bandwidth. Complementary DNA strands with fluorophore “Cy5” and quencher “Iowa Black RQ” were purchased from IDT and pre-annealed in TAE buffer with specified $MgCl_2$ concentration by incubating at 90 °C for 5 min and then cooling to room temperature. PNA was added and mixed within a 10 sec period and data points were recorded every 0.1 sec and subsequently averaged with a three data point period. Fluorescence data was translated to concentration values by setting base level to 0 μM dissociated duplex and recording maximum fluorescence following thermal melting and annealing of duplex

with PNA and equating this to the original concentration of duplex. A 10 second period following mixing was used to fit a linear equation giving the initial rate of reaction. All rates were measured in triplicate and the average used to calculate the exponents in the rate equation.

III.6 References

(1) Yan, H. *Science* **2004**, *306*, 2048.

(2) Krishnan, Y.; Simmel, F. C. *Angew. Chem., Int. Ed.* **2011**, *50*, 3124.

(3) Bhatia, D.; Sharma, S.; Krishnan, Y. *Curr. Opin. Biotechnol.* **2011**, *22*, 475.

(4) Dietz, H.; Douglas, S. M.; Shih, W. M. *Science* **2009**, *325*, 725.

(5) Rothemund, P. W. K. *Nature* **2006**, *440*, 297.

(6) Seeman, N. C. *Annu. Rev. Biochem.* **2010**, *79*, 65.

(7) Liu, X.; Xu, Y.; Yu, T.; Clifford, C.; Liu, Y.; Yan, H.; Chang, Y. *Nano letters* **2012**, *12*, 4254.

(8) Verena J. Schuller, S. H., Nadja Sandholzer, Philipp C. Nickels, Nina A. Suhartha, Stefan Endres, Carole Bourquin, Tim Liedl† *ACS Nano* **2011**, *5*, 9696.

(9) Li, J.; Pei, H.; Zhu, B.; Liang, L.; Wei, M.; He, Y.; Chen, N.; Li, D.; Huang, Q.; Fan, C. *ACS nano* **2011**, *5*, 8783.

(10) Samano, E. C.; Pilo-Pais, M.; Goldberg, S.; Vogen, B. N.; Finkelstein, G.; LaBean, T. H. *Soft Matter* **2011**, *7*, 3240.

(11) Ding, B.; Deng, Z.; Yan, H.; Cabrini, S.; Zuckermann, R.; Bokor, J. *Journal of the American Chemical Society* **2010**, *132*, 3248.

(12) Pilo-Pais, M.; Goldberg, S.; Samano, E.; Labean, T. H.; Finkelstein, G. *Nano letters* **2011**, *11*, 3489.

(13) Chen, Z.; Lan, X.; Wang, Q. *Small* **2013**, *9*, 3567.

(14) Endo, M.; Yang, Y.; Emura, T.; Hidaka, K.; Sugiyama, H. *Chemical communications (Cambridge, England)* **2011**, *47*, 10743.

(15) Schreiber, R.; Do, J.; Roller, E.-M.; Zhang, T.; Schüller, V. J.; Nickels, P. C.; Feldmann, J.; Liedl, T. *Nature nanotechnology* **2014**, *9*, 74.

(16) Sharma, J.; Chhabra, R.; Andersen, C. S.; Gothelf, K. V.; Yan, H.; Liu, Y. *Journal of the American Chemical Society* **2008**, *130*, 7820.

(17) Ding, B.; Deng, Z.; Yan, H.; Cabrini, S.; Zuckermann, R. N.; Bokor, J. *J. Am. Chem. Soc.* **2010**, *132*, 3248.

(18) Hung, A. M.; Micheel, C. M.; Bozano, L. D.; Osterbur, L. W.; Wallraff, G. M.; Cha, J. N. *Nat Nano* **2010**, *5*, 121.

(19) Chen, Z.; Lan, X.; Wang, Q. *Small (Weinheim an der Bergstrasse, Germany)* **2013**, 3567.

(20) Voigt, N. V.; Torring, T.; Rotaru, A.; Jacobsen, M. F.; Ravnsbaek, J. B.; Subramani, R.; Mamdouh, W.; Kjems, J.; Mokhir, A.; Besenbacher, F.; Gothelf, K. V. *Nature Nanotechnology* **2010**, *5*, 200.

(21) Jahn, K.; Tørring, T.; Voigt, N. V.; Sørensen, R. S.; Bank Kodal, A. L.; Andersen, E. S.; Gothelf, K. V.; Kjems, J. *Bioconjugate Chemistry* **2011**, *22*, 819.

(22) Yoshidome, T.; Endo, M.; Kashiwazaki, G.; Hidaka, K.; Bando, T.; Sugiyama, H. *Journal of the American Chemical Society* **2012**, *134*, 4654.

(23) He, Y.; Tian, Y.; Ribbe, A. E.; Mao, C. *Journal of the American Chemical Society* **2006**, *128*, 12664.

(24) Chhabra, R.; Sharma, J.; Ke, Y.; Liu, Y.; Rinker, S.; Lindsay, S.; Yan, H. *Journal of the American Chemical Society* **2007**, *129*, 10304.

(25) Shen, W.; Zhong, H.; Neff, D.; Norton, M. L. *Journal of the American Chemical Society* **2009**, *131*, 6660.

(26) Williams, B. a. R.; Lund, K.; Liu, Y.; Yan, H.; Chaput, J. C. *Angewandte Chemie (International ed. in English)* **2007**, *46*, 3051.

(27) Saccà, B.; Meyer, R.; Erkelenz, M.; Kiko, K.; Arndt, A.; Schroeder, H.; Rabe, K. S.; Niemeyer, C. M. *Angewandte Chemie International Edition* **2010**, *49*, 9378.

(28) Meyer, R.; Niemeyer, C. M. *Small* **2011**, *7*, 3211.

(29) Carter, J. D.; LaBean, T. H. *ACS nano* **2011**, *5*, 2200.

(30) Nakata, E.; Liew, F. F.; Uwatoko, C.; Kiyonaka, S.; Mori, Y.; Katsuda, Y.; Endo, M.; Sugiyama, H.; Morii, T. *Angew. Chem. Int. Ed.* **2012**, *51*, 2421.

(31) Tian, Y.; He, Y.; Chen, Y.; Yin, P.; Mao, C. *Angewandte Chemie, International Edition* **2005**, *44*, 4355.

(32) He, Y.; Chen, Y.; Liu, H.; Ribbe, A. E.; Mao, C. *Journal of the American Chemical Society* **2005**, *127*, 12202.

(33) Andersen, E. S.; Dong, M.; Nielsen, M. M.; Jahn, K.; Subramani, R.; Mamdouh, W.; Golas, M. M.; Sander, B.; Stark, H.; Oliveira, C. L. P.; Pedersen, J. S.; Birkedal, V.; Besenbacher, F.; Gothelf, K. V.; Kjems, J. *Nature (London, United Kingdom)* **2009**, *459*, 73.

(34) Han, D.; Pal, S.; Nangreave, J.; Deng, Z.; Liu, Y.; Yan, H. *Science* **2011**, *332*, 342.

(35) Park, S. Y.; Lytton-Jean, A. K. R.; Lee, B.; Weigand, S.; Schatz, G. C.; Mirkin, C. A. *Nature* **2008**, *451*, 553.

(36) MacFarlane, R. J.; Lee, B.; Jones, M. R.; Harris, N.; Schatz, G. C.; Mirkin, C. A. *Science (Washington, DC, United States)* **2011**, *334*, 204.

(37) Pistol, C.; Dwyer, C.; Lebeck, A. R. *Micro, IEEE* **2008**, *28*, 7.

(38) Strano, M. S. *Science* **2012**, *338*, 890.

(39) Fu, J.; Liu, M.; Liu, Y.; Yan, H. *Accounts of Chemical Research* **2012**, *45*, 1215.

(40) Douglas, S. M.; Bachelet, I.; Church, G. M. *Science* **2012**, *335*, 831.

(41) Braun, E.; Eichen, Y.; Sivan, U.; Ben-Yoseph, G. *Nature (London)* **1998**, *391*, 775.

(42) Pearson, A. C.; Liu, J.; Pound, E.; Uprety, B.; Woolley, A. T.; Davis, R. C.; Harb, J. N. *Journal of Physical Chemistry B* **2012**, *116*, 10551.

(43) Ding, B.; Deng, Z.; Yan, H.; Cabrini, S.; Zuckermann, R. N.; Bokor, J. *Journal of the American Chemical Society* **2010**, *132*, 3248.

(44) Pal, S.; Deng, Z.; Ding, B.; Yan, H.; Liu, Y. *Angewandte Chemie, International Edition* **2010**, *49*, 2700.

(45) Pal, S.; Dutta, P.; Wang, H.; Deng, Z.; Zou, S.; Yan, H.; Liu, Y. *Journal of Physical Chemistry C* **2013**, *117*, 12735.

(46) Sacca, B.; Meyer, R.; Erkelenz, M.; Kiko, K.; Arndt, A.; Schroeder, H.; Rabe, K. S.; Niemeyer, C. M. *Angewandte Chemie, International Edition* **2010**, *49*, 9378.

(47) Stephanopoulos, N.; Liu, M.; Tong, G. J.; Li, Z.; Liu, Y.; Yan, H.; Francis, M. B. *Nano Letters* **2010**, *10*, 2714.

(48) Zhao, Z.; Liu, Y.; Yan, H. *Organic & Biomolecular Chemistry* **2013**, *11*, 596.

(49) Nie, Z.; Li, X.; Li, Y.; Tian, C.; Wang, P.; Mao, C. *Chemical Communications (Cambridge, United Kingdom)* **2013**, *49*, 2807.

(50) Liu, M.; Fu, J.; Hejesen, C.; Yang, Y.; Woodbury, N. W.; Gothelf, K.; Liu, Y.; Yan, H. *Nature Communications* **2013**, *4*, 2127/1.

(51) Ke, Y.; Sharma, J.; Liu, M.; Jahn, K.; Liu, Y.; Yan, H. *Nano Letters* **2009**, *9*, 2445.

(52) Liu, Z.; Li, Y.; Tian, C.; Mao, C. *Biomacromolecules* **2013**, *14*, 1711.

(53) Zhao, Z.; Jacovetty, E. L.; Liu, Y.; Yan, H. *Angewandte Chemie, International Edition* **2011**, *50*, 2041.

(54) Wei, X.; Nangreave, J.; Jiang, S.; Yan, H.; Liu, Y. *Journal of the American Chemical Society* **2013**, *135*, 6165.

(55) Mei, Q.; Wei, X.; Su, F.; Liu, Y.; Youngbull, C.; Johnson, R.; Lindsay, S.; Yan, H.; Meldrum, D. *Nano Letters* **2011**, *11*, 1477.

(56) Nielsen, P. E.; Egholm, M. *Current issues in molecular biology* **1999**, *1*, 89.

(57) De Costa, N. T. S.; Heemstra, J. M. *PloS one* **2013**, *8*, e58670.

(58) Nielsen, P. E.; Egholm, M. *Curr. Issues Mol. Biol.* **1999**, *1*, 89.

(59) Flory, J. D.; Shinde, S.; Lin, S.; Liu, Y.; Yan, H.; Ghirlanda, G.; Fromme, P. *Journal of the American Chemical Society* **2013**, *135*, 6985.

(60) Mischiati, C.; Borgatti, M.; Bianchi, N.; Rutigliano, C.; Tomassetti, M.; Feriotto, G.; Gambari, R. *J. Biol. Chem.* **1999**, *274*, 33114.

(61) Saviano, M.; Romanelli, A.; Bucci, E.; Pedone, C.; Mischiati, C.; Bianchi, N.; Feriotto, G.; Borgatti, M.; Gambari, R. *J. Biomol. Struct. Dyn.* **2000**, *18*, 353.

(62) Lukeman, P. S.; Mittal, A. C.; Seeman, N. C. *Chemical communications (Cambridge, England)* **2004**, 1694.

(63) Chakrabarti, R.; Klibanov, A. M. *Journal of the American Chemical Society* **2003**, *125*, 12531.

(64) Xiaodi, S.; Kanjanawarut, R. *ACS Nano* **2009**, *3*, 2751.

(65) Ananthanawat, C.; Hoven, V. P.; Vilaivan, T.; Su, X. *Biosensors & bioelectronics* **2011**, *26*, 1918.

(66) Kameshima, W.; Ishizuka, T.; Minoshima, M.; Yamamoto, M.; Sugiyama, H.; Xu, Y.; Komiyama, M. *Angewandte Chemie International Edition* **2013**, *52*, 13681.

(67) Stadler, A. L.; Sun, D.; Maye, M. M.; Lelie, D. V. D.; Gang, O. *ACS Nano* **2011**, 2467.

(68) Sun, D.; Stadler, A. L.; Gurevich, M.; Palma, E.; Stach, E.; van der Lelie, D.; Gang, O. *Nanoscale* **2012**, *4*, 6722.

(69) Ackermann, D.; Famulok, M. *Nucleic acids research* **2013**, *41*, 4729.

(70) Yamazaki, T.; Aiba, Y.; Yasuda, K.; Sakai, Y.; Yamanaka, Y.; Kuzuya, A.; Ohya, Y.; Komiyama, M. *Chemical communications (Cambridge, England)* **2012**, *48*, 11361.

(71) Gu, H.; Chao, J.; Xiao, S.-J.; Seeman, N. C. *Nature* **2010**, *465*, 202.

(72) Andersen, E. S.; Dong, M.; Nielsen, M. M.; Jahn, K.; Subramani, R.; Mamdouh, W.; Golas, M. M.; Sander, B.; Stark, H.; Oliveira, C. L. P.; Pedersen, J. S.; Birkedal, V.; Besenbacher, F.; Gothelf, K. V.; Kjems, J. *Nature* **2009**, *459*, 73.

(73) Tomac, S.; Sarkar, M.; Ratilainen, T.; Wittung, P.; Nielsen, P. E.; Norde´n, B.; Graslund, A. *Journal of the American Chemical Society* **1996**, *118*, 5544.

(74) Rothemund, P. W. K. *Nature* **2006**, *440*, 297.

(75) Baker, B. a.; Mahmoudabadi, G.; Milam, V. T. *Soft Matter* **2013**, *9*, 11160.

(76) LaBean, T. H.; Yan, H.; Kopatsch, J.; Liu, F.; Winfree, E.; Reif, J. H.; Seeman, N. C. *Journal of the American Chemical Society* **2000**, *122*, 1848.

(77) Li, H.; Park, S. H.; Reif, J. H.; LaBean, T. H.; Yan, H. *Journal of the American Chemical Society* **2004**, *126*, 418.

(78) Tomac, S.; Sarkar, M.; Ratilainen, T.; Wittung, P.; Nielsen, P. E.; Norden, B.; Graeslund, A. *Journal of the American Chemical Society* **1996**, *118*, 5544.

(79) Wittung, P.; Nielsen, P.; Norde, B. *Journal of the American Chemical Society* **1996**, *118*, 7049.

(80) Borgatti, M.; Romanelli, A.; Saviano, M.; Pedone, C.; Lampronti, I.; Breda, L.; Nastruzzi, C.; Bianchi, N.; Mischiati, C.; Gambari, R. *Oncology Research* **2003**, *13*, 279.

(81) Gambari, R. *Current Medicinal Chemistry* **2004**, *11*, 1253.

(82) Maier, M. A.; Esau, C. C.; Siwkowski, A. M.; Wancewicz, E. V.; Albertshofer, K.; Kinberger, G. A.; Kadaba, N. S.; Watanabe, T.; Manoharan, M.; Bennett, C. F.; Griffey, R. H.; Swayze, E. E. *Journal of Medicinal Chemistry* **2006**, *49*, 2534.

(83) Garner, P.; Sherry, B.; Moilanen, S.; Huang, Y. *Bioorganic & Medicinal Chemistry Letters* **2001**, *11*, 2315.

(84) Nielsen, P. E.; Editor *Peptide Nucleic Acids: Protocols and Applications, Second Edition*, 2004.

CHAPTER IV. CHARGE TRANSFER IN MODIFIED PNA DUPLEXES IN SOLUTION

IV.1 Introduction

Nucleic acids are interesting building blocks for supramolecular assemblies because of their predictable and programmable Watson-Crick base pairing, which in turn makes possible the encoding of self-assembled three-dimensional architectures with specificity.[1-5] Hence nucleic acids have recently emerged as a novel material for nanotechnology applications.[6] Chemical synthesis has created either nucleic acid analogues, such as peptide nucleic acids (PNAs), or nucleic acids with functional groups, including redox centers and fluorophores, that impart functionality to the nucleic acid based nanostructures. These functionalized nucleic acids can therefore be utilized together with the encoding properties of nucleic acid to assemble three-dimensional molecular devices specializing in programmable, sequence specific, nucleic acid related sensing and responding.

Our lab and others[7-11] have appended to PNA electroactive groups, such as ferrocene (Fc),[12] ruthenocene (Rc), tris(bipyridine) ruthenium ($[Ru(Bpy)_3]^{2+}$), and other metal complexes with excellent electrochemistry and luminescence properties and studied the modified PNAs for different reasons, including to understand charge transfer,[9-11] to detect nucleic acids in a sequence-specific manner, to modulate the PNA•DNA hybridization

and use it for making gene-targeted drugs,[13-15] and to create molecular probes useful in the study of cellular biology.[16]

Several methods have been developed to incorporate functional groups in PNA. The substitution of the natural bases with metal complexes in PNA monomer is one strategy for the incorporate of ligand and/or metal complexes at specific, variable positions within a PNA strand. The most straightforward method to incorporate the metal complexes in PNA is by coupling the amino group at the N-end of PNA with the carboxylic acid group of a carboxy- or an acetic acid- derivative of the metal complex (Figure IV-1a and b).[15,17-19] The advantage of this method is the straightforward organic synthesis route. However, this strategy can only place the metal complexes at the N-end of the PNA. To overcome this limitation, other strategies were developed in Metzler-Nolte and other labs, such as click chemistry between azide derivatives of the metal complexes and alkynes on the backbone of nucleic acid monomer (Figure IV-1c)[20,21] or Sonogashira coupling between the alkyne derivatives of the metal complexes and aryl halides situated on either the side chain[22] or the base (Figure IV-1d)[23,24] of the nucleic acid monomer.

The incorporation of a $[Ru(Bpy)_3]^{2+}$ complex in PNA was first described by the Spiccia group.[25] They coupled the carboxylic acid derivative of the ruthenium complex to the PNA backbone through several different linkers (Figure IV-1e and f) and found that the linker had only a small effect on the luminescence and electrochemistry properties of the metal complex. Later Joshi et al. investigated the thermal stability of metalated PNA•DNA hetero-duplexes and compared their melting temperatures to that of non-modified ones.[26] The enhanced thermal stability of the metal-containing PNAs was

attributed to the stabilization effect of attractive electrostatic interaction between the cationic metal complex and the polyanionic DNA backbone. To increase the sensitivity in the detection of the metal complex label, Baldoli et al. synthesized a triferrocenyl PNA monomer.[27,28]

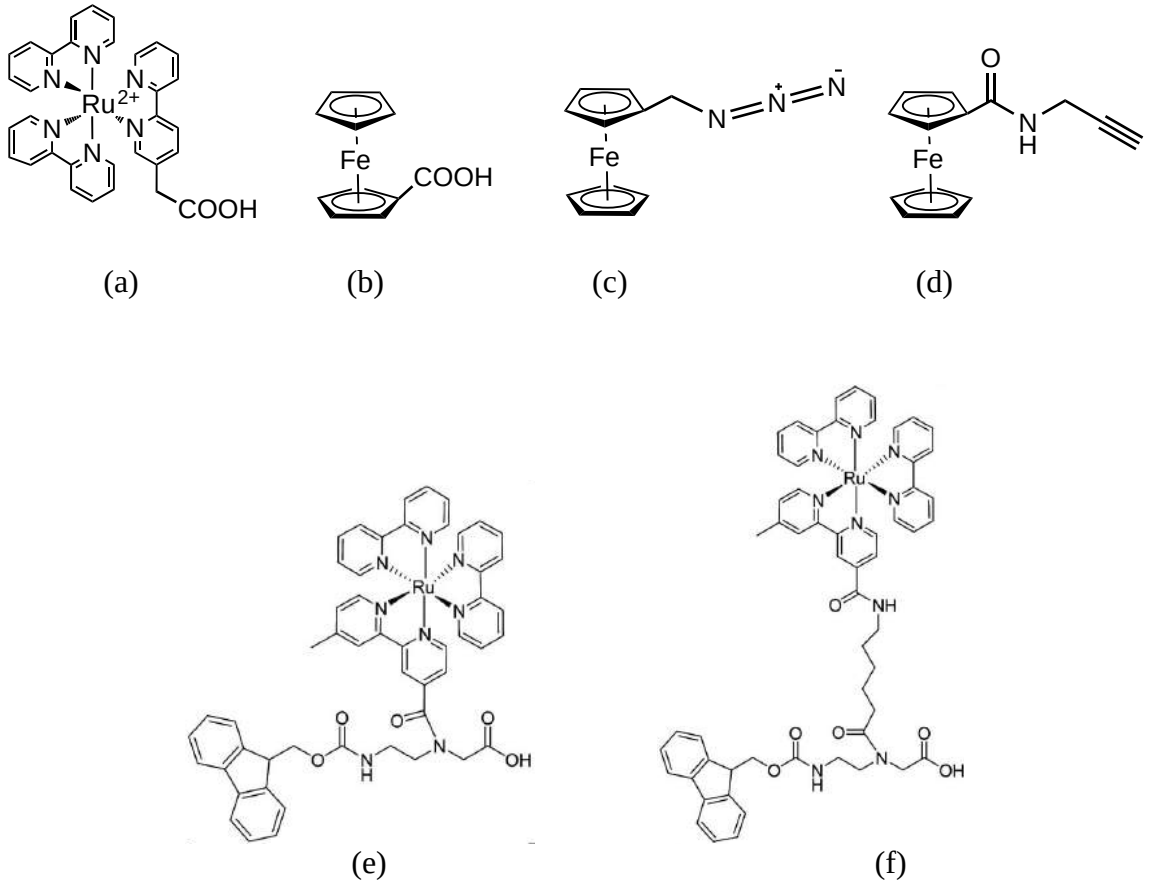

Figure IV-1. Chemical structures of moieties of metal complexes for incorporation in nucleic acids with alternative strategies.

The oxidative hole transfer and the reductive electron transfer in DNA-based systems have been extensively investigated.[29,30] The hole transfer can take place by superexchange-mediated tunneling over short distances (< 10 Å), by hopping over long

distances (up to 200 Å) or by a combination of the two mechanisms. The mechanism of the reductive electron transfer was less studied when compared to the detailed investigation of oxidative hole transfer in nucleic acids. Experimental and theoretical studies have suggested that cytosine (C) and thymine (T) may be responsible for the reductive electron transfer. Although T and C have comparable reduction potentials, the slightly lower reduction potential of T renders it the favorable intermediate for electron transfer.[31-35] It was proposed that the electron transfer occurs by hopping over long distances with the pyrimidine radical anions being the intermediate electron carrier.[36] γ-pulse radiolysis studies showed that the electron transfer in DNA follows a superexchange-mediated electron tunneling mechanism below 77 K and that the rate constant is distance dependent.[37-39] Below 170 K, the electron transfer is mainly intermediated by $T^{\bullet-}$ instead of $C^{\bullet-}$. Above 170 K, a thermally activated hopping mechanism governs the electron transfer in DNA.

In contrast to photoinduced hole and electron transfer through DNA in solution, which have been studied extensively, studies of charge transfer through PNA in solution have not yet been reported. Such studies of PNA can help elucidate fundamental features of charge transfer in nucleic acids in general, and thus provide information useful for the pursuit of nucleic acid based molecular devices in electronic, biomedical, and nanotechnological applications.

IV.2 Research Design

In order to study photoinduced electron transfer through PNA in solution, we chose $[Ru(Bpy)_3]^{2+}$ and [Cu(8-hydroxyquinolinate)$_2$] [Cu**Q**$_2$] as electron donor and acceptor, respectively. A PNA monomer that contains a $[Ru(Bpy)_3]^{2+}$ complex tethered to the PNA backbone was synthesized (Figure IV-2a) and was introduced into PNA oligomers at different positions, terminal and central, by solid phase peptide synthesis. When the $[Ru(Bpy)_3]^{2+}$ complex was situated in a central position of the duplex, an abasic PNA monomer in which the secondary amine of the backbone unit, N-2(-aminoethyl) glycine (aeg), was capped with an acetyl group (Figure IV-2b) was introduced at the position complementary to the Ru complex. The acceptor was created by Cu^{2+} coordination to a pair of 8-hydroxyquinoline ligands (**Q**) situated in complementary positions in the duplexes (Figure IV-2c).[40,41]

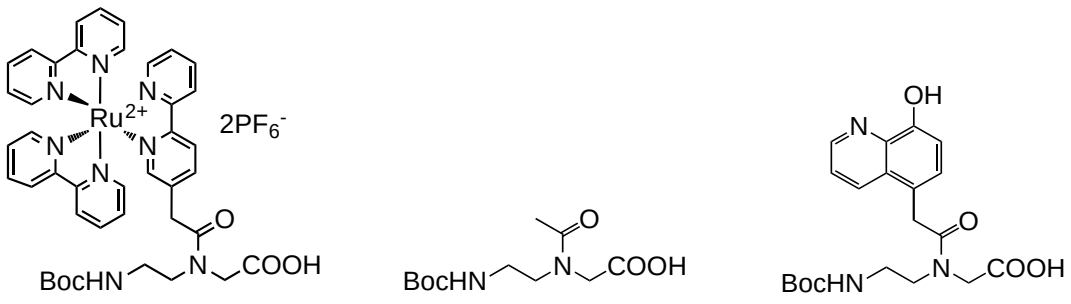

(a) (b) (c)

*Figure IV-2.The structure of the PNA monomers that contain (a) $[Ru(Bpy)_3]^{2+}$ (**R**); (b) backbone unit (**B**); and (c) 8-hydroxyquinoline (**Q**).*

IV.3 Results

IV.3.i PNA synthesis

Table IV-1 shows the sequences of the PNA duplexes synthesized for this study. PNA monomers that contains $[Ru(Bpy)_3]^{2+}$, backbone, and 8-hydroxyquinoline are represented with symbol **R**, **B** and **Q**, individually. In these duplexes, the donor and acceptor are separated by two or five base pairs. For the case of two base pairs, the chemical nature of the base pairs was varied. The position of the Donor–PNA bridge-Acceptor unit in the PNA duplexes was also varied from center to terminal position. The sequence design is based on the well studies 10-bp PNA duplex (**P**). The unit of Donor–PNA bridge-Acceptor is either inserted or replacing the base pairs in the duplex P.

Table IV-1. PNA Duplexes and Sequences.

PNA	Sequences	Strand ID
P	H-AGTGATCTAC-Lys-NH_2	α
	H_2N-Lys-TCACTAGATG-H	β
P-R	H-AGTGATCTAC-Lys-NH_2	α
	H_2N-Lys-TCACTAGATG-**R**-H	β
P-AA	H-**R**-AA-**Q**-GATCTAC-Lys-NH_2	α
	H_2N-Lys-TT-**Q**-CTAGATG-H	β
P-AG	H-**R**-AG-**Q**-GATCTAC-Lys-NH_2	α
	H_2N-Lys-TC-**Q**-CTAGATG-H	β
P-AGTGA	H-**R**-AGTGA-**Q**-CTAC-Lys-NH_2	α
	H_2N-Lys-TCACT-**Q**-GATG-H	β
P-AA-P'	H-AGTGA-**R**-AT-**Q**-TCTAC-Lys-NH_2	α
	H_2N-Lys-TCACT-**B**-TA-**Q**-AGATG-H	β
P-AG-P'	H-AGTGA-**R**-AG-**Q**-TCTAC-Lys-NH_2	α
	H_2N-Lys-TCACT-**B**-TC-**Q**-AGATG-H	β

IV.3.ii UV-Vis Spectroscopy Titrations

The binding of Cu^{2+} to the duplexes has been studied by UV-Vis titrations. For the PNA duplexes with $[Ru(Bpy)_3]^{2+}$ at either the terminal (Figure IV-3) or the center (Figure IV-4), the spectroscopic changes of the UV titrations were observed as a bathochromic shift from 247 to 260 nm, which is the diagnostic peak shift for the binding between Cu^{2+} and **Q** observed in all the other **Q**-modified PNA duplexes. Therefore the wavelengths at 247 and 260 nm were used to monitor the change in the UV spectra. From the titration curves, the stoichiometry between Cu^{2+} and ligand **Q** is 0.3 and 0.4 for the ratio of Cu/ssPNA when $[Ru(Bpy)_3]^{2+}$ is positioned two base pairs away at the terminal (Figure IV-3) and the center (Figure IV-4), respectively.

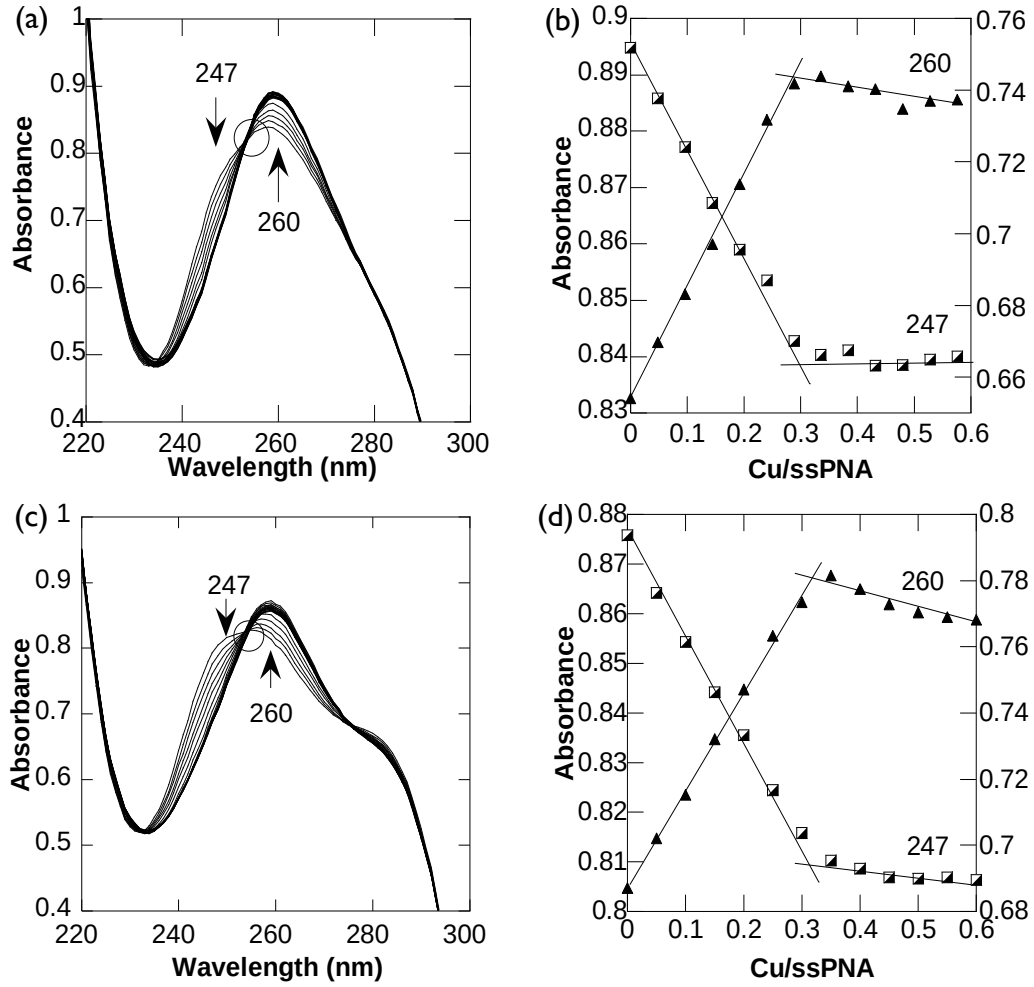

Figure IV-3. Titration spectra of 5 μM solution of (a) ***P-AA*** *and (b)* ***P-AG****. Titration curves of 5 μM solution of (a)* ***P-AA*** *and (b)* ***P-AG*** *by 0.4 mM $CuCl_2$ at 260 nm (▲) and 247 nm (◩) in pH 7.0 10 mM sodium phosphate buffer.*

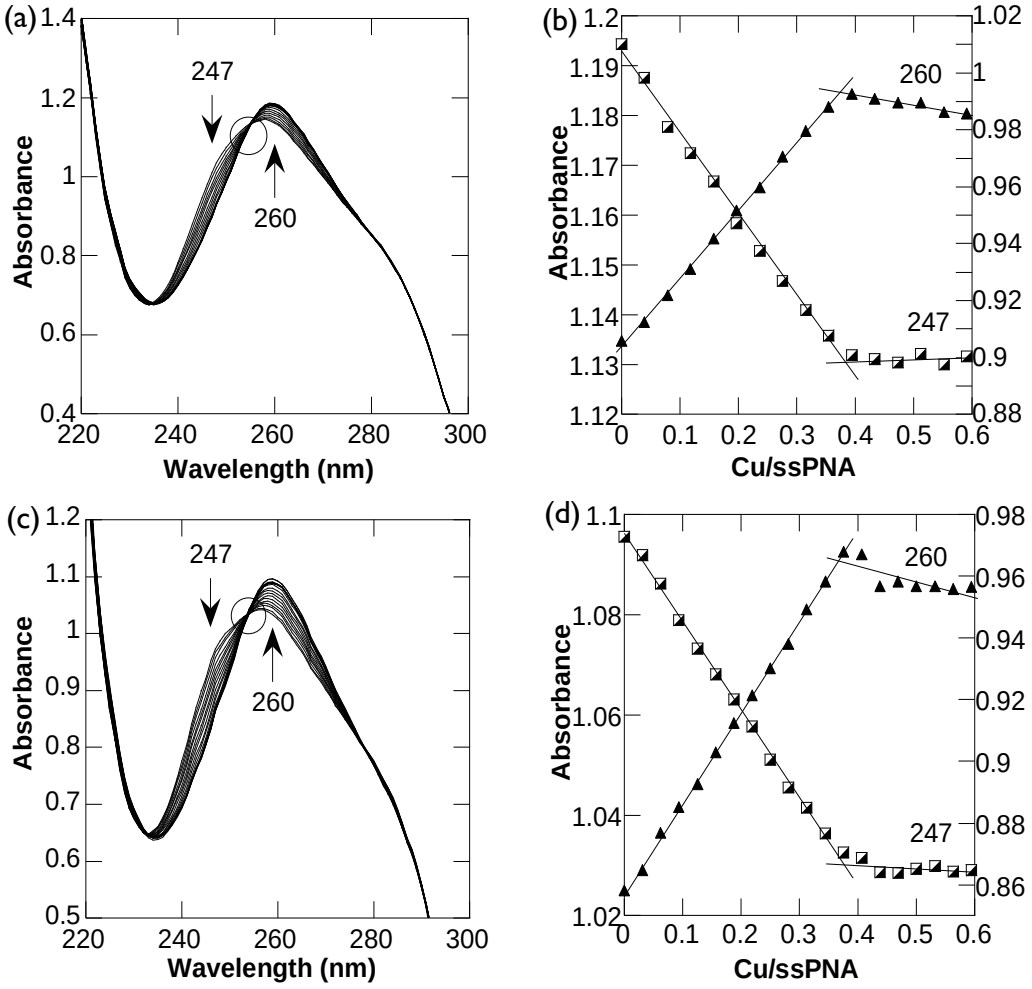

Figure IV-4. Titration spectra of 5 μM solution of (a) ***P-AA-P'*** *and (b)* ***P-AG-P'****. Titration curves of 5 μM solution of (a)* ***P-AA-P'*** *and (b)* ***P-AG-P'*** *by 0.4 mM $CuCl_2$ at 260 nm (▲) and 247 nm (◩) in pH 7.0 10 mM sodium phosphate buffer.*

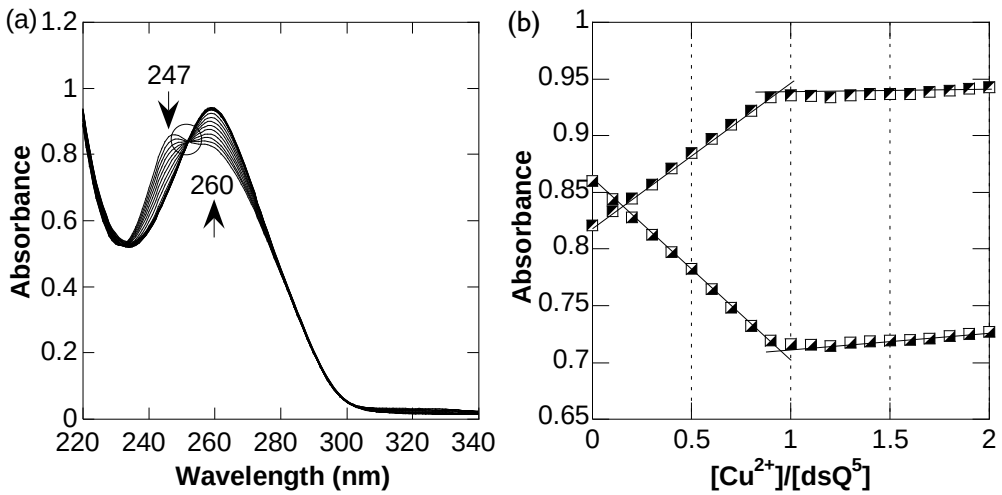

Figure IV-5. UV spectra of titration of 5 μM solution of dsQ^5 (a) with a 0.5 mM $CuCl_2$ solution, and titration curves of dsQ^5 (b) at 247 nm (◪) and 260 nm (◩) in pH = 7.7 10 mM Tris buffer in acetonitrile/water solvent (1/3, v/v).

Typically, the binding ratio of Cu/ssPNA is 0.5 between Cu^{2+} and **Q**-modified PNA with one copper bond per PNA duplex (Figure IV-5). To investigate the reason for the lower stoichiometry, a control experiment of ligand **Q** titration with Cu^{2+} in the presence of the $[Ru(Bpy)_3]^{2+}$ containing PNA monomer R was performed (Figure IV-6). The bathochromic shift from 240 to 254 nm resembles the titration of ligand **Q** with Cu^{2+} in the absence of R and the titration curves showed a 0.5 ratio of Cu/**Q**. This result showed that the complex $[Ru(Bpy)_3]^{2+}$ does not interfere with the titration of **Q** by Cu^{2+}. The lower stoichiometry only occurs when the complex $Ru(Bpy)_3]^{2+}$ and the ligand **Q** are tethered with one another in the same PNA strand. Therefore, we attribute this lower stoichiometry of Cu/ssPNA a result of the steric interactions between the $[Ru(Bpy)_3]^{2+}$ complex and the ligand **Q**, which have a stronger effect when the $[Ru(Bpy)_3]^{2+}$ complex is at the (fraying) end of the duplex (Cu/ssPNA is 0.3) than when the complex is in the middle of the duplex (Cu/ssPNA is 0.4).

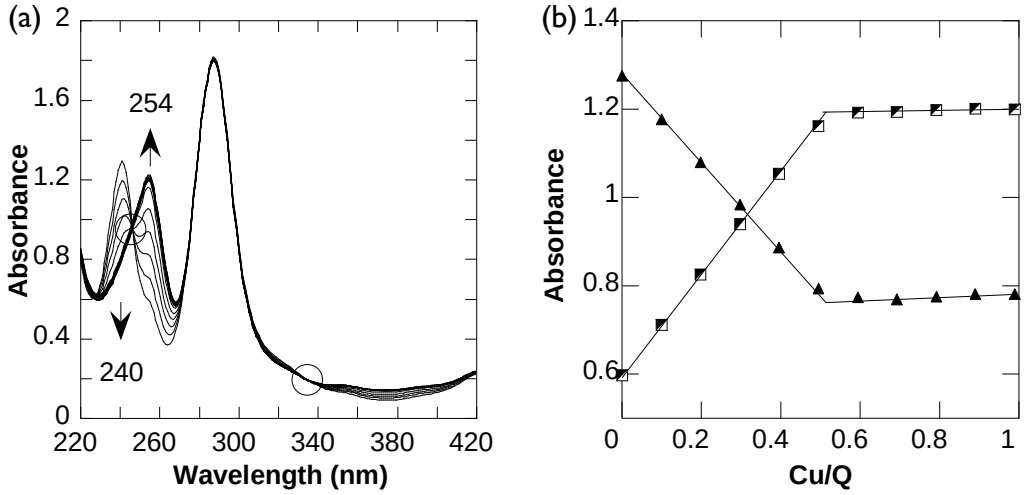

*Figure IV-6. Titration spectra (a) and curve (b) of a mixture of 20 μM ligand **Q** and 20 μM PNA monomer **R** by 0.4 mM $CuCl_2$ at 240 nm (◪) and 254 nm (▲) in pH 7.0 10 mM sodium phosphate buffer.*

This explanation is supported by two experimental facts. First, the titration of **P-AGTGA** by Cu^{2+}, where the complex is 5-bp instead of 2-bp away from ligand **Q**, showed a higher stoichiometry of Cu/ssPNA at 0.35 than that of **P-AG** and **P-AA** at 0.3 (Figure IV-7). Apparently the steric interaction between the $[Ru(Bpy)_3]^{2+}$ complex and the ligand **Q** is weaker when $[Ru(Bpy)_3]^{2+}$ and **Q** are farther apart (5-bp) than when they are closely situated (2-bp). Therefore, the weaker steric interaction in **P-AGTGA** coincides with the higher stoichiometry. The second fact that supports the explanation is that titrations with Cu^{2+} of the β strand of the **P-AG** duplex, which does not contain the $[Ru(Bpy)_3]^{2+}$ complex, changes in absorbance occurred up to a Cu/ssPNA ratio of 1:2 (Figure IV-8c and d), but for titrations of the α strand of the **P-AG** duplex, which contains the $[Ru(Bpy)_3]^{2+}$ complex, changes occurred only up to 1:3 values of the Cu/ssPNA ratio (Figure IV-8a and b). In addition, the ssPNA titration of a short 4-bp strand **Q**-AG-**R** by Cu^{2+} also showed a 0.3 stoichiometry at the selected wavelengths

(Figure IV-8e and f). These facts stated above reinforced the explanation that the lower stoichiometry is due to the steric interaction between $[Ru(Bpy)_3]^{2+}$ complex and ligand **Q**. The stoichiometry obtained by UV titrations was later confirmed by isothermal titration calorimetry in Section IV.3.v . The simulation of UV titration in Section IV.3.iv has shown that the formation of inter-duplex complex can also explain the low stoichiometry of UV titration.

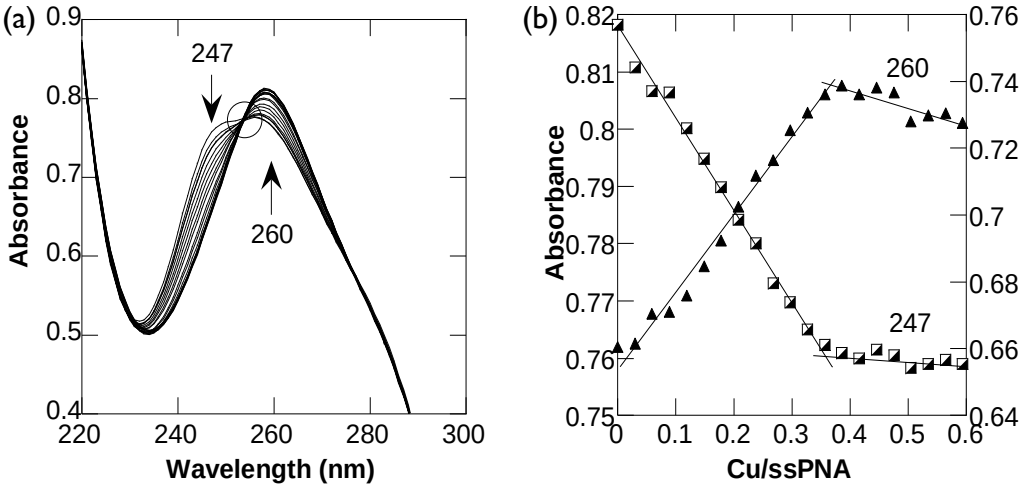

*Figure IV-7. Titration spectra (a) and curve (b) of 5 μM solution of **P-AGTGA** by 0.4 mM $CuCl_2$ at 260 nm (▲) and 247 nm (◪) in pH 7.0 10 mM sodium phosphate buffer.*

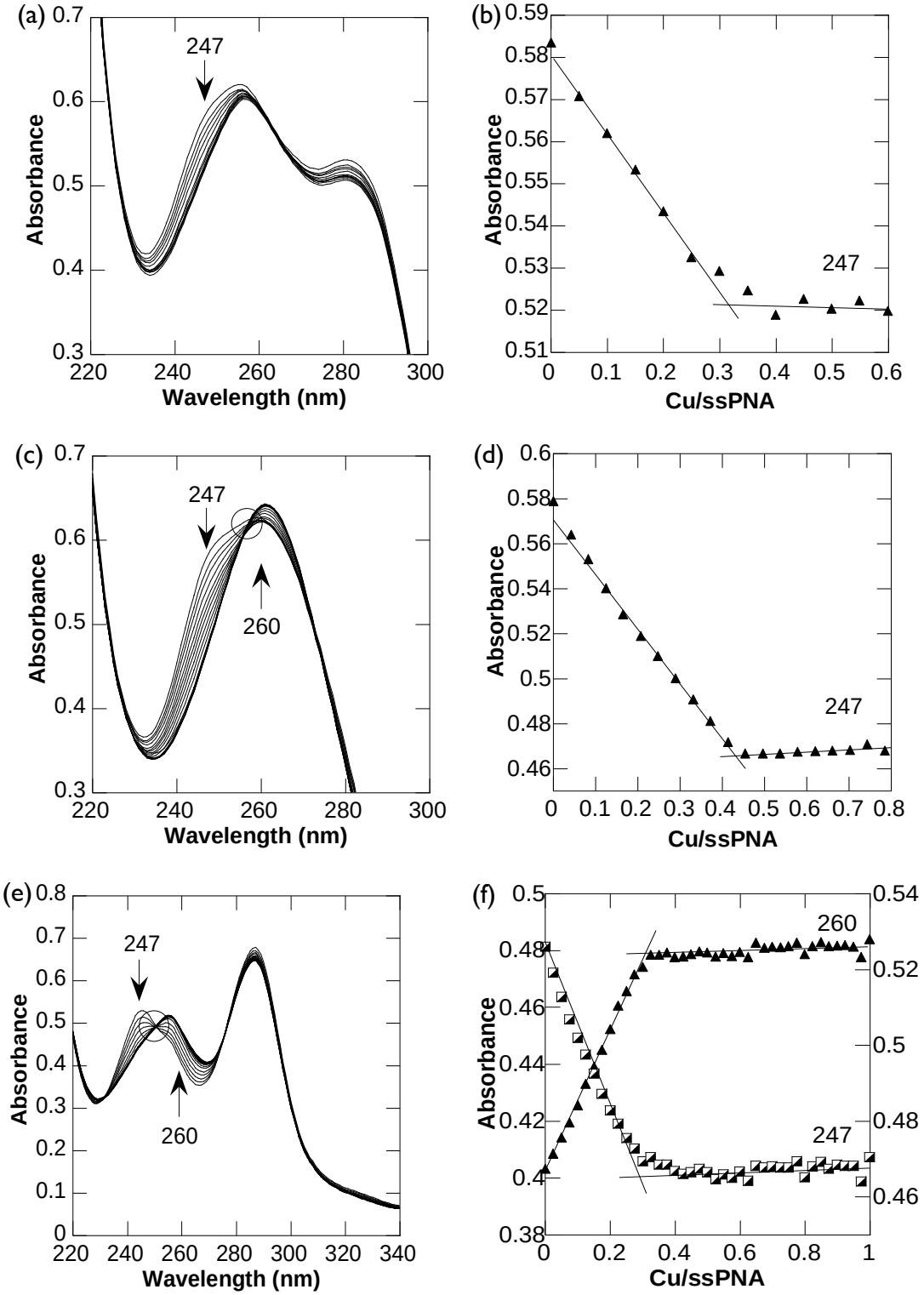

*Figure IV-8. Titration spectra of 5 μM solution of ssPNA **P-AG-P'** α-strand (a) and β-strand (c) by 0.4 mM $CuCl_2$ in pH 7.0 10 mM sodium phosphate buffer and the titration curves of ssPNA **P-AG-P'** α-strand (b) and β-strand (d) at 247 nm (▲).Titration spectra (e) and curve (f) of 10 μM solution of 4-bp short ssPNA **Q**-AG-**R** by 0.4 mM $CuCl_2$ at 260 nm (▲) and 247 nm (◪) in pH 7.0 10 mM sodium phosphate buffer.*

IV.3.iii Fluorescence Spectroscopy Titrations

Luminescence titrations measures the emission intensity of the $[Ru(Bpy)_3]^{2+}$ complex with the addition of different amount of Cu^{2+}. Since the complex formed between Cu^{2+} and ligand **Q** quenches the luminescence of $[Ru(Bpy)_3]^{2+}$, the titration of PNA duplex by Cu^{2+} shows a gradually decreased light intensity with increased amount of $[Cu\mathbf{Q}_2]$ formed (Figure IV-9). The fluorescence titration of **P-AA** and **P-AA-P'** resemble the UV titrations. However, the stoichiometry of fluorescence titrations is 0.4 of the ratio Cu/ssPNA regardless of the position of the $[Ru(Bpy)_3]^{2+}$ complex in the duplex. The UV titrations are based on monitoring the absorbance of the 8-hydroxyquinoline ligands, while the fluorescence titrations monitor the emission of the $[Ru(Bpy)_3]^{2+}$ complex. Variations may exist in the observed stoichiometry due to the mechanisms of different methods used.

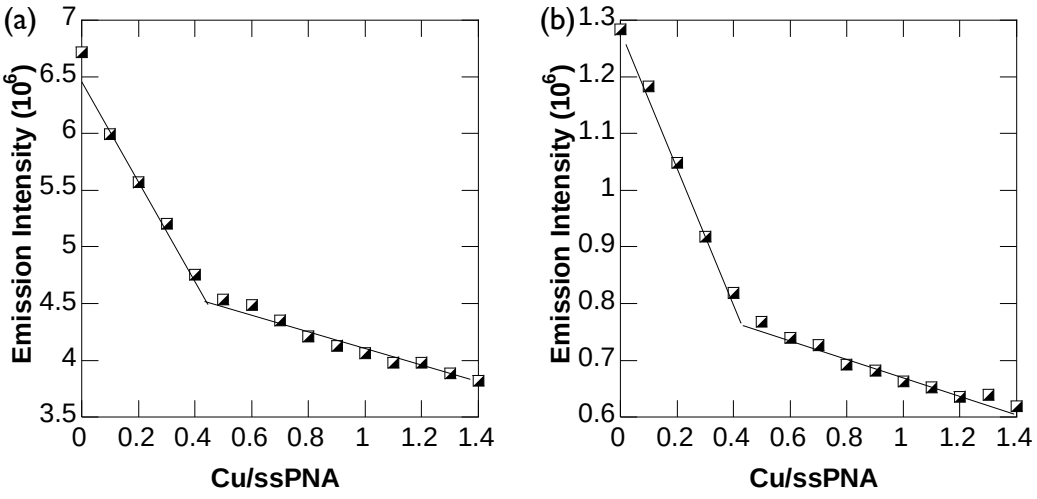

*Figure IV-9. (a) The titration curve for 10 µM **P-AA** with excitation wavelength at 440nm. (b) Emission spectrum of 10 µM **P-AA-P'** with excitation wavelength at 480nm. All spectra were measured in 10 mM pH=7 phosphate buffer and the emissions were monitored at 620nm.*

IV.3.iv Fittings of UV Spectroscopy Titration

The fitting of UV data is done by Mathematica under the help from Heather Stout. The inflection point of Cu/ssPNA between 0.25 and 0.5, which is between 0.5 and 1.0 for Cu/dsPNA, suggests a sequential binding mechanism in the formation of [Cu**Q**$_2$]. As shown in Equation IV-1, the first step gives a 1.0 stoichiometry between M and L to form ML (Cu^{2+}, dsPNA and the intra-duplex complex are referred as M, L, and ML for the convenience of the following discussion). As in and Equation IV-2, the second step gives a 0.5 stoichiometry to form ML_2 (referred to the inter-duplex complex). The coexistence of the two steps in equilibrium results in the in stoichiometry between 0.5 and 1.0 as mentioned at the beginning of this section.

$$M + L \overset{K_1}{\rightarrow} ML \qquad \textit{Equation IV-1}$$

$$ML + L \overset{K_2}{\rightarrow} ML_2 \qquad \textit{Equation IV-2}$$

where K_1 and K_2 are the equilibrium constants for each step, which lead to the following relations shown in the following equations:

$$[ML] = [M] \cdot [L] \cdot K_1 \qquad \textit{Equation IV-3}$$

$$[ML_2] = [ML] \cdot [L] \cdot K_2 \qquad \textit{Equation IV-4}$$

$$M_o = [M] + [ML] + [ML_2] \qquad \textit{Equation IV-5}$$

$$L_o = [L] + [ML] + 2[ML_2] \qquad \textit{Equation IV-6}$$

where M_0 is the total concentration of Cu^{2+}, L_0 is the total concentration of PNA duplex, which are known values for each addition in UV titration. $[M]$, $[L]$, $[ML]$, and $[ML_2]$ are the concentration of each species in solution. K_1 and K_2 are the two equilibrium constant to be fitted. Substituting $[ML]$ and $[ML_2]$ in Equation IV-5 with Equation IV-3 and Equation IV-4 gives Equation IV-7,

$$M_o = [M] + [M] \cdot [L] \cdot K_1 + [M] \cdot K_1 \cdot K_2 \cdot [L]^2 \qquad \textit{Equation IV-7}$$

Isolating term $[M]$ allows the presentation of $[M]$ by unknown values shown in Equation IV-8.

$$[M] = M_o/(1 + K_1 \cdot [L] + K_1 \cdot K_2 \cdot [L]^2) \qquad \textit{Equation IV-8}$$

Replacing $[L]$, $[ML]$, and $[ML_2]$ in Equation IV-6 with Equation IV-3 and Equation IV-4 gives Equation IV-9,

$$L_o = [L] + [M] \cdot [L] \cdot K_1 + 2[M] \cdot K_1 \cdot K_2 \cdot [L]^2 \qquad \textit{Equation IV-9}$$

Bringing Equation IV-8 into Equation IV-9 gives a cubic equation with one unknown $[L]$ to solve.

$$K_1 \cdot K_2 \cdot [L]^3 + (K_1 + 2K_1 \cdot K_2 \cdot M_o - K_1 \cdot K_2 \cdot L_o)[L]^2 + (1 + K_1 \cdot M_o - K_1 \cdot L_o)[L] = L_o \qquad \textit{Equation IV-10}$$

Once the solution to the above equation $[L]$ is solved, then the concentrations $[M]$, $[ML]$, and $[ML_2]$ are all solved according to Equation IV-8, Equation IV-3 and Equation IV-4. Therefore, the absorbance (A) of PNA solution for UV titration can then be obtained by using previously measured or assumed extinction coefficients by the following Equation IV-11:

$$A = b(\varepsilon_L \cdot [L] + \varepsilon_{ML} \cdot [ML] + \varepsilon_{ML_2} \cdot [ML_2]) + B_0 \qquad \textit{Equation IV-11}$$

where b is the length of light path (1 cm) and B_0 is a constant accounting for the baseline shift. The absorption coefficients ε_L, ε_{ML}, $\varepsilon_{ML_2}$and For **P-AG**, the parameters that are used for the fitting are summarized in Table IV-2. The UV titration and its fitting of **P-AG** is shown in Figure IV-10.

Table IV-2. Fitting parameters for UV titration of **P-AG**

PNA	ε_L	ε_{ML}	ε_{ML_2}	K_1	K_2	B_0
P-AG	162,000	186,000	350,000	10,000	1,000,000	-0.005

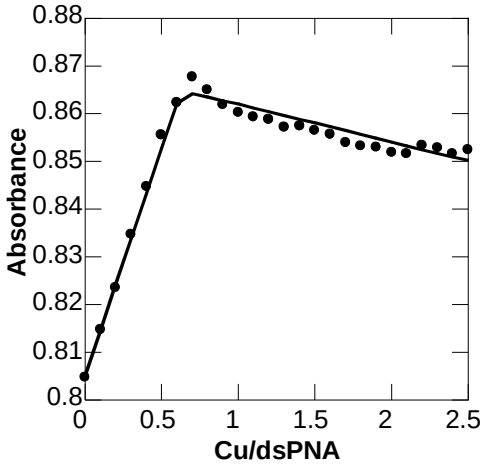

Figure IV-10. UV titrations and simulated results for 5 μM ***P-AG****. (a) Experimental and simulated absorbance. Blue: Monitored at 247nm, Black: Monitored at 260nm; (b) Simulated concentrations.*

From the above analysis we found that the fitting requires that K_2, the binding constant for the second step is much larger ($\geq$ 1000 fold) than that of the first step K_1. Under this condition, the formation of the inter-duplex complex is favored at the beginning of the UV titration. Later on when Cu^{2+} is added in excess to the solution, the equilibrium is driven to form the intra-duplex complex. Although the inter-duplex complex (ML_2) did form at the beginning of the titrations, it eventually dissociates and is converted to the intra-duplex complex (ML). The decreasing trend after the inflection point is a result of the decrease of absorption coefficient when the inter-duplex complex (ML_2) is converted to the intra-duplex complex (ML). The same conclusion can be drawn for duplexes with central $[Ru(Bpy)_3]^{2+}$ group as well.

IV.3.v Isothermal Titration Calorimetry

To investigate the lower stoichiometry of Cu/ssPNA observed in UV titrations in more detail, Isothermal Titration Calorimetry (ITC) is used to monitor the binding between Cu^{2+} and **Q**-modified PNA. The stoichiometry results of UV titrations agree with the stoichiometry measured by ITC very well (Table IV-3). Besides the identical stoichiometry observed between UV and ITC, ITC has also shown a slight feature of a stepwise binding event when the $[Ru(Bpy)_3]^{2+}$ complex is in the center of the strand (Figure IV-11b and c). The feature of a stepwise binding event is shown as a curvature at the beginning of ITC titration before the stoichiometry is reached. The two-step binding was observed in Dr. Zhijie Ma's thesis of the study of **Q**-modified PNA duplex by ITC, in which it is hypothesized that the first step involves the coordination of Cu^{2+} to two **Q** ligands from two different duplexes thus form the intermolecular [Cu$\mathbf{Q}_2$]. The second step followed is the entropy driven reorganization and the formation of intramolecular [Cu$\mathbf{Q}_2$] within the duplex. Compared with Zhijie's result, the curvature observed is not as profound. Therefore, it is not conclusive that whether or not an intermolecular complex [Cu$\mathbf{Q}_2$] was formed as an intermediate before the formation of the intramolecular complex [Cu$\mathbf{Q}_2$]. This confusion is addressed by the measurement of thermal UV-Vis in the next section.

Table IV-3. Comparison of the stoichiometry from UV titration and ITC

PNA	UV Cu/ssPNA	ITC Cu/ssPNA
P-AA	0.30±0	0.30±0
P-AA-P'	0.37±0.04	0.40
P-AG-P'	0.35±0.05	0.40
Q-AG-R	0.3	0.3

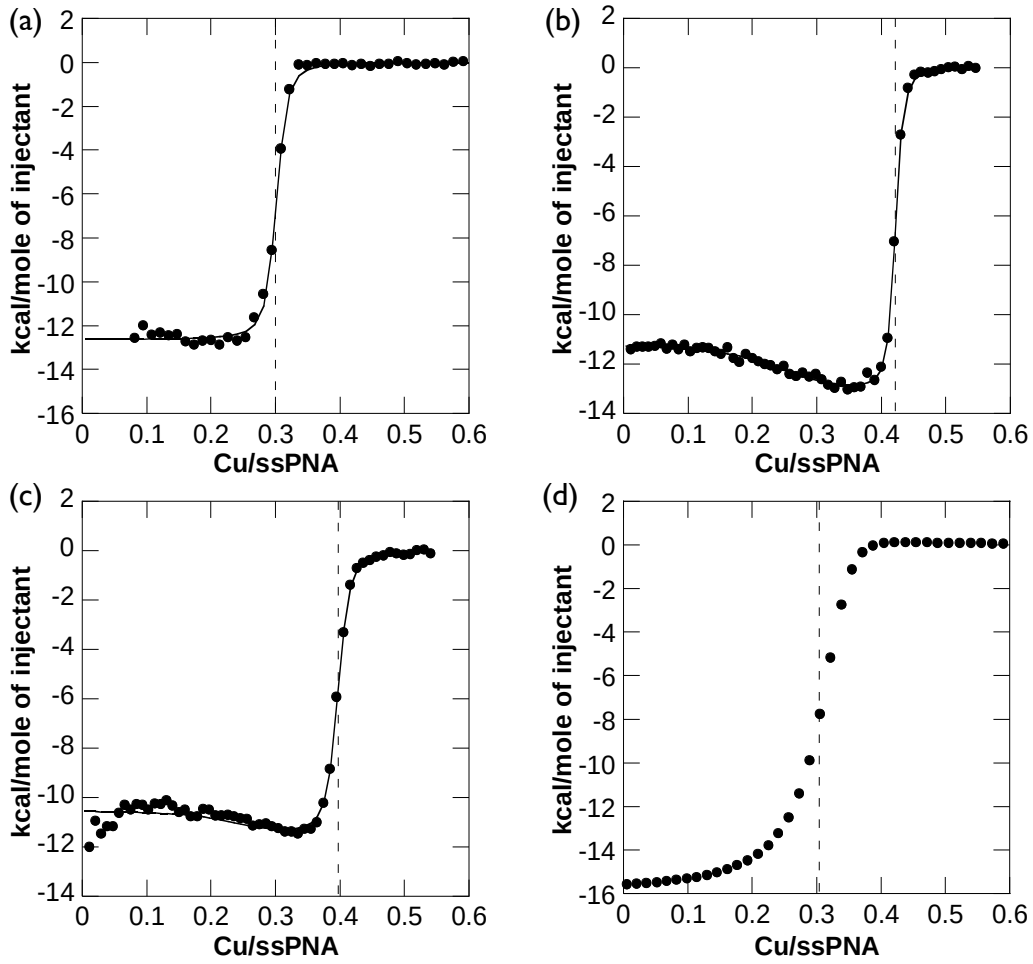

*Figure IV-11. ITC titration of 0.03 mM (a) **P-AA**, (b) **P-AA-P'**, (c) **P-AG-P'** and 0.06 mM (d) 4-bp short ssPNA **Q**-AG-**R** with $CuCl_2$ in pH 8.1 50 mM Tris buffer at 25 °C.*

IV.3.vi UV-Vis Spectroscopy Melting Curves

The thermal UV-Vis measures the absorbance change at 260 nm with elevated temperature from 10 to 95 °C. The melting temperature observed from the melting curve provides information on the thermal stability of the duplex. Representative melting curves of **P**, **P-AA**, **P-AA-P'** and a mismatch PNA duplexes in the absence and presence of Cu^{2+} are shown in Figure IV-12 and the melting temperatures T_m are listed in Table

IV-4. The T_m of the non-modified, 10-base pair PNA duplex, **P** on which the modified **P-XY** and **P-XY-P'** duplexes are based, was 67°C. The T_m of duplexes that contained one or two **Q** ligands was lower than that of **P** by 9-20°C, a decrease similar to that caused by a mismatch. In the presence of Cu^{2+}, the T_m of all PNAs that contain two **Q** ligands was 18-26°C higher than the T_m of the corresponding duplexes in the absence of Cu^{2+}, an increase attributed to the formation in the duplex of a [Cu$\mathbf{Q}_2$] complex that functions as an alternative base pair. In contrast, the T_m of duplexes that contained only one **Q** ligand, **P-AA**(α)/**P**(β) and **P-AG**(α)/**P**(β), was lower in the presence of Cu^{2+}, a change attributed to distortions of the duplex upon Cu^{2+} coordination to the **Q** ligand.

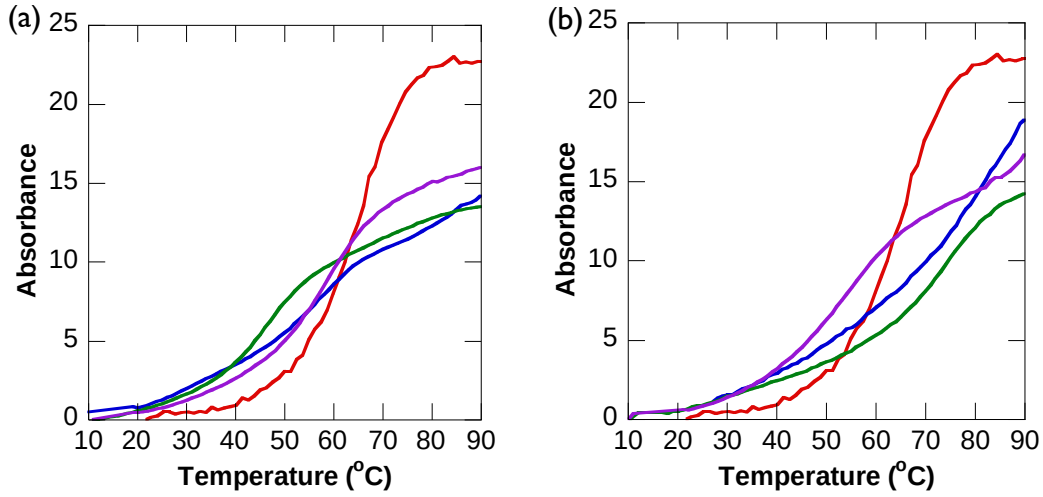

*Figure IV-12. Melting curves of duplexes **P** (red), **P-AA** (blue), **P-AA-P'** (green), and **P-AA**(α)/**P**(β) (purple) in the absence (a) and presence (b) of Cu^{2+}.*

Table IV-4. Melting Temperatures (°C) in the Absence and Presence of Cu^{2+}

PNA	w/o Cu^{2+}	w/ Cu^{2+}	ΔT
P	67	67	0
P-AA	56	82	26
P-AG	56	78	22
P-AGTGA	47	67	20
P-AA-P'	48	70	22
P-AG-P'	48	66	18
P-AA(α)/**P**(β)	58	56	-2
P-AG(α)/**P**(β)	58	52	-6

To clarify the confusion about the stepwise binding event which was mentioned above in the ITC experiments, the melting temperatures of the PNA duplexes **P-AA** and **P-AA-P'** with 0, 0.5 and 1 equivalence of Cu^{2+} were measured (Figure IV-13). Based on the destabilization effect observed for the mismatched duplex **P-AA**(α)/**P**(β) and **P-AG**(α)/**P**(β), it is expected that if a complex is formed without serving as the alternative base pair but a inter-duplex complex, the melting temperature of the duplex in the presence of 0.5 and 1 equivalence Cu^{2+} would be similar with each other. Otherwise, if the complex is inter-duplex at lower stoichiometry of Cu^{2+} and intra-duplex at higher stoichiometry, an increase of thermal stability is anticipated. As shown in Figure IV-13, the melting curves of duplex in the presence of 0.5 or 1.0 equivalence of Cu^{2+} almost overlap with each other indicating that the thermal stability of the complexes formed at 0.5 or 1.0 equivalence of Cu^{2+} are very similar. This result suggests that there is no distinct difference in the thermal stability if PNA duplex with the extra amount of Cu^{2+} added which is responsible to drive the equilibrium from inter- to intra-duplex complex formation. The stabilization induced by Cu^{2+} to the duplex indicates a combination of inter- and intra-duplexes in the solution.

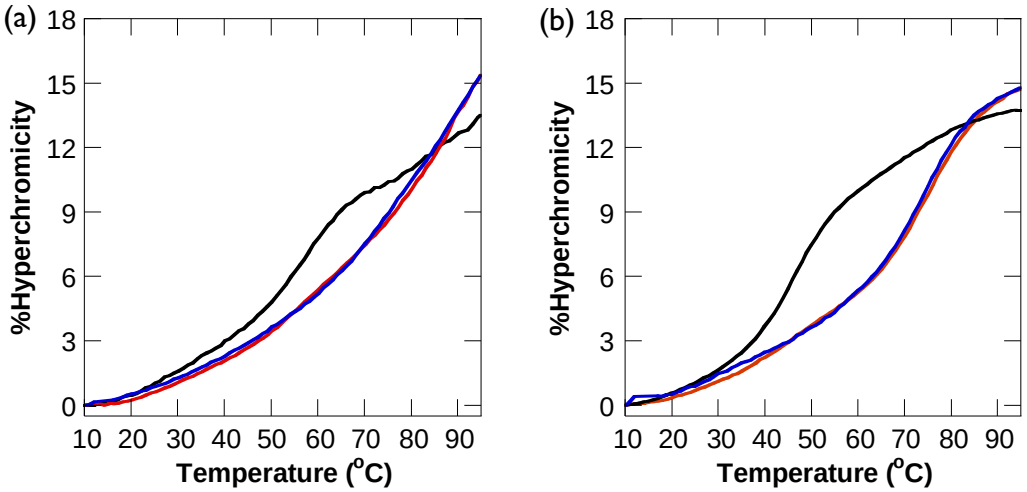

*Figure IV-13. Melting curves of duplexes (a) **P-AA** and (b) **P-AA-P'** in the absence (black), 0.5 equivalence (red) and 1.0 equivalence (blue) of Cu^{2+}.*

IV.3.vii Electron Paramagnetic Resonance (EPR) Spectroscopy

Andrew Weitz from Dr. Hendrich lab performed the EPR experiments reported in this section. Data analysis and discussion are written by me. EPR spectra have been recorded for 200 µM solutions of the PNA duplexes to study the Cu^{2+} coordination environment and the quantitative analysis of the Cu^{2+} concentration (Figure IV-14). The EPR spectra showed a close resemblance of the one previously measured for [Cu$\mathbf{Q}_2$] complexes in PNA duplex (Figure IV-15).[40] The g values observed are very close to the reported values of both the synthetic complex [Cu$\mathbf{Q}_2$] and the complex within the PNA context (Table IV-5). Even though the signal-to-noise ratio is not ideal, the superhyperfine features of the spectra indicate the coordination of Cu^{2+} to the nitrogen and oxygen atoms of **Q** monomers at the complementary positions in the same manner as reported earlier in by Watson et al. and Ma et al., especially when the sample is concentrated enough and the superhyperfine features are well defined (Figure IV-14e). The slight difference in the

parameters of the three EPR spectra for [Cu$\mathbf{Q}_2$] indicates the change in the environment of [Cu$\mathbf{Q}_2$] when it is free, incorporated in PNA context, and placed close to the $[Ru(Bpy)_3]^{2+}$ complex.

Besides the coordination environment, quantitative analysis of EPR spectra also gives information on the stoichiometry of the complex formed. The EPR samples are recorded in the presence of sodium phosphate buffer. Under this condition, Cu^{2+} and the phosphate anions form poly-nuclear complexes, which is EPR-silent. In this way, the EPR spectra only measure the Cu^{2+} that coordinated with a stronger ligand such as **Q**. The concentration of PNA and Cu^{2+} used to prepare the EPR sample and the measured concentration of coordinated Cu^{2+} are collected in Table IV-6. Except for the concentrated **P-AA-P'** and the **P-AA** with extra amount of Cu^{2+}, the stoichiometry calculated from the ration between measured Cu^{2+} and the concentration of PNA agrees well with the stoichiometry observed in UV and ITC (Table IV-6a, b, c, and f). With the extra amount of Cu^{2+}, the stoichiometry moves from 0.65 to 1.1 (Table IV-6c and d). It is also clear from that the binding of Cu^{2+} is enhanced by the addition of extra Cu^{2+}, indicating there is equilibrium responsible for the low stoichiometry observed earlier in the UV titrations and ITC between Cu^{2+} and PNA. As for the fluorescence decay experiments illustrated in the next section, extra amount of Cu^{2+} is used to insure the complete binding of Cu^{2+} to the ligand.

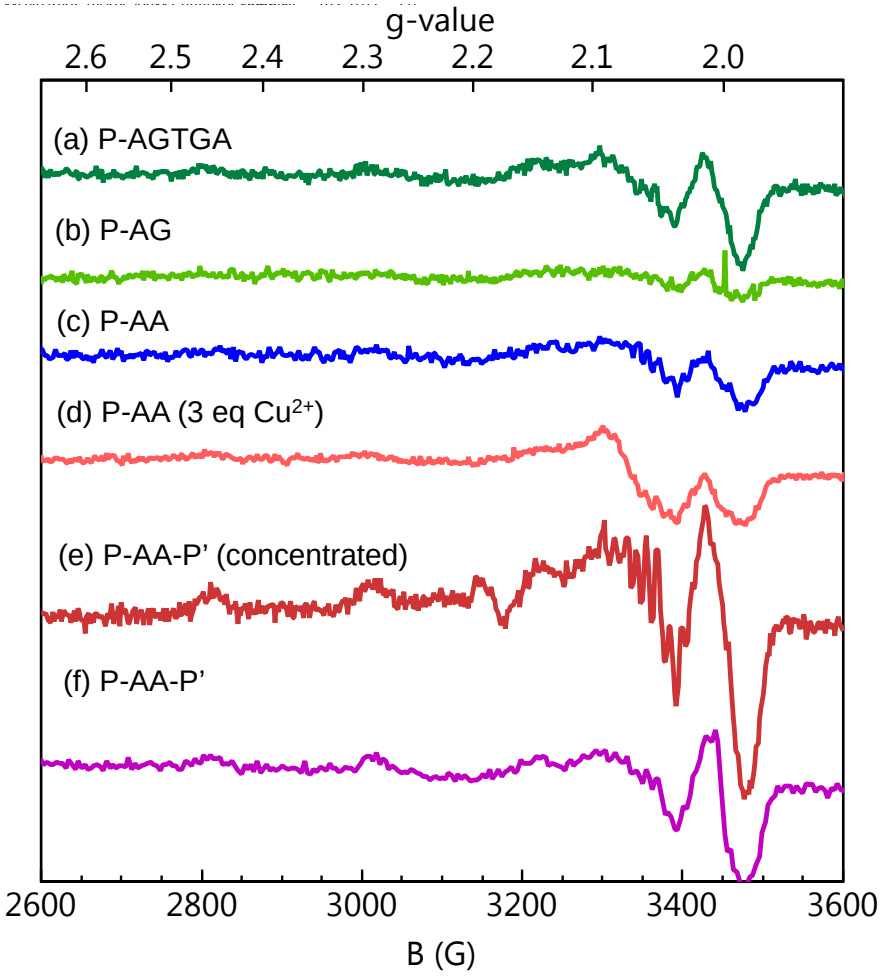

Figure IV-14. EPR spectra of (a) 20 µM ***P-AGTGA*** *and 20 µM* Cu^{2+}*, (b) 20 µM* ***P-AG*** *and 20 µM* Cu^{2+}*, (c) 20 µM* ***P-AA*** *and 20 µM* Cu^{2+}*, (d) 20 µM* ***P-AA*** *and 60 µM* Cu^{2+}*, (e) 100 µM* ***P-AA-P'*** *and 100 µM* Cu^{2+}*, and (f) 20 µM* ***P-AA-P'*** *and 20 µM* Cu^{2+} *in 25 % glycerol and 10 mM pH 7.0 sodium phosphate buffer.*

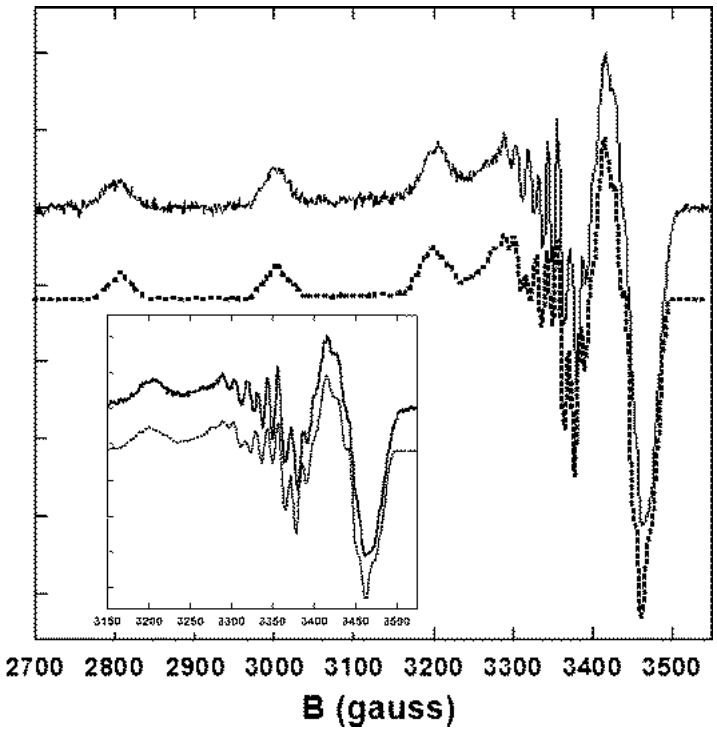

*Figure IV-15. EPR spectra (solid line) and simulation (dotted line) of 100 µM PNA duplex ds**Q**5 (H-GTAG**Q**TCACT-Lys-NH_2•NH_2-Lys-CATC**Q**AGTGA-H) and 100 µM Cu^{2+} in 25 % glycerol and 10 mM pH 7.0 sodium phosphate buffer with a zoomed-in inset of the superhyperfine structures. Figure is taken from published reference.*[40]

Table IV-5. EPR parameters for [Cu**Q**$_2$] within the PNA and in the synthetic complex

	ds**Q**$_5$[40]	[Cu**Q**$_2$][42]	**P-AGTGA**	**P-AA-P'**
g_1	2.06	2.06	2.06	2.06
g_2	2.05	2.05	2.05	2.05
g_3	2.22	2.22	2.22	2.22
A_1	72	72	72	72
A_2	80	80	79	79
A_3	611	611	635	630
A_{1N}	39	39	42	42
A_{2N}	32	32	37	33
A_{3N}	36	36	30	35

Table IV-6. Concentration (μM) of PNA and Cu^{2+} in sample preparation and the measured concentration of [Cu**Q**$_2$] by EPR

	P-AGTGA	**P-AG**	**P-AA**	**P-AA**	**P-AA-P'**	**P-AA-P'**
PNA	20	20	20	20	100	20
Cu^{2+}	20	20	20	60	100	20
[Cu**Q**$_2$]	10	10	13	23	30	15
Cu/dsPNA	0.50	0.50	0.65	1.1	0.33	0.75
Notation [a]	(a)	(b)	(c)	(d)	(e)	(f)

[a] *The notations correspond to the notation used in Figure IV-14.*

IV.3.viii Fluorescence Quenching by Photo-Induced Electron Transfer

Collaborator Xing from University of Pittsburgh performs the fluorescence quenching experiments. The discussion and presentation of result is written by me. The **P-AG** and **P-AGTGA** duplexes were used to evaluate the effect of distance between the $[Ru(Bpy)_3]^{2+}$ donor and the [Cu**Q**$_2$] acceptor on their electron transfer. In the absence of Cu^{2+}, the luminescence of the $[Ru(Bpy)_3]^{2+}$ complex in duplexes **P-AG** and **P-AGCTA** is similar to that of the "free" $[Ru(Bpy)_3]^{2+}$ complex in solution (Figure IV-16a). Addition of Cu^{2+} to the solution of the duplexes modified with **R**, but with no **Q** ligands, left the luminescence of $[Ru(Bpy)_3]^{2+}$ unaffected (Figure IV-16b). In contrast, the addition of one or more equivalents of Cu^{2+} to a solution of the duplexes modified with both **R** and **Q** quenches the $[Ru(Bpy)_3]^{2+}$ luminescence (Figure IV-12a). These results indicate that quenching of the $[Ru(Bpy)_3]^{2+*}$ in the **P-AG** or **P-AGCTA** involves the [Cu**Q**$_2$] complex that is part of the PNA duplex. Energy transfer from $[Ru(Bpy)_3]^{2+}$* to [Cu**Q**$_2$] is discounted as a decay pathway because of the poor overlap between the emission spectrum of $[Ru(Bpy)_3]^{2+}$ and the absorption spectrum of [Cu**Q**$_2$] (Figure IV-17). On the other hand, the electron transfer reaction $[Ru(Bpy)_3]^{2+*}$+[Cu**Q**$_2$] → $[Cu\mathbf{Q}_2]^-$ +

$[Ru(Bpy)_3]^{3+}$ is thermodynamically favorable.[43,44] Hence we conclude that the good electron donor $[Ru(Bpy)_3]^{2+}$* is quenched by the electron acceptor $[Cu\mathbf{Q}_2]$. This conclusion was corroborated by the observation of strong luminescence with the redox inactive $[Zn\mathbf{Q}_2]$ in the **P-AG** duplex (Figure IV-18).

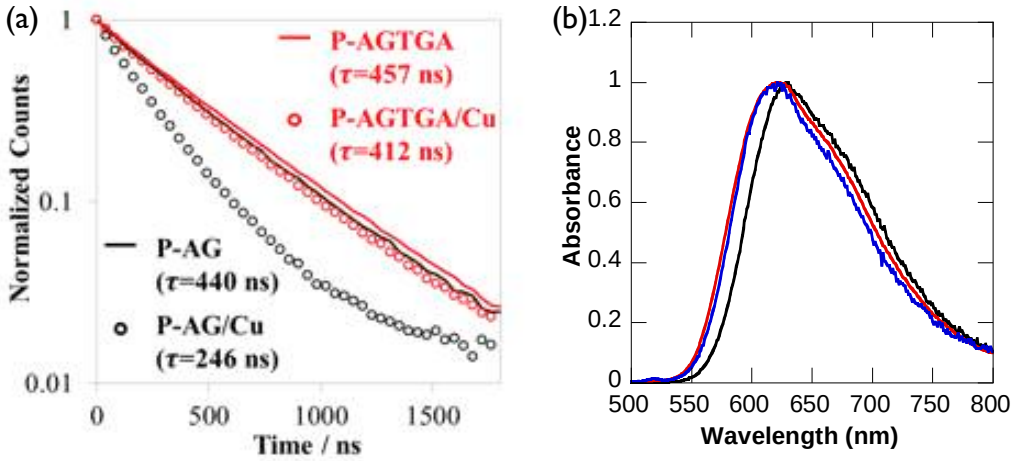

*Figure IV-16. (a) Luminescence decay for 20 μM solutions of **P-AG** (black) and **P-AGTGA** (red) in pH 7.0 10 mM phosphate buffer in the absence (solid lines) and presence (open circles) of two Cu^{2+} equiv. (b) Emission spectra of free $[Ru(Bpy)_3]^{2+}$ in water (black), **P-AG** (red) and **P-AGTGA** (blue) in 10 mM pH=7 phosphate buffer excited at 450nm.*

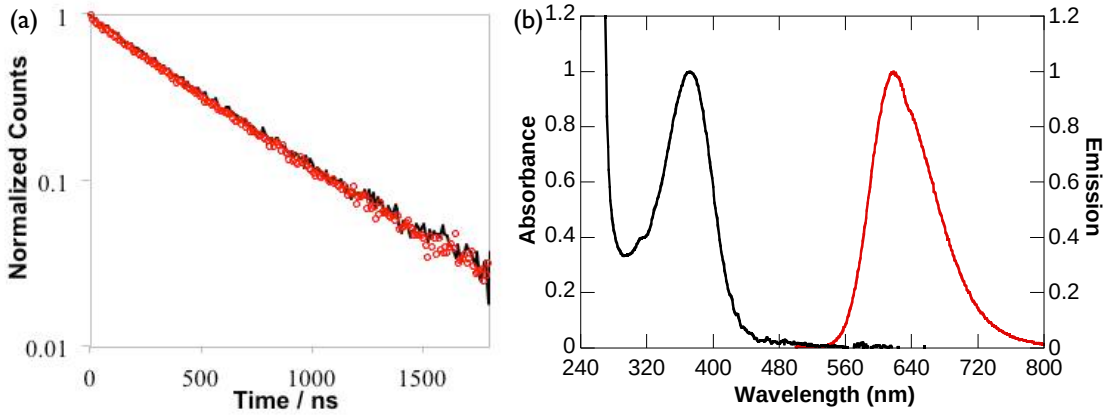

*Figure IV-17. (a) The decay curves of **P-R** PNA without (black) and with (red) 100μM Cu in 10mM phosphate buffer. (b) Absorption spectra of $[Cu\mathbf{Q}_2]$(black) and $[Ru(Bpy)_3]^{2+}$ and the emission spectrum of $[Ru(Bpy)_3]^{2+}$*

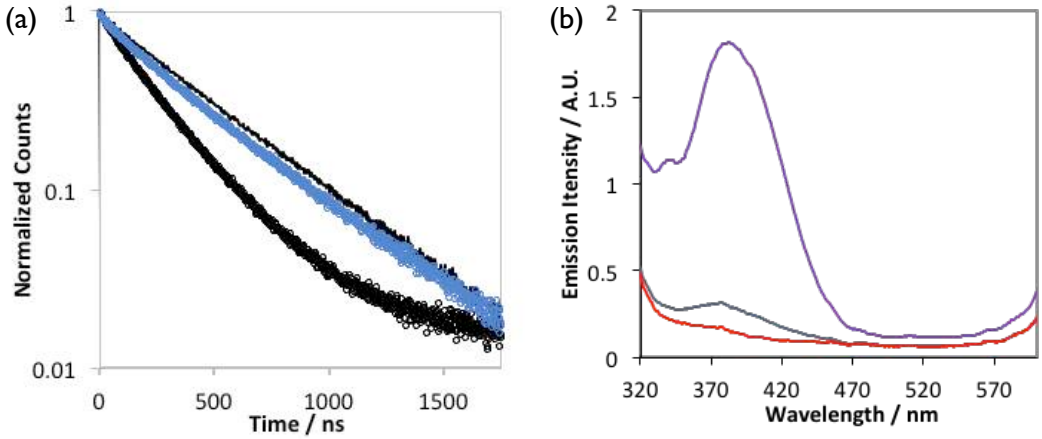

*Figure IV-18. (a) Luminescence decay curves are shown for **P-AG** without (navy line) and with two equivalents of Cu^{2+} (black circle) and Zn^{2+} (blue circle). b) The steady state excitation spectra are shown for **P-AG** measured at 620nm in the absence (grey) and presence of Cu^{2+} (red) or Zn^{2+} (purple), showing the fluorescence enhancement with Zn^{2+}.*

IV.3.viii.a Length Dependence of Photo-Induced Electron Transfer

The luminescence decays for $[Ru(Bpy)_3]^{2+}$* in duplexes of **P-AG** and **P-AGTGA** were used to probe the length dependence of the charge transfer rate (Figure IV-16a). In each case the luminescence decay law could be described by a single exponential exponential, and the addition of Cu^{2+} caused a decrease of the luminescence lifetime of the $[Ru(Bpy)_3]^{2+}$ complex for both duplexes. Assuming that the increase in the nonradiative decay rate of $[Ru(Bpy)_3]^{2+}$ upon addition of Cu^{2+} is caused by electron transfer, the rate constant for charge transfer between the $[Ru(Bpy)_3]^{2+}$ donor and [Cu**Q**$_2$] acceptor can be calculated as: $k_{ET} = 1/\tau - 1/\tau_0$ (Equation IV-12), where τ is average lifetimes determined from the fitting the luminescence decay with a (multi)exponential decay. τ_0 is that measured in the absence of the electron transfer quencher [Cu**Q**$_2$]. One obtains a value of $1.8\times10^6\ s^{-1}$ for **P-AG** and of $0.24\times10^6\ s^{-1}$ for **P-AGTCA** (Table

IV-7). Although these values are for only two donor-acceptor distances, if one assumes that $k_{ET} \propto \exp(-\beta \cdot D_{DA})$, in which D_{DA} is the distance between the Ru^{2+*} and the Cu^{2+}, a decay parameter of β of ~ 0.2 $Å^{-1}$ is obtained. This value should be considered an upper limit because of differences in $\Delta_r G$ ($\Delta_r G$ is probably more negative for **P-AG** than **P-AGTGA**) that arise from the Coulomb field stabilization being different for the **P-AG**/Cu and the **P-AGTGA**/Cu.[45,46] The β value of 0.2 $Å^{-1}$ lies between the electrochemically measured values in earlier work,[11,43,47] for single stranded PNAs (0.7~0.8 $Å^{-1}$) and double stranded PNAs (0.07 $Å^{-1}$).[47] The difference between β measured by luminescence in solution and by electrochemistry in SAMs of PNA may be caused by differences in the PNA geometry and/or in the mechanism hole-mediated[10,11,47] versus electron-mediated.[48,49]

Table IV-7. Luminescence lifetimes and electron transfer rates in **P-AG** and **P-AGTGA**

PNA	τ/ns	τ_0/ns	k_{ET}/s^{-1}
P-AG	246	440	1.8×10^6
P-AGTGA	412	457	0.24×10^6

IV.3.viii.b Position Effect of Photo-Induced Electron Transfer

The nature of the luminescence decay of the $[Ru(Bpy)_3]^{2+*}$ complex depends on its position in the duplex, as can be seen by comparing the data for **P-AG** and **P-AG-P'** in the presence of Cu^{2+} (Figure IV-19a). Figure IV-19b shows fits of the luminescence decay using a log-normal distribution of lifetimes. The peak width for the distribution of

lifetimes of the Ru complex in **P-AG** and **P-AG-P'** (solid red and solid black lines in Figure IV-19b) represents a lower limit because these decays can be fit by a single exponential decay law. In the presence of Cu^{2+}, the luminescence decay of the $[Ru(Bpy)_3]^{2+}$ complex in **P-AG** can be fit by a single modal distribution with a large peak width, while the decay of the Ru complex in **P-AG-P'** requires a bimodal distribution. The mean value for the long lifetime component for **P-AG-P'** in the presence of Cu^{2+} is similar to the mean lifetime observed for **P-AG** and **P-AG-P'** in the absence of Cu^{2+}, but it has a larger width. The observation of two different lifetimes may be caused by different conformations adopted by the PNA duplexes in solution. In the PNA duplexes that contain a terminal $[Ru(Bpy)_3]^{2+}$, the $[Ru(Bpy)_3]^{2+}$ complex could adopt a variety of positions with respect to the duplex because (1) the complex is attached to the PNA backbone through a flexible linker, (2) the terminal base pairs are subject to fraying, and (3) the complex has two optical isomers, Λ- and Δ-$[Ru(Bpy)_3]^{2+}$. The fact that the luminescence decay for **P-AG** in the presence of Cu^{2+} has a single modal distribution indicates that the different relative positions of the $[Ru(Bpy)_3]^{2+*}$ complex, with respect to the Cu^{2+} acceptor, are similar for this duplex. The bimodal distribution of lifetimes observed for the luminescence decay in the case of PNA duplexes with a central $[Ru(Bpy)_3]^{2+}$ complex suggests that the PNA exists in (at least) two distinct conformations for which the charge transfer between the $[Ru(Bpy)_3]^{2+*}$ and the $[Cu\mathbf{Q}_2]$ are significantly different and the interchange between them is slow compared to the charge transfer timescale. The lifetime distribution will be discussed furthr in the section of dynamic molecular simulation.

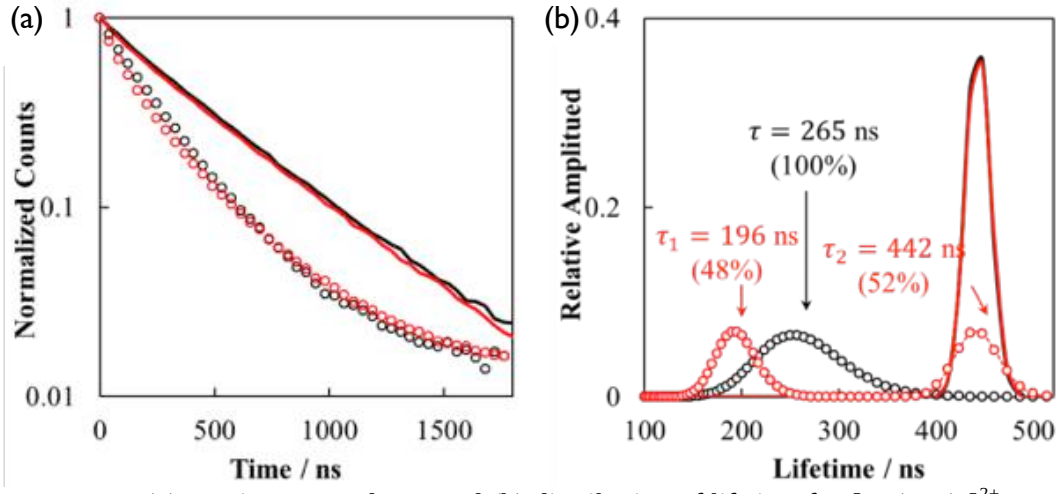

*Figure IV-19. (a) Luminescence decay and (b) distribution of lifetime for $[Ru(Bpy)_3]^{2+}$ complex in duplexes **P-AG** (black) and **P-AG-P'** (red) in the absence (solid lines) and presence (open circles) of Cu^{2+}.*

IV.3.viii.c Sequence Dependence of Photo-Induced Electron Transfer

As an experimental test of the conformation hypothesis, a base pair mismatch was introduced between the $[Ru(Bpy)_3]^{2+}$ and the **Q** ligands simply by mix and match the α and β strands of the perfect match PNA duplexes, which are **P-AA**(α)/**P-AG**(β), **P-AG**(α)/**P-AA**(β), **P-AA-P'**(α)/**P-AG-P'**(β), and **P-AG-P'**(α)/**P-AA-P'**(β). The $[Ru(Bpy)_3]^{2+*}$ lifetime shows a sequence dependence for the case of the PNA with terminally-attached $[Ru(Bpy)_3]^{2+}$, **P-AA**(α)/**P-AG**(β) and **P-AG**(α)/**P-AA**(β), but not for the PNA that contains $[Ru(Bpy)_3]^{2+}$ in the middle of the duplex **P-AA-P'**(α)/**P-AG-P'**(β), and **P-AG-P'**(α)/**P-AA-P'**(β). The fast luminescence lifetime component measured for the latter PNA duplexes is the same as for fully matched duplex **P-AG-P'** (Table IV-8). The sequence dependence of the luminescence for PNA duplexes with a terminal $[Ru(Bpy)_3]^{2+}$ suggests that charge transfer occurs through the nucleobase stack, and the lack of a sequence dependence for the luminescence decays in the case of PNA duplexes

containing a central $[Ru(Bpy)_3]^{2+}$ donor indicate that direct interactions occur between the donor and acceptor rather than nucleobase-mediated charge transfer.

Table IV-8. Sequence independence of fully matched PNA

PNA	Fast Peak		Slow Peak	
	Mean/ns	Weight (%)	Mean/ns	Weight (%)
P-AG	265	100	-	-
P-AA	278	100	-	-
P-AG-P'	196	48	442	52
P-AA-P'	193	43	444	57

IV.3.ix Molecular Dynamics (MD) Simulations

The section is simulated by collaborator Yongle from University of New Mexico, discussed and presented by me. Molecular dynamics (MD) simulations were performed for models of the **P-AG** and **P-AG-P'** duplexes, using published parameter sets for the PNA and the $[Ru(Bpy)_3]^{2+}$ complex.[10,50] In this modeling, the $[Cu\mathbf{Q}_2]$ was replaced by an AT base pair because an accurate $[Cu\mathbf{Q}_2]$ force field is not available. Figure IV-20 shows the average structure of typical trajectories. In Figure IV-20a, one of the three bipyridine ligands participates in π-π interaction with a terminal base pair. This interaction may restrict the flexibility of the $[Ru(Bpy)_3]^{2+}$ and favor positions of the complex in which π–π stacking is possible. Note that the steric interactions between the two $[Ru(Bpy)_3]^{2+}$ enantiomers and the left handed PNA duplex are slightly different and may contribute to broadening of the overall distribution shown in Figure IV-20b.

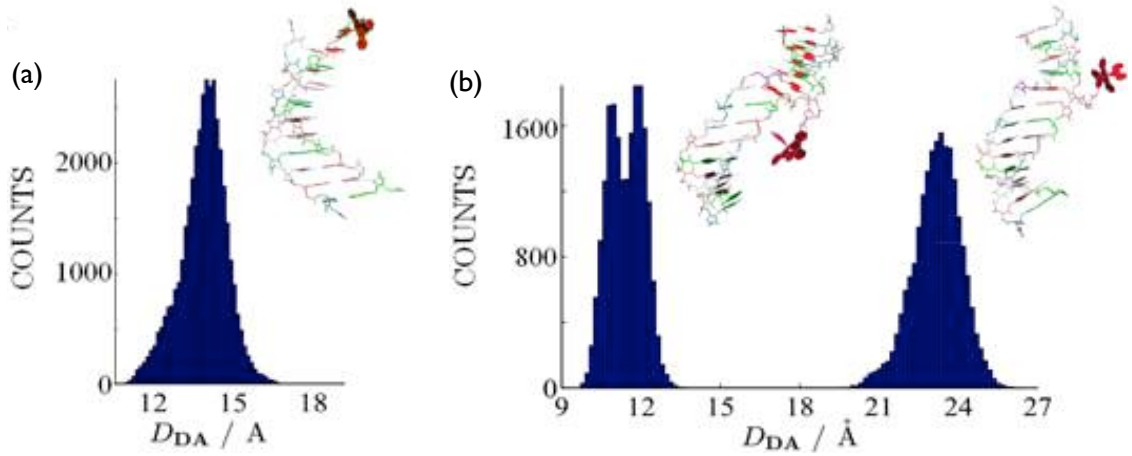

*Figure IV-20. The D_{DA} distributions calculated using MD simulations for the analogue of **P-AG** (a) and of **P-AG-P'** (b). The insets are the average structure for one MD trajectory.*

The donor-acceptor distance D_{DA} was calculated for snapshots of each trajectory at every 0.2 ps. The D_{DA} for the duplexes with a terminal $[Ru(Bpy)_3]^{2+}$ complex had a single mode distribution while the D_{DA} for the duplexes with a central $[Ru(Bpy)_3]^2$ complex had a bimodal distribution. Moreover, the mean value of the short-distance peak in duplexes with a terminal $[Ru(Bpy)_3]^2$ complex is smaller than the corresponding value for duplexes with a central complex, indicating that the latter duplexes should have a shorter luminescence lifetime than the former ones, as observed in experiments.

IV.4 Discussion

Previous UV and ITC titrations with Cu^{2+} of PNA duplexes that contained two **Q** ligands but no $[Ru(Bpy)_3]^{2+}$ showed that one Cu^{2+} binds to one duplex, indicating formation of $[Cu\mathbf{Q}_2]$ in the duplex.[40,41] This result was confirmed by EPR spectroscopy.[40,41] The $[Ru(Bpy)_3]^{2+}$ modification in PNA strand induced steric hindrance in the PNA duplex, which lead to a lower stoichiometry between Cu^{2+} and **Q**-modified

PNA. Due to the steric hindrance of the bulky $[Ru(Bpy)_3]^{2+}$, less **Q** ligand is available to the coordination of Cu^{2+}. According to the simulations of the UV-Vis and the fluorescence titrations, there is possibly an equilibrium between the inter- and intra-duplex complex formations as a result of the incorporation of $[Ru(Bpy)_3]^{2+}$. When the amount of Cu^{2+} is inadequate compared to PNA, the formation of inter-duplex $[Cu\mathbf{Q}_2]$ gives a 1:4 ratio (0.25) between Cu^{2+} and ssPNA. With more Cu^{2+} added to the solution, the formation of inter-duplex $[Cu\mathbf{Q}_2]$ is enhanced, driving the ratio toward 1:2 (0.5) between Cu^{2+} and ssPNA. As a result, the UV titration shows a ratio that is between 0.25 and 0.5, indicating a mixture of inter- and intra-duplex complexes. However, due to the existence of the mixture of both inter- and intra-duplex complexes, similar experimental results are observed for the $[Ru(Bpy)_3]^{2+}$ modified **Q**-containing PNA: 1) the addition of metal ion stabilizes the PNA duplex, 2) the formed $[Cu\mathbf{Q}_2]$ quenches the fluorescence of $[Ru(Bpy)_3]^{2+}$ through electron transfer and 3) exhibit the same physical parameters and superhyperfine structure in EPR spectrum indicating similar coordination environment as in the non-$[Ru(Bpy)_3]^{2+}$ **Q**-containing PNAs.

The incorporation of bulky metal complex into a PNA duplex poses synthetic challenges with the traditional solid phase peptide synthesis. Current research in our lab with $[Ru(Bpy)_3]^{2+}$ modification involves a linker between the $[Ru(Bpy)_3]^{2+}$ monomer and the adjacent monomer. The linker is basically a relief of the steric tension introduced by the $[Ru(Bpy)_3]^{2+}$ complex. Observation of the Kaiser test and the synthetic yield proved that the coupling is much better with a linker in between.

PNAs with terminal and central $[Ru(Bpy)_3]^{2+}$ modification and shorter (2-bp) or longer (5-bp) bridge in between the donor and the acceptor were synthesized to study the binding and luminescence properties of the modified PNAs. The terminal $[Ru(Bpy)_3]^{2+}$ modification is more flexible at the fraying end of the PNA duplex, demonstrating a higher degree of interaction with the ligand **Q** in UV titration (0.3 Cu/ssPNA in Figure IV-2 and 5), ITC (Figure IV-8a and d), and fluorescence lifetime distribution and MD simulation (broad peak in Figure IV-15b and 16a). The central $[Ru(Bpy)_3]^{2+}$ modification is more restricted by the hydrogen bonds from the neighboring base pairs, therefore, is less interactive with the ligand **Q** in UV titration (0.4 Cu/ssPNA in Figure IV-3), ITC (Figure IV-8b and c), and fluorescence lifetime distribution and MD simulation (narrow peak in Figure IV-15b and 16b). The position difference of the donor $[Ru(Bpy)_3]^{2+}$ complex allows the electron transferring to the acceptor $[Cu\mathbf{Q}_2]$ via different mechanism. Sequence dependence was observed in the mismatched PNA duplex showing the pathway of electron transfer is through the bases between the donor and the acceptor when $[Ru(Bpy)_3]^{2+}$ is terminal while no sequence dependence was observed for the central $[Ru(Bpy)_3]^{2+}$ modified PNA.

The rate constant for charge transfer was determined from the analysis of the luminescence decay curves. Significant difference was found in the electron transfer rates of the PNAs bridged with different lengths. The luminescence lifetime of **P-AGTGA** was not affected significantly by the addition of Cu^{2+}, which means the electron transfer is very slow. In contrast, the luminescence lifetime of **P-AG** was reduced significantly in the presence of Cu^{2+} indicating fast electron transfer rate between $[Ru(Bpy)_3]^{2+}$ and $[Cu\mathbf{Q}_2]$.

IV.5 Conclusions

This work demonstrates that $[Ru(Bpy)_3]^{2+}$ can transfer an electron to a [Cu**Q**$_2$] complex that is incorporated into the nucleobase stack of a PNA duplex. The presence of $[Ru(Bpy)_3]^{2+}$ causes the low stoichiometry between ligand **Q** and Cu^{2+}, which is possibly a result of the steric hindrance of the bulky $[Ru(bpy)_3]^{2+}$. When the $[Ru(bpy)_3]^{2+}$ complex can access the terminus of the duplex and interact with the nucleobase π system the rate shows a clear dependence on nucleobase stacking (matched versus mismatched) and length between $[Ru(Bpy)_3]^{2+}$ and [Cu**Q**$_2$] (two versus five nucleobases). If the complex is blocked from accessing the PNA terminus, then the charge transfer proceeds from the $[Ru(bpy)_3]^{2+}$ directly through nonbonded contacts to the acceptor and displays a dependence of rate on conformation. Thus PNA duplexes provide a useful scaffold to connect metal complexes and study charge transfer between them.

IV.6 Experimental

Materials. The Boc-protected 8-hydroxyquinolinyl PNA monomer 2-(N-(tert-butyloxycarbonyl-2-aminoethyl)-2-(8-hydroxyquinolin-5-yl)acetamido)acetic acid (**Q**, Figure 1C) and precursor 2,2'-bipyridyl PNA monomer **1** (Figure S1) 2-(N-(tert-butyloxycarbonyl-2-aminoethyl)-2-(2,2'-bipyridin-4-yl)acetamido)acetic acid, which are needed for synthesizing ruthenium(II) tris(bipyridyl) PNA monomer (Ru, Figure 1A), were synthesized as reported previously.[1,2] The ruthenium(II) tris(bipyridyl) PNA monomer **2**, namely 2-(N-(tert-butyloxycarbonyl-2-aminoethyl)-2-(2,2'-bipyridin-4-yl) acetic acid)-bis(2,2'-bipyridine)ruthenium(II), was synthesized from precursor **1**, Bpy

PNA monomer (Figure IV-17).[3] The backbone monomer was synthesized from the coupling between tert-butyl 2-(2-(tert-butoxycarbonyl)ethylamino)acetate and acetic anhydride, followed by hydrolysis, as reported previously.[4] All other reagents were commercially available, analytical grade quality, and used without further purification.

Synthesis of $[Ru(Bpy)_3]^{2+}$-containing PNA Monomer. All manipulations were carried out under low light. Bpy PNA monomer **1** (415 mg, 1mmol) was suspended in 43 ml of a 70% ethanol solution. cis-Bis(2,2'-bipyridine)dichlororuthenium(II) hydrate (500 mg, 0.96 mmol) was added to the suspension. The reaction mixture was refluxed for 16 h and the solvent was removed by vacuum (Figure IV-21). The compound was purified by cation exchange chromatography using CM-sepharose resin, with an ammonium chloride step gradient. The desired product precipitated out of the solution upon addition of ammonium hexafluorophosphate. The precipitate was filtered and washed several times with water and ether. An orange residue remained. Yield: 42% (447 mg). Mass Spectral data (ESI) give molecular masses of calc/found 827.9/827.2. ^{1}H NMR (300 MHz, CD_3CN): *d* 8.5 (m, 6H), 8.05 (m, 5H), 7.95 (m, 1H), 7.75 (m, 5H), 7.6 (m, 1H), 7.4 (m, 5H), 5.5 (1H, br, NH), 4.0 (m, 2H, CH_2), 3.6 (m, 2H, CH_2), 3.3 (m, 2H, CH_2), 3.1 (m, 2H, CH_2), 1.4 (d, 7H(should be 9H), Boc).

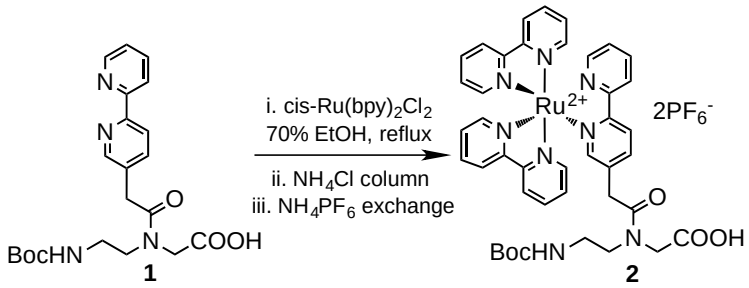

Figure IV-21.Synthesis of Ruthenium(II) tris(bipyridyl) monomer.

Solid Phase PNA Synthesis. PNA oligomers were synthesized with the Boc-protection strategy. PNA monomers were purchased from ASM Research Chemicals and were used without further purification. PNA was precipitated using diethyl ether after cleavage and was purified by reversed-phase HPLC using a C18 silica column on a Waters 600 model. Absorbance was measured at 260 nm with a Waters 2996 Photodiode Array Detector. The concentration of PNA oligomers was determined by UV absorption at 90°C using the sum of the extinction coefficients of the constituent PNA monomers at 260 nm taken from the literature. (ε_{260} were taken to be 8600 M^{-1} cm^{-1} for T, 6600 M^{-1} cm^{-1} for C, 13700 M^{-1} cm^{-1} for A, and 11700 M^{-1} cm^{-1} for G.[5] The extinction coefficient for the $[Ru(bpy)_3]^{2+}$ at 260 nm is taken to be the same as that of $Ru(bpy)_3Cl_2$ in water (ε_{260} = 13250 $M^{-1}cm^{-1}$). The extinction coefficient for 8-hydroxyquinoline ε_{260} = 2570 M^{-1} cm^{-1} (at pH 7.0) was determined from the slope of a plot of A_{260} versus concentration.

Characterization of the oligomers was performed by MALDI-ToF mass spectrometry on an Applied Biosystems Voyager Biospectrometry Workstation with Delayed Extraction and an R-cyano-4-hydroxycinnamic acid matrix (10 mg/mL in 1:1 water/acetonitrile, 0.1% TFA). m/z for $(M+H)^+$ were calculated and found to be **P-AA** α 3565.44/3568.05, **P-AA** β 2879.88/2882.03, **P-AG** α 3582.63/3582.39, **P-AG** β 2864.87/2864.95, **P-AGTGA** α 3582.63/3579.06, **P-AGTGA** β 2864.87/2863.12, **P-AA-P'** α 4390.71/4392.44, **P-AA-P'** β 3824.73/3824.83, **P-AG-P'** α 4415.82/4417.45, **P-AG-P'** β 3799.10/3800.87.

UV-Vis Spectroscopy Titrations. UV-Vis titrations were performed on a Varian Cary 50 Bio spectrophotometer with a 10 mm quartz cell. PNA stock solutions were prepared

with nanopure water (> 18.3 $M\Omega.cm^{-1}$) and have been stored at -18 °C to avoid depurination. PNA solutions were prepared in 10 mM pH 7.0 sodium phosphate buffer. To prepare each PNA duplex for titrations, the PNA solutions were held at 95 °C for 10 min first and then annealed from 95 °C to 10 °C at a rate of 1 °C/min. Concentration of the annealed PNA duplex were 5 μM. UV-Vis titrations were carried out by addition of 0.4 mM $CuCl_2$ solutions to PNA solutions at room temperature. The absorbance after each addition was corrected for dilution.

UV-Vis Spectroscopy Melting Curves. UV melting curves were recorded at 260 nm in the temperature range of 10-95 °C for both cooling and heating modes, at the rate of 1 °C/min. Prior to the measurement of the melting profiles, solutions of 5 μM of each ss PNA in 10 mM pH 7.0 sodium phosphate buffer were kept at 95 °C for 10 min before cooling down. T_m is the inflection point of a sigmoidal function used to fit the melting curve.

ITC. A MicroCal VP-ITC was used for all ITC experiments. A solution of one of the solution was placed in the cell (volume 1.46 mL) and the titrant solution (about 281.5 μM) in a syringe with the stirring speed at 300 rpm. Typically 58 injections of 5 μL each and 210 s apart have been made. The integrated peaks of the heat have been plotted as a function of the molar ratio. Tris(hydroxymethyl)-aminomethane (Tris) buffer solutions have been made by dissolving calculated amounts of solid in Nanopure water, and adjusting to the desired pH with HCl. The concentration of Cu^{2+} was corrected by Cu-EDTA ITC experiment.

EPR Spectroscopy. EPR spectra have been recorded on an X-band (9 GHz) Bruker ESP 300 spectrometer equipped with an Oxford ESR 910 cryostat. The microwave frequency was calibrated with a frequency counter and the magnetic field with a NMR gaussmeter. The temperature was calibrated using devices from Lake Shore Cryonics. Spectra have been collected under nonsaturating conditions. Samples have been prepared in pH 7.0 10 mM sodium phosphate buffer with 25% glycerol as glassing agent. Samples containing PNA and Cu^{2+} in appropriate molar ratio have been heated at 95 °C for 10 min, slowly cooled to room temperature, and then transferred into EPR tubes and frozen. EPR spectra have been simulated using the program SpinCount written by Prof. Michael P. Hendrich. Spin quantitation was done relative to a 0.499 mM Na_2[Cu(EDTA)] standard, the copper concentration of which was determined by plasma emission spectroscopy.

Luminescence Lifetime Spectroscopy. PNA solutions were prepared in pH 7.0 10 mM sodium phosphate buffer with concentrations of 10 or 20 μM. The PNA solutions were freeze-pump-thawed before measurement. A PicoHarp 300 TCPSC System is used to monitor the luminescence of $[Ru(bpy)_3]^{2+}$ at 620nm. The excitation laser has a repetition rate of 200 kHz and a wavelength of 440 nm. It is generated from a PiLas laser head controlled by a PIL044 driver. The recorded decay curves were fitted using the DAS 6 software package.

IV.7 References

(1) Rothemund, P. W. K. *Nature* **2006**, *440*, 297.

(2) Dietz, H.; Douglas, S. M.; Shih, W. M. *Science* **2009**, *325*, 725.

(3) Yan, H. *Science* **2004**, *306*, 2048.

(4) Bhatia, D.; Sharma, S.; Krishnan, Y. *Curr. Opin. Biotechnol.* **2011**, *22*, 475.

(5) Krishnan, Y.; Simmel, F. C. *Angew. Chem., Int. Ed.* **2011**, *50*, 3124.

(6) Seeman, N. C. *Annu. Rev. Biochem.* **2010**, *79*, 65.

(7) Hüsken, N.; Gasser, G.; Köster, S. D.; Metzler-Nolte, N. *Bioconjugate Chem.* **2009**, *20*, 1578.

(8) Baldoli, C.; Rigamonti, C.; Maiorana, S.; Licandro, E.; Falciola, L.; Mussini, P. R. *Chem.--Eur. J.* **2006**, *12*, 4091.

(9) Wierzbinski, E.; de Leon, A.; Davis, K. L.; Bezer, S.; Wolak, M. A.; Kofke, M. J.; Schlaf, R.; Achim, C.; Waldeck, D. H. *Langmuir* **2012**, *28*, 1971.

(10) Wierzbinski, E.; de Leon, A.; Yin, X.; Balaeff, A.; Davis, K. L.; Reppireddy, S.; Venkatramani, R.; Keinan, S.; Ly, D. H.; Madrid, M.; Beratan, D. N.; Achim, C.; Waldeck, D. H. *J. Am. Chem. Soc.* **2012**, *134*, 9335.

(11) Paul, A.; Watson, R. M.; Lund, P.; Xing, Y.; Burke, K.; He, Y.; Borguet, E.; Achim, C.; Waldeck, D. H. *J. Phys. Chem. C* **2008**, *112*, 7233.

(12) van Staveren, D. R.; Metzler-Nolte, N. *Chemical Reviews (Washington, DC, United States)* **2004**, *104*, 5931.

(13) Liu, J.; Tiefenauer, L.; Tian, S.; Nielsen, P. E.; Knoll, W. *Anal. Chem.* **2006**, *78*, 470.

(14) Huesken, N.; Gebala, M.; Schuhmann, W.; Metzler-Nolte, N. *ChemBioChem* **2010**, *11*, 1754.

(15) Huesken, N.; Gebala, M.; Battistel, A.; La Mantia, F.; Schuhmann, W.; Metzler-Nolte, N. *ChemPhysChem* **2012**, *13*, 131.

(16) Gross, A.; Huesken, N.; Schur, J.; Raszeja, L.; Ott, I.; Metzler-Nolte, N. *Bioconjugate Chem.* **2012**, *23*, 1764.

(17) Maurer, A.; Kraatz, H.-B.; Metzler-Nolte, N. *Eur. J. Inorg. Chem.* **2005**, 3207.

(18) Verheijen, J. C.; van der Marel, G. A.; van Boom, J. H.; Metzler-Nolte, N. *Bioconjugate Chem.* **2000**, *11*, 741.

(19) Hess, A.; Metzler-Nolte, N. *Chemical Communications (Cambridge)* **1999**, 885.

(20) Sosniak, A. M.; Gasser, G.; Metzler-Nolte, N. *Org. Biomol. Chem.* **2009**, *7*, 4992.

(21) Sudhir, V. S.; Venkateswarlu, C.; Musthafa, O. T. M.; Sampath, S.; Chandrasekaran, S. *Eur. J. Org. Chem.* **2009**, 2120.

(22) Hoffmanns, U.; Metzler-Nolte, N. *Bioconjugate Chem.* **2006**, *17*, 204.

(23) Zatsepin, T. S.; Andreev, S. Y.; Hianik, T.; Oretskaya, T. S. *Russ. Chem. Rev.* **2003**, *72*, 537.

(24) Beilstein, A. E.; Grinstaff, M. W. *J. Organomet. Chem.* **2001**, *637-639*, 398.

(25) Nickita, N.; Gilles, G.; Alan, M. B.; Leone, S. *Eur. J. Inorg. Chem.* **2009**, *2009*.

(26) Joshi, T.; Barbante, G.; Francis, P.; Hogan, C.; Bond, A.; Gasser, G.; Spiccia, L. *Inorg. Chem.* **2012**, *51*, 3302.

(27) Baldoli, C.; Rigamonti, C.; Maiorana, S.; Licandro, E.; Falciola, L.; Mussini, P. R. *Chem. - Eur. J.* **2006**, *12*, 4091.

(28) Baldoli, C.; Oldani, C.; Licandro, E.; Ramani, P.; Valerio, A.; Ferruti, P.; Falciola, L.; Mussini, P. *J. Organomet. Chem.* **2007**, *692*, 1363.

(29) Wagenknecht, H.-A. *Angew. Chem., Int. Ed.* **2003**, *42*, 2454.

(30) Venkatramani, R.; Keinan, S.; Balaeff, A.; Beratan, D. N. *Coordination Chemistry Reviews* **2011**, *255*, 635.

(31) Seidel, C. A. M.; Schulz, A.; Sauer, M. H. M. *J. Phys. Chem.* **1996**, *100*, 5541.

(32) Steenken, S.; Telo, J. P.; Novais, H. M.; Candeias, L. P. *J. Am. Chem. Soc.* **1992**, *114*, 4701.

(33) Voityuk, A. A.; Michel-Beyerle, M. E.; Rosch, N. *Chem. Phys. Lett.* **2001**, *342*, 231.

(34) Wesolowski, S. S.; Leininger, M. L.; Pentchev, P. N.; Schaefer, H. F., III *J. Am. Chem. Soc.* **2001**, *123*, 4023.

(35) Li, X.; Cai, Z.; Sevilla, M. D. *J. Phys. Chem. A* **2002**, *106*, 1596.

(36) Giese, B. *Annu. Rev. Biochem.* **2002**, *71*, 51.

(37) Razskazovskii, Y.; Swarts, S. G.; Falcone, J. M.; Taylor, C.; Sevilla, M. D. *J. Phys. Chem. B* **1997**, *101*, 1460.

(38) Cai, Z.; Gu, Z.; Sevilla, M. D. *J. Phys. Chem. B* **2000**, *104*, 10406.

(39) Messer, A.; Carpenter, K.; Forzley, K.; Buchanan, J.; Yang, S.; Razskazovskii, Y.; Cai, Z.; Sevilla, M. D. *J. Phys. Chem. B* **2000**, *104*, 1128.

(40) Watson, R. M.; Skorik, Y. A.; Patra, G. K.; Achim, C. *J. Am. Chem. Soc.* **2005**, *127*, 14628.

(41) Ma, Z.; Olechnowicz, F.; Skorik, Y. A.; Achim, C. *Inorg. Chem.* **2011**, *50*, 6083.

(42) Walker, F. A. S., H.; McCormick, D. B. *Inorg. Chem.* **1972**, *11*, 2756.

(43) Monzon, L. M. A.; Burke, F.; Coey, J. M. D. *J. Phys. Chem. C* **2011**, *115*, 9182.

(44) Kalyanasundaram, K. *Coord. Chem. Rev.* **1982**, *46*, 159.

(45) Zimmt, M. B.; Waldeck, D. H. *J. Phys. Chem. A* **2003**, *107*, 3580.

(46) Tachiya, M. *J. Phys. Chem.* **1993**, *97*, 5911.

(47) Paul, A.; Watson, R. M.; Wierzbinski, E.; Davis, K. L.; Sha, A.; Achim, C.; Waldeck, D. H. *J. Phys. Chem. B* **2010**, *114*, 14140.

(48) Daublain, P.; Thazhathveetil, A. K.; Wang, Q.; Trifonov, A.; Fiebig, T.; Lewis, F. D. *J. Am. Chem. Soc.* **2009**, *131*, 16790.

(49) Daublain, P.; Thazhathveetil, A. K.; Shafirovich, V.; Wang, Q.; Trifonov, A.; Fiebig, T.; Lewis, F. D. *J. Phys. Chem. B* **2010**, *114*, 14265.

(50) Moret, M.-E.; Tavernelli, I.; Rothlisberger, U. *J. Phys. Chem. B* **2009**, *113*, 7737.

CHAPTER V. Summary and Outlook

Beyond its role as the carrier of genetic information, DNA as well as its synthetic analogues such as PNA, LNA, GNA, or UNA has been used as a new material for nanotechnology applications. The Watson-Crick base pairing between nucleic acids allows the self-assembly between the complementary sequences. The success in the synthesis of ligand-containing nucleic acid monomers makes possible new rules of complementarity between modified nucleic acid strands. In the presence of metal ions, the coordination bonds between metal and ligand support as alternative base pairs just as hydrogen bonds support natural nucleobase pairs. The incorporations of metal ions and complexes that respond to redox, current, light, pH, temperature and other environmental changes offer great opportunities to add more functionality to the self-assembled structures based on a nucleic acid scaffold.

Chapter II in this thesis reports a molecular switch made from PNA, ligands and metal ions. The switch is based on the difference between the binding constants of the same metal ion in different oxidation states to different ligands. The addition of an oxidant or reductant triggers the "translocation" of a copper ion between two metal binding sites based on different ligands. Attempts have been made to study the copper translocation mechanism by stopped-flow instrument. Two approaches have been tried to understand whether the copper ions translocate between the two ligand sites through the bases within the PNA duplex or through the solutions outside the PNA duplex. One approach to understand the mechanism is to study the concentration dependence of the Cu(II)

translocation rate constant in solutions with different PNA concentrations. If the translocation occurs inside the PNA duplex as a unimolecular process, the rate constant of the translocation would be independent on the concentration of the PNA. On the other hand, if the translocation occurs outside the PNA, the rate constant would be dependent on the concentration of the copper ion and the PNA duplex. Another way to address the mechanism of Cu(II) translocation would be by the study of PNA duplexes that contain metal binding sites based on either ligands **Q** or **B** situated at different distances, e.g. ds$\mathbf{Q}^5\mathbf{B}^9$ in which the **Q** and **B** sites are separated by 3 nucleobase pairs, and ds$\mathbf{Q}^5\mathbf{B}^6$ in which the two sites are adjacent. If the translocation happens inside the PNA duplex, the translocation rate would be larger for ds$\mathbf{Q}^5\mathbf{B}^6$ than for ds$\mathbf{Q}^5\mathbf{B}^9$ because of the shorter distance between the two ligand sites in the former duplex. If the translocation happens outside the PNA duplex, the rate for ds$\mathbf{Q}^5\mathbf{B}^6$ and ds$\mathbf{Q}^5\mathbf{B}^9$ would be similar.

The molecular switch could be used as an optical sensor for the oxidation state of copper because the binding of copper in different oxidation state to the **Q** and **B** ligands can be monitored at distinct wavelengths in the UV range. It would be useful to find other ligands to make possible the detection in the visible or NIR range.

The research presented in this thesis shows that PNA could be used as an "active" linker of copper complexes, possibly including copper enzymes,[1-3] to a DNA- or peptide-based platform for nanodevices. Built in a robot-like nanodevice for drug delivery for example, a nucleic acid-based molecular switch could confer to the device the ability to transform its own structure as a function of the (type of) copper present in solution or the

pH of the solution and consequently release a drug at the site where prescribed, specific environmental conditions are met.[4-8]

Chapter III outlined the results of a study in which different molecular groups have been attached to DNA origami through a PNA linker. The study showed that a PNA strand modified with biotin can be positioned on a rectangular DNA origami at predefined locations such as corner, edge and center. The enhanced binding efficiency of a PNA strand over a DNA strand and the realization of post-annealing invasion by PNA prove that functionalization of DNA origami using PNA is effective. PNA functionalization of DNA origami opens a door to creating dynamic nanostructures in which structure transformation are implemented through the use of modified PNAs as described in the paragraph above this one. The detection of the changes could be by fluorescence, absorption or electrochemistry produced by the functional group on the PNA. Such dynamic changes based on the use of PNA have advantages over other current strategies for the modification of DNA origami because (1) modifications made by covalent means applied to DNA are not reversible under ambient conditions, (2) modifications made using ss DNA require a raise of the temperature above the melting temperature of the DNA origami. Given the already established means to modify PNA itself, it is easy to envision that modified PNAs can be organized either on the long DNA single strand that makes the DNA origami or on the staple strands that hold the DNA origami together, to achieve dynamic functionalization and create DNA origami capable of a measurable response to the environmental input.

The studies presented in chapter IV addressed the electronic properties and charge transfer through PNA in solution. The electron transfer rate constants were measured by monitoring the fluorescence quenching of the electron donor $[Ru(Bpy)_3]^{2+}$ by the electron acceptor [Cu**Q**$_2$]. Analysis of the dependence of the electron transfer rate constant on distance, sequence and conformation revealed that 1) the electron transfer rate decreases quickly with the distance between the donor and the accepter, 2) the rate constant of electron transfer depends on the sequence between the donor and the acceptor, 3) the conformation of PNA affects the electron transfer between the donor and acceptor. The study also established that the stoichiometry of Cu^{2+} binding to the **Q** ligands in PNA is low, which is possibly due to the steric hindrance exerted by $[Ru(Bpy)_3]^{2+}$ on the duplex. A two-step binding mechanism for Cu^{2+} in which Cu^{2+} first forms an inter-molecular complex with two PNA duplexes followed by the partial transformation of this inter-duplex complex into a PNA duplex containing one Cu^{2+} ion could explain the low stoichiometry. One way to test this hypothesis, is by using DNA to create negatively charged hetero PNA•DNA complexes that could be studied in turn by gel electrophoresis to distinguish the inter- and intra-molecular complexes by their different size and molecular weight. One requirement of applying is the studied molecular should carry charge whereas PNA is neutral.

This thesis provides basic concepts and experimental results that can be used in the building of molecular components of nanodevices based on PNA and the organization of the molecular components on DNA origami. This knowledge could be applied to rationally design and create smart molecular devices capable of providing a measurable outcome in response to signals from the environment.

V.1 References

(1) Brown, K.; Tegoni, M.; Prudencio, M.; Pereira, A. S.; Besson, S.; Moura, J. J.; Moura, I.; Cambillau, C. *Nature Structural Biology* **2000**, *7*, 191.

(2) Speers, A. E.; Adam, G. C.; Cravatt, B. F. *Journal of the American Chemical Society* **2003**, *125*, 4686.

(3) Speers, A. E.; Cravatt, B. F. *Chemistry & Biology* **2004**, *11*, 535.

(4) Nie, Z.; Li, X.; Li, Y.; Tian, C.; Wang, P.; Mao, C. *Chemical Communications (Cambridge, United Kingdom)* **2013**, *49*, 2807.

(5) Liu, M.; Fu, J.; Hejesen, C.; Yang, Y.; Woodbury, N. W.; Gothelf, K.; Liu, Y.; Yan, H. *Nature Communications* **2013**, *4*, 2127/1.

(6) Ke, Y.; Sharma, J.; Liu, M.; Jahn, K.; Liu, Y.; Yan, H. *Nano Letters* **2009**, *9*, 2445.

(7) Liu, Z.; Li, Y.; Tian, C.; Mao, C. *Biomacromolecules* **2013**, *14*, 1711.

(8) Zhao, Z.; Jacovetty, E. L.; Liu, Y.; Yan, H. *Angewandte Chemie, International Edition* **2011**, *50*, 2041.